Proceedings of

7th NIRS Research Center for Charged Particle Therapy Symposium

# Progress in Heavy Ion Radiotherapy

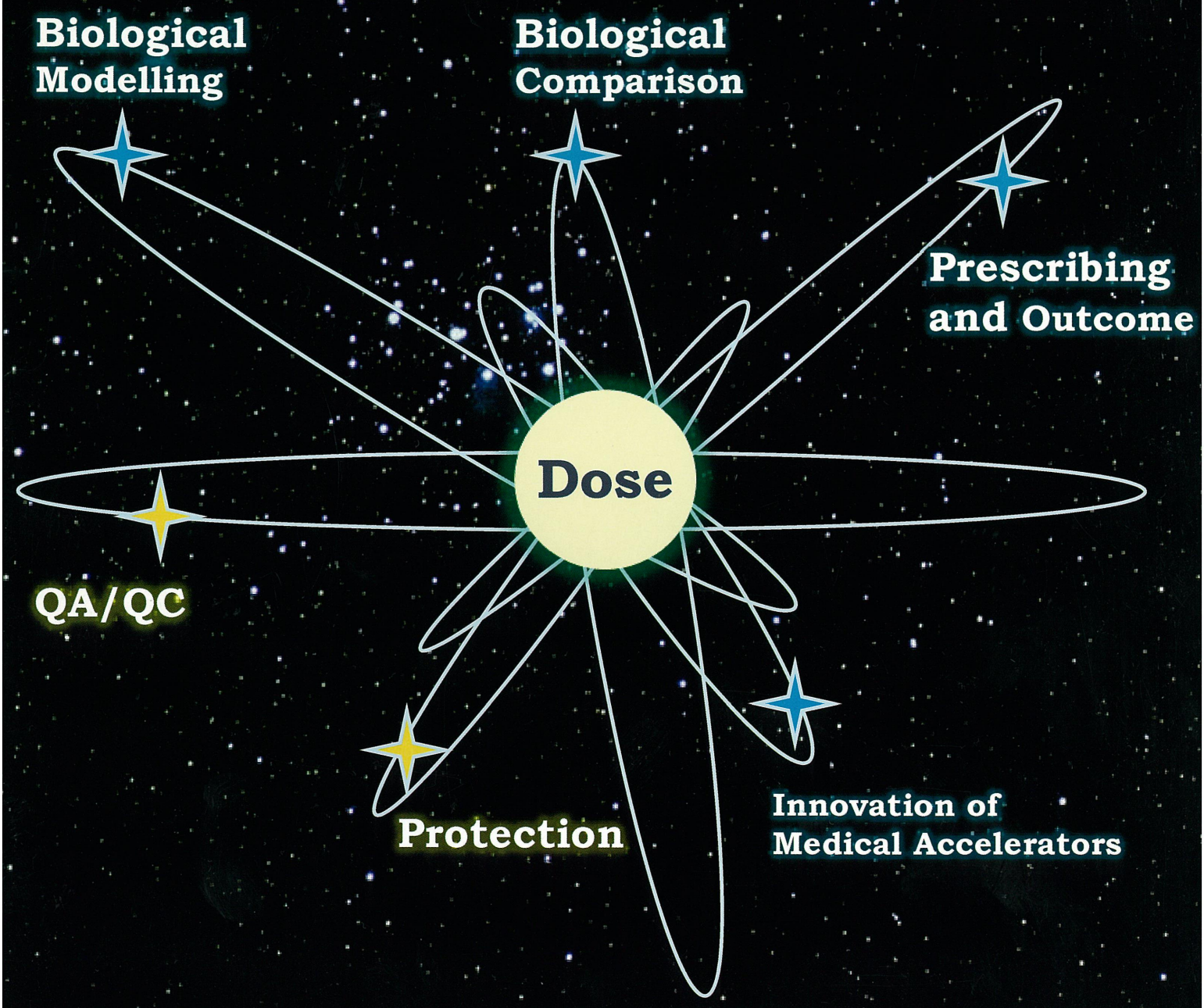


NIRS-M-209
978-4-938987-48-0

NIRS International Symposium on

# Progress in Heavy Ion Radiotherapy

November 30 & December 1 , 2007, NIRS

Organized by
National Institute of Radiological Sciences (NIRS), Chiba, Japan

Editor-in-Chief : Tatsuaki Kanai, Ph.D

Secretariat: International and Research Cooperation Section
Dept. of Planning and Management, NIRS

# Contents


7th NIRS Research Center for Charged Particle Therapy Symposium
Progress in Heavy Ion Radiotherapy
Nov. 30 & Dec. 1, 2007 NIRS, Chiba, Japan

# Upgrade of HIMAC Accelerator Complex

Koji Noda*, Takuji Furukawa, Takashi Fujisawa, Taku Inaniwa, Yoshiyuki Iwata,
Tatsuaki Kanai, Mitsutaka Kanazawa, Atsushi Kitagawa, Yuka Kobayashi, Masataka Komori,
Shinichi Minohara, Takeshi Murakami, Masayuki Muramatsu, Shinji Sato, Kota Torikai, Masami Torikoshi

Research Center for Charged Particle Therapy, National Institute of Radiological Sciences, Chiba, Japan
*Corresponding: noda_k@nirs.go.jp

**Abstract**

The first clinical trial with carbon beams generated from the HIMAC was conducted in June 1994. The total number of patients treated is now in excess of 3,500 as of October 2007. The impressive advance of the carbon-ion therapy using the HIMAC has been supported by high-reliability operation and by the development of the accelerator technology. Furthermore, we have carried out the beam intensity and quality upgrades of the HIMAC accelerator complex in order to increase the irradiation accuracy and the treatment efficiency.

## 1. Introduction

Heavy-ion beams are very suitable for the treatment of deeply seated cancer because of an excellent physical-dose distribution and high-LET characteristics around the Bragg peak. Therefore, NIRS decided to carry out heavy-ion cancer therapy with HIMAC [1]. Since the first clinical trial on three patients in June 1994 with 290 MeV/n carbon beam, the total number of patients treated at HIMAC exceeded 3,500 as of October 2007. At an early stage of the clinical trials, the number of fractional irradiations was typically 18 and the treatment required 6 weeks, besides the extra time needed for diagnostics and treatment planning. The number of fractions, however, has been decreased for some protocols, especially for the lung and liver, without encountering any serious side effects. At present, for lung- and liver-cancer treatments, only one fractional irradiation is carried out. Such decrease in fraction number can increase the number of treatments. As a result of the accumulating numbers of protocols, at 2003, carbon therapy at NIRS was approved as a highly advanced medical technology by the Japanese government. Such advances of carbon therapy with HIMAC have been supported by highly reliable operation [2] and by the development of beam-delivery and accelerator technologies [3-5]. The HIMAC accelerator complex has been upgraded especially for increasing the irradiation accuracy and the treatment efficiency. Based on the study for the upgrade of the HIMAC accelerator complex, we have designed a compact carbon-ion therapy facility for widespread use in Japan, and the Gunma University has been constructing the compact facility since April 2006. Owing to upgrade of the HIMAC accelerator, further, a design of a new treatment facility as our future plan has been successfully progressed. We review the upgrade of the HIMAC accelerator complex.

## 2. Study for upgrade of HIMAC accelerator complex

### 2.1. Gated irradiation with patient' s respiration

Damage to normal tissues around tumor was inevitable in treatment of a tumor moving along with respiration of a patient. A respiration-gated irradiation system, therefore, which can respond quickly to irregular respiration, was developed [3]. In this system, the irradiation-gate signal is generated only when target is at the design position and the synchrotron can extract a beam. This method has been applied to liver, lung and uterus cancers

since February 1996. At present, this irradiation method has applied to one-third of the HIMAC treatment. Figure 1 shows the view of irradiation gated with respiration.

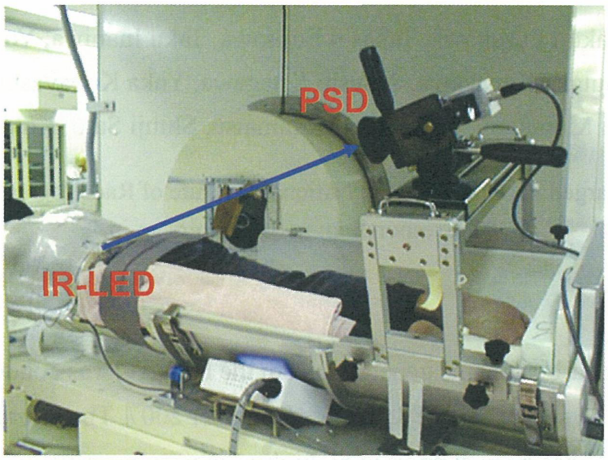


Fig. 1. The view of irradiation gated with respiration using the horizontal irradiation port.

This irradiation method requires the quick response of beam on/off according to the irradiation-gate signal. For the purpose, the RF-KO extraction method with AM and FM was developed. This RF-KO slow extraction method in synchrotron is based on the transverse beam heating while keeping the separatrix constant. One of great advantages in this method has a quick response within 1 ms to a gate-signal of beam on/off, as shown in Fig. 2. As a result, this RF-KO slow extraction method has realized the irradiation gated with respiration.

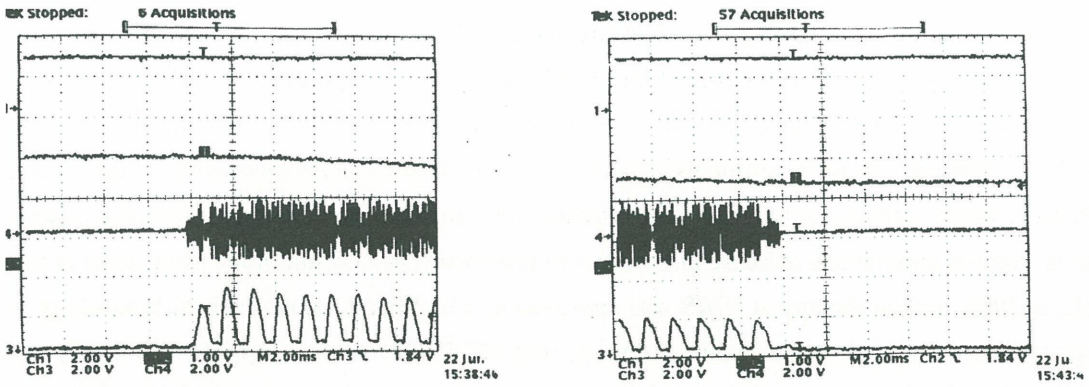


Fig.2. Time response of the RF-KO slow extraction method to the gate signal. (a) From upper trace, sextupole field for the extraction, circulating-beam current, transverse RF wave-form and the time structure of the extracted beam in time scale of 50 ms/div., (b) Beam-on (Left) and -off (Right) response in time scale of 2 ms/div.

### 2.2. Improvement of time structure of extracted beam through RF-KO slow extraction

The RF-KO method has been a key-technology of the gated irradiation method, although the method brought a huge ripple of the time structure of the extracted beam (spill). The huge spill ripple has never disturbed the dose distribution in the wobbler method, because the ripple frequency of around 1 kHz is much different from the wobbling one of around 60 Hz. On the other hand, sophisticated irradiation-methods such as a spot scanning and a raster one (beam-scanning method) have successfully been developed, because they can provide a high irradiation accuracy even for an irregular target shape and bring a high beam-utilization efficiency [6-9]. In the beam-scanning method, it was anticipated that the huge ripple affects the lateral dose distribution, because the scanning frequency is closed to the ripple one. Further, the intensity modulation of the extracted beam is an im-

portant technology for the beam-scanning method. Therefore, both the control method for the microscopic structure (kHz-order) and for the global one (Hz-order) were investigated.

*2.2.1 Improvement of microscopic time structure of extracted beam*

Since microscopic time structure of extracted beam (spill ripple) should be significantly suppressed in the beam-scanning methods, the source of the spill ripple in the RF-KO method was investigated through both the experiment and simulations [10], as follows; The frequency region of the transverse RF filed, which can extract the beam, was measured. Further, the spill structure during one period of the FM were measured and simulated in various sizes of the horizontal chromaticity. As the results of the investigation, it was found that the RF-KO slow extraction with the FM consists of two processes depending on the RF frequency regions; (1) The particles near the boundary of the separatrix can be extracted mainly due to the amplitude growth of the betatron oscillation when the frequency of the transverse RF field matches with the tune region near a boundary of the separatrix (extraction region). (2) The particles deeply inside the separatrix are diffused toward the boundary of the separatrix when the RF frequency matches with the tune region inside the separatrix (diffusion region). They are overlapped in each other, because of the dependence of the tune on the betatron-amplitude in the third-order resonance. The spill structures during one period of the FM are quite different in each frequency region and they are repeated with the repletion frequency of the FM, which is very source of the spill ripple in the RF-KO method. Therefore we proposed the dual FM method in order to suppress the spill ripple [11]. During the no-beam period, applying an additionally RF field with a frequency that matches that of the extraction region, the particles in the extraction region can be extracted due to the betatron-amplitude growth and/or due to the synchrotron oscillation. Thus, in this scheme, the spill ripple was considerably suppressed compared with that in the original RF-KO method (single FM). Furthermore, applying a transverse RF field with a mono-frequency that matches the tune in the extraction region, the particles in the extraction region can be extracted at a constant rate, because the amplitude-growth rate is almost constant due to satisfying the resonance condition. In this case, the spill ripple is considerably small under the condition that there is no other perturbation. However, the extraction efficiency is considerably degreased in this scheme, because no particle can be delivered to the extraction region from the diffusion one. Thus, the spill ripple will be improved, while keeping the extraction efficiency high, by adding a diffusion function to the mono-frequency RF-field, which we call the separate function method [11]. In this case, the dual FM method can be utilized for the diffusion function. The microscopic time structure, which was improved by the separate function method, is shown in Fig. 3.

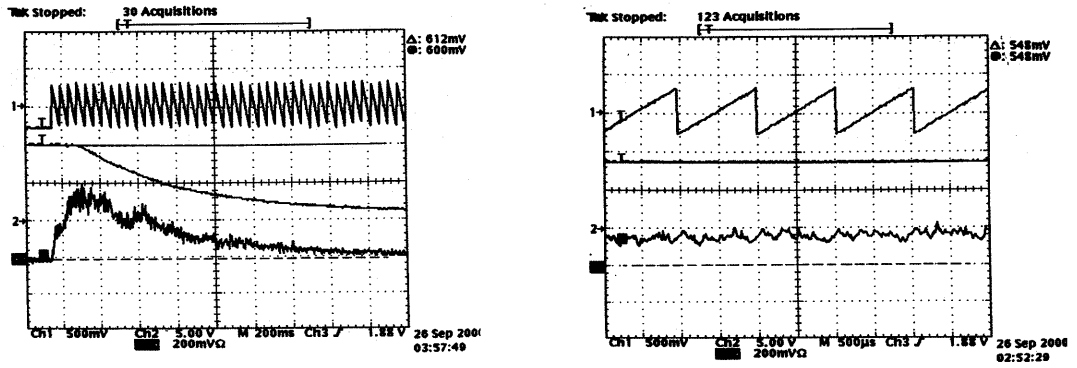


Fig. 3. Improved time structure by the separate function method. (a) Time scale is 200ms/div., (b) enlarged figure (a). Time scale is 0.5 ms/div.

*2.2.2 Improvement of global time structure of extracted beam*

In the RF-knockout extraction, the global time structure should be control, because it has been strongly required for medical and other applications. Especially for the beam-scanning irradiation method, the uniform spill significantly contributes to obtain easily uniform dose distribution in the lateral direction. For the purpose, we proposed to optimize the AM function for the transverse RF-field. In this optimization process for the AM, the radial distribution function of particles in the normalized phase-space was assumed to be expressed by the Rayleigh distribution function. The width of the Rayleigh distribution is widened by the transverse RF heating and the larger part than a constant width is extracted from the ring. Using this model, we estimated analytically the global spill structure. A diffusion constant by RF kick was obtained experimentally, and we predicted the RF kick angle so as to keep the extracted intensity constant. As a result of the study, it was verified that the function for the AM with the above-mentioned parameters could provide the flat spill within ?23% in both the simulation and the experiment at HIMAC synchrotron. Cooperating with the feedback system, finally, the global spill structure was suppressed less than ?5% [12].

Based on the control of the global time structure mentioned above, further, we have developed a system to control the spill structure and the beam intensity by the AM of the transverse RF-field for extraction [13], because the flat spill and the intensity control allow precise irradiation with a larger dynamic range of dose modulation. The core part of this control system (AM function controller) needs to achieve: 1) calculate and output AM signal based on the requirement comes from the irradiation system, 2) real-time processing more than 1ms time resolution, and 3) feed-forward and feedback control to realize the extracted intensity as same as requested. In order to realize these requirements, we employed a single-chip microcomputer for main processing. By cooperating with the feedback control, the intensity of extract beam was controlled dynamically while keeping its flatness. This system allows us to control the beam current almost as requested, which was experimentally verified at the HIMAC synchrotron. The time structure of extracted beam, which was obtained through the intensity control system, is shown in Fig. 4.

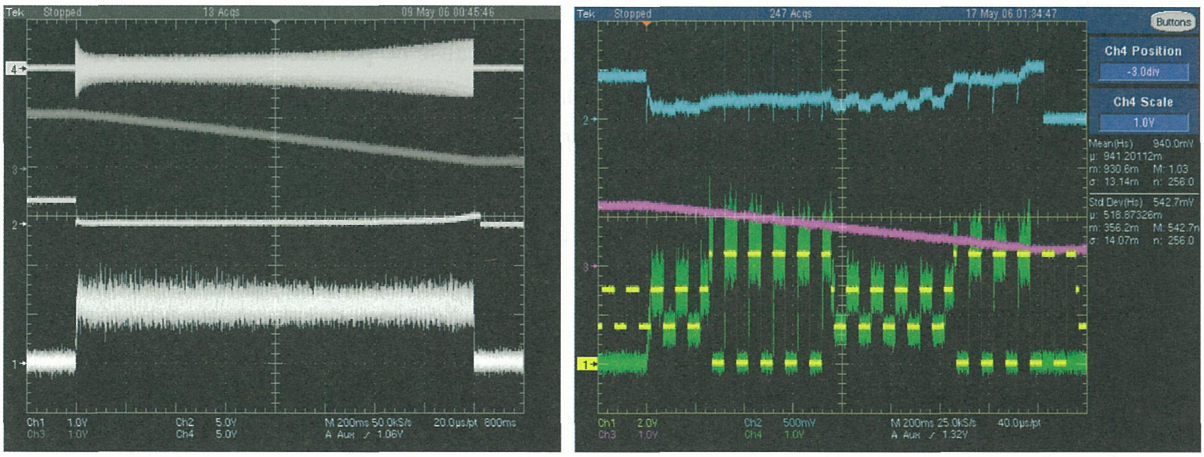


Fig. 4. Time structure of extracted beam obtained by the intensity control system. Left: Constant spill structure (bottom trace) in the time scale of 200 ms/div. Right: Intensity controlled spill structure (green trace) and request signal (yellow trace).

## 2.3. Control of beam profile and position

*2.3.1 Control of beam size*

In order to deliver the desired beam size and profiles at a target through a beam-transport line, it has been an essential technology to match the optical parameters, such as the emittance, twiss parameters and dispersion

function at an extraction channel of the ring. However, an optical matching at the extraction channel has not been easy, because it has been difficult to directly measure the optical parameters there as an initial condition of the transport line. Thus, an effort has also been made to match the optical parameters by predicting them at the extraction channel based on a simulation. However, the simulation result has a relatively large error compared with a direct measurement due to errors of the magnetic fields and an unexpected non-linear field in the ring. Therefore, we have developed a more accurate prediction method of the optical parameters at the extraction channel. The procedure in the proposed method is as follows: (A) For horizontal plane; (1) An outgoing separatrix was measured at the entrance of the extraction channel by using thin tantalum rods [14]. (2) The lattice parameters in the ring model, such as the horizontal tune and the strength of the separatrix exciters, were modified so as to reconstruct the measured outgoing-separatrix. (3) A simulation with the modified lattice parameters predicts the optical parameters of the extracted beam at the extraction channel. (B) For vertical plane; the optical parameters are estimated by measuring the vertical beam profile of the circulating beam by a non-destructive profile monitor [15] and using the twiss parameters of the ring at the entrance of the extraction channel. In order to verify the proposed method, we compared the predicted beam envelopes and dispersion function along the transport line with the measurement result. As a result, it was verified that the optical parameters reconstructed well the actual beam profile in the beam transport line [16], as shown in Fig. 5.

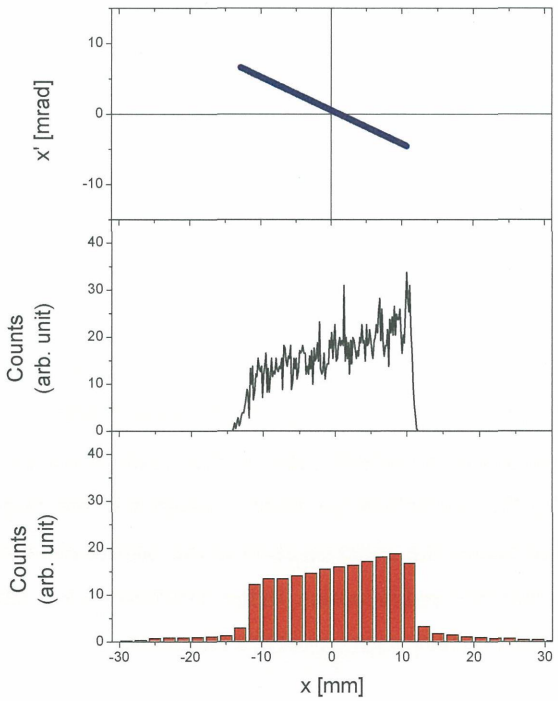


Fig. 5. Comparison of the horizontal beam profile between the simulation and the experiment. From the upper figure, phase-space distribution estimated by the rod-monitor measurement, horizontal profile estimated by the simulation and the measured profile.

As can be seen in Fig. 5, particle distribution in the horizontal plane is not Gaussian distribution, while the vertical one is Gaussian. It is inevitably that the difference between the horizontal and vertical distribution brings the rotating-angle dependence of the beam distribution in a rotating gantry. Therefore, we developed the compensation method for such an asymmetric distribution in the phase space and the difference between the horizontal emittance and the vertical one. This method is based on employing a thin scatterer (thin scatterer method), although the emittance is slightly enlarged by multiple scattering. As a result of particle tracking, the followings were verified [17]: 1) The asymmetric distribution was compensated by the thin scatterer set at the

optimum phase-advance from the entrance of the extraction channel. 2) The proposed method could realize the symmetric beam condition at the entrance of the gantry. 3) The horizontal and vertical profiles at the iso-center had no correlation between the rotation angles of the gantry while keeping their Gaussian profile.

*2.3.2 Control of beam position*

We have investigated the beam-position stability in order to deliver the stable beam for the beam-scanning. It was found from the measurement that beam position of vertical port from the upper synchrotron showed relatively poor reproducibility, especially in horizontal axis, corresponding to the extraction direction. Further, it was confirmed that large change was observed at particular conditions: 1) At the cold start, 2) After high energy operation with 800MeV/n and 3) After low energy operation such as a proton beam with 100MeV/u. it seems that 2) and 3) are caused by the change of residual field of the magnet.

Concerning the cold start, temperature of the cooling water for power supplies and magnets varies according to the excitation level etc. It was found from the measurement that 7 degrees rise in water temperature in the first one hour after the cold start, corresponding to more than 3 mm change of horizontal beam position. We should take an extra time for keeping the water temperature constant in the case of cold start.

It can be conceived that the extreme condition such as maximum energy and lower than minimum-design-value may cause variation of magnetic field via different residual magnetization. Owing to initializing procedure, the magnetic field reproducibility of the DC magnets was measured to be less than 5?10-5 by NMR measurement. Such slight change of the magnetic field in the transport line would not affect the beam quality, such as the position, profile and intensity. On the other hand, the magnetic field reproducibility of the pattern operation magnet was measured to be around 10-4 by search-coil measurement. The slight difference of the magnetic field in the ring brings the tune difference. Since a slight change of the horizontal tune causes the separatrix size difference in the resonant slow extraction, the extraction angle and the emittance change. It was verified by a computer simulation using RF-knockout simulation code. It means the beam quality at the end of HEBT strongly depends on the magnetic field stability of the pattern operation magnet in the synchrotron ring. Since daily fluctuation of the horizontal tune strongly affects beam quality, we have developed the system to compensate the daily fluctuation of the horizontal tune. In this system, we employ online-monitoring system and pulse-to-pulse correction by the correction quadrupole magnet in the ring. The current of the correction quadrupole magnet is changed to center the beam position at the profile monitor, based on measured beam response, which depends on the beam line and its optics. In the preliminary test results, this system makes it possible to keep the beam position and intensity constant at the iso-center.

**2.4. Intensity upgrade and extended flattop operation**

When the delivered beam intensity can be considerably increased to more than $2 \cdot 10^{10}$ carbon ions, we can complete the one fractional irradiation of almost treatment with one operation cycle of the HIMAC synchrotron, because the scanning method has high beam-utilization efficiency. This one cycle operation can increase the treatment efficiency in the gated irradiation. Therefore, we have pay much effort to increase the beam intensity from the synchrotron.

*2.4.1 Intensity upgrade*

In order to suppress the beam loss due to space-charge effect, resonance characteristics were investigated at the HIMAC synchrotron by means of a tune survey (Qx = 3.68~3.75, Qy = 3.0~3.5) with a high-intensity beam.

The working point is close to the integer resonance through the incoherent tune-shift under high ion density after bunching. Thus we changed the vertical tune from 3.13 to 3.23. Since the effect of the 3rd-order coupling resonance (Qx + 2Qy = 10) is not negligible, however, we tested the resonance correction by using 4 sextupoles. After the correction, the beam lifetime was increased by more than 5 times under (Qx,Qy) = (3.74,3.23).
Reducing bunching factor can suppress the space-charge effect. Therefore, an un-tuned RF-cavity, having a Co-based amorphous core, has been developed so as to make multi-harmonics operation possible for reducing the longitudinal space-charge effect [18,19]. By the multi-harmonics operation, the beam intensity was increased by 40%.

*2.4.2 Extended flattop operation*

Concerning the extended flattop operation of the HIMAC synchrotron, the stability of the beam was tested, firstly. In this test, $2 \cdot 10^{10}$ carbon ions were accelerated up to 400 MeV/n and extracted with the constant rate of $2 \cdot 10^{8}$ particles/s during 100 s of the extended flattop. The extraction beam rate is highly stabilized owing to a dynamic intensity control system with RF-knockout slow-extraction. In the 3D pencil beam scanning irradiation, on the other hand, the stability of the pencil beam is very important issue to assure the scanned field quality. As a result of the simulation study, it was clearly found that the dose uniformity was intolerably deteriorated under the position change of ±2 mm with sinusoidal frequency of 50Hz. Further, it was founded that the long-term difference of the beam position and size during the irradiation bring more critical disturbance on the dose distribution. Therefore, the beam position and profile during 100s extraction was also measured. Figure 6 shows the measured beam profiles during 100s extraction. The measurement was carried out by using the wire grid profile monitor in the beam line where the beta functions are larger than that of the iso-center. By the analysis of this measurement result, it was calculated that both the position and size during the extended flattop are stabilized within ±0.5 mm at the iso-center position.

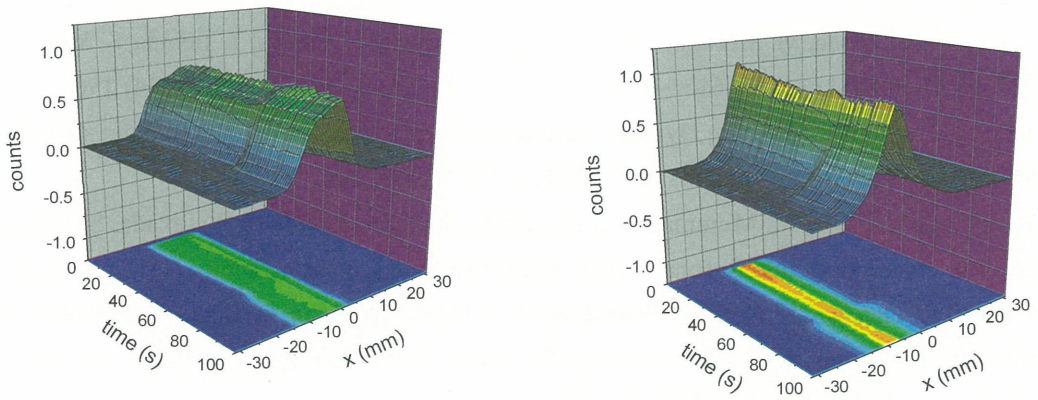


Fig. 6. Measured result of beam profile during 100s extraction.

## 4. Summary

For the upgrade of the HIMAC accelerator complex, the beam-studies have been carried out. Owing to the studies, not only a compact carbon-therapy facility for widespread use in Japan, but also the new treatment facility at HIMAC with the scanning method has been successfully progressed.

## References

[1] Y. Hirao et al., Heavy ion synchrotron for medical use-HIMAC project at NIRS-Japan, Nucl. Phys. A 538

(1992) 541c.

[2] T. Furukawa et al., Development toward turn-key beam delivery for therapeutic operation at HIMAC, Proceedings of 10th EPAC, Edinburgh, 2006, pp.2352-2354.

[3] S. Minohara, T. Kanai, M. Endo, K. Noda and M. Kanazawa, Respiration gated irradiation system for heavy-ion radiotherapy, Int. J. Rad. Oncol. Bio. Phys. 47, 1097-1103 (2000).

[4] T. Kanai et al., Commissioning of a conformal irradiation system for heavy-ion radiotherapy using a layer-stacking method, Med. Phys. 33, 2989-2997 (2006).

[5] K. Noda et al., Slow beam extraction by a transverse RF field with AM and FM, Nucl. Instrum. Meth.. A 374 (1996) 269-277.

[6] T. Kanai, K. Kawachi, H. Matsuzawa, T. Inada, Three-dimensional beam scanning for proton therapy. Nucl. Instrum. Meth. 214 (1983) 491.

[7] E. Pedroni, R. Bacher, H. Blattmann et al. The 200 MeV proton therapy project at PSI: Conceptual design and practical realization. Med Phys. 22 (1995) 37.

[8] Th. Haberer, W. Becher, D. Schardt, G. Kraft, Magnetic scanning system for heavy ion therapy. Nucl. Instrum Meth. A 330 (1993) 296.

[9] E. Urakabe, T. Kanai, M. Kanazawa, A. Kitagawa, K. Noda, T. Tomitani, M Suda, Y. Iseki, K. Hanawa, K. Sato, M. Shimbo, H. Mizuno, Y. Hirata, Y. Futami, Y. Iwashita, A. Noda, Spot Scanning Using Radioactive 11C Beams for Heavy-Ion Radiotherapy, Jpn. J. Appl. Phys. 40 (2001) 254.

[10] K. Noda, T. Furukawa, S. Shibuya, M. Muramatsu, T. Uesugi, M. Kanazawa, M. Torikoshi, E. Takada, S. Yamada, Source of spill ripple in the RF-KO slow-extraction method with FM and AM, Nucl. Instrum. Meth. A 492 (2002) 241-252.

[11] K. Noda, T. Furukawa, S. Shibuya, T. Uesugi, M. Muramatsu, M. Kanazawa, E. Takada. S. Yamada, Advanced RF-KO slow-extraction method for the reduction of spill ripple, Nucl. Instrum. Meth. A 492 (2002) 253-263.

[12] T. Furukawa, K. Noda, M. Muramatsu, T. Uesugi, S. Shibuya, H. Kawai, T. Takada, S. Yamada, Global Spill Control in RF-knockout Slow-Extraction, Nucl. Instrum. Meth. A 522 (2004) 196.

[13] S. Sato, T. Furukawa, K. Noda, Dynamic intensity control system with RF-knockout slow-extraction in the HIMAC synchrotron, Nucl. Instrum. Meth. A 574 (2007) 226.

[14] T. Furukawa, K. Noda, M. Muramatsu, T. Uesugi, S. Shibuya, H. Kawai, T. Takada, S. Yamada, New Approach toward Optimum Resonant Slow-Extraction, Nucl. Instrum. Meth. A515 (2003) 861-869.

[15] T. Honma, D. Ohsawa, K. Noda, T. Iwashima, H. Y. Ogawa, Y. Sano, E. Takada, S. Yamada, Design and performance of a non-destructive beam-profile monitor utilizing charge-division method at HIMAC, Nucl. Instrum. Meth. A 490 (2002) 435-443.

[16] T. Furukawa, K. Noda, T. Fujimoto, T.H. Uesugi, S. Shibuya and M. Torikoshi, Optical matching of a slowly extracted beam with transport line, Nucl. Instrum. Meth. A 560 (2006) 191-196.

[17] T. Furukawa and K. Noda, Compensation of the asymmetric phase?space distribution for a slowly extracted beam from a synchrotron, Nucl. Instrum. Meth. A 565 (2006) 430-438.

[18] M. Kanazawa et al., RF cavity with Co-based amorphous core, Nucl. Instrum. Meth. A 566 (2006) 195-204.

[19] M. Kanazawa et al., RF cavity with Co-based amorphous core, Proceedings of 10th EPAC, Edinburgh, 2006, pp.983-985.

# Status and Developments of the Heavy Ion Therapy Facility HIT at Heidelberg

H. Eickhoff, GSI, Darmstadt, Germany

Corresponding: H.Eickhoff@gsi.de

## Introduction

The Heavy Ion Therapy Facility HIT at the University Clinics of Heidelberg [1] is designed to treat about 1000 cancer patients per year, mainly with p- and carbon-beams; in addition the extension to helium and oxygen beams is foreseen. The 'intensity controlled raster-scan procedure' will be applied, which has been successfully demonstrated at the GSI Experimental Therapy Program [2]. Since 1997 about 400 patients have been treated with this treatment modality.

The accelerator complex of the HIT facility comprises two ECR- low energy branches, a linac with a compact RFQ- and IH- structure, a synchrotron, a high energy beam transport system, leading the ion beam to 2 horizontal treatment places, an isocentric light ion gantry and a 'QA' -place for quality assurance and further developments.

## Description of the Heidelberg Facility

The main requirements of the proposed facility can be summarized as follows:

- treatment both with low- and high- LET-ions
- fast change of ion species
- 3 treatment areas to treat a large number of patients
- integration of an isocentric gantry
- ion-species : p, He, C, O
- ion-range (in water) : 20 - 300 mm
- ion-energy (*) : 50 - 430 MeV/u
- extraction-time : 1 - 10 s
- beam-diameter : 4 - 10 mm (h/v)
- intensity (ions/spill)(*) : $1*10^6$ to $4*10^{10}$

(*) (dependent upon ion species)

These requirements are similar to those already established at the GSI-pilot project, but extended by additional ion species and the gantry application.

In addition to $^{12}C$-ion irradiations, proton treatments are requested for special tumor species in order to compare the medical results of C-treatments to those achieved with p-beams, for which an extended medical data base is available. For protons there is a significant blow-up of the beam diameter over the path length, which restricts the localization for deeply seated tumors. As this effect is much smaller for He-ions, this ion species will be favorable for a low-LET-ion treatment.

*The structure of the facility*

The building consists of 3 floors; the accelerator complex is located on the first and a major part of the additional technical installations on the second underground level.

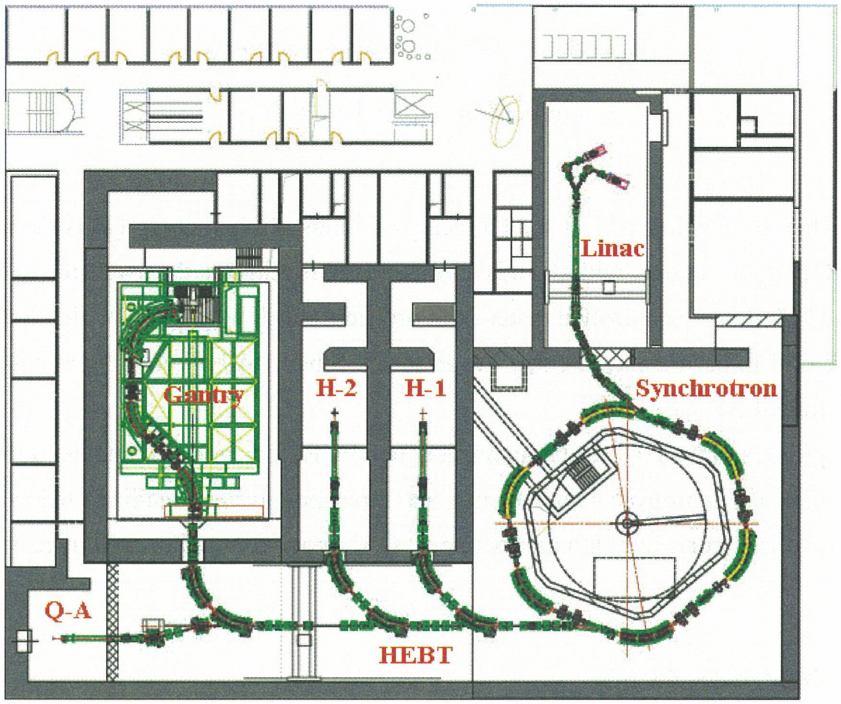


Fig. 1: Layout of the first underground floor, housing the accelerator complex

On ground level offices are located as well as the upper part of the gantry cave, that extends over all 3 floors.

Fig. 1 shows the layout of the first underground floor of this facility with the accelerator sections and treatment places.

The accelerator and beam transport sections consist of the following subsections:

*a) Injector and low energy beamline*

For the ion generation two parallel ECR-sources are installed, giving the possibility to switch from proton to carbon treatment within a short time.

The ECR source is chosen, as this type provides a very stable beam intensity over a long time without adjustment of the source parameters.

The required particle currents between 80 µA for $^{16}O^{6+}$ and 1.2 mA for p are rather conservative; both the current and the requested beam emittance can easily be achieved. The extraction energy of the ECR-source is 8 keV/u.

Within the low energy beam line the requested intensity reduction down to 0.1% of the maximal ion intensity is be performed by means of appropriate beam defocusing.

*b) Linac, Medium energy beam transport*

A combination of an RFQ and IH-linac structure with a total length of about 6 m is installed to accelerate the ions up to 7 MeV/u [3-7]. The RF-frequency of these structures is 216 MHz. The pulse length is about 200 µs, the maximal repetition frequency is 5 Hz. The normalized beam emittance is about 0.8 π mm mrad, the momentum spread ±0.15%.

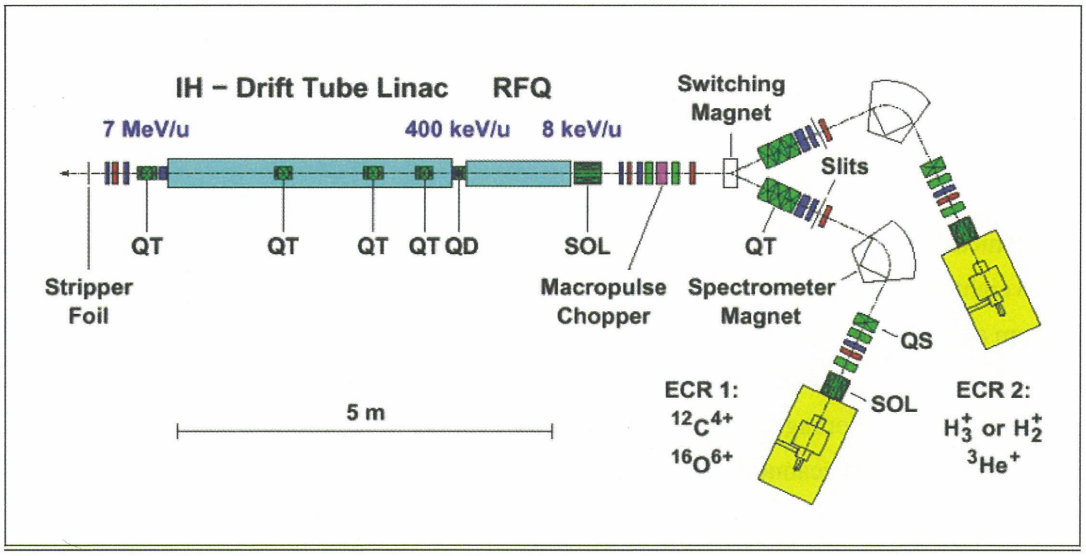


Fig. 2: Layout of the injector-linac

The medium energy beam transport system to the synchrotron consists of a stripping and a matching section. In addition, for multiturn injection a chopper system is provided to match the pulse length for the synchrotron injection. An rf debuncher cavity is installed to reduce the momentum spread for the synchrotron injection in order to maximize the multiturn injection efficiency.

*c) Synchrotron*

For the synchrotron [8] with a circumference of about 65 meters 6 bending magnets with a maximum flux density of 1.53 T are provided. Four long and two short straight sections are available for the installation of injection and extraction elements and the RF-cavity. After a 15 to 20 turn injection, corresponding to an injection time of about 30 μs, the acceleration to the maximal extraction energy takes place within 1.0 s.

The synchrotron has a doublet focusing structure with a slightly different ion optical setting for beam injection and extraction.

For slow extraction the 'transverse knock out' method is applied with variable extraction time between 1 and 10 s and multiple beam extraction at the same flat top. The easy realization of multiple beam extraction in the same cycle with this method gives great advantages both for respiration gated treatments and for the minimization of the treatment duration using the rasterscan method.

*d) High energy beam transport (HEBT)*

The high energy beam transport system delivers the slowly extracted beam to three treatment places. After the synchrotron extraction section a fast deflecting magnet prohibits the beam delivery in case of interlocks.

At the end of the high energy transport line a 'Quality-Assurance' (QA)-place is installed for beam diagnostic purposes, further developments of the treatment technique and biophysical research activities.

*e) Treatment areas*

In order to meet the demand for a patient flow of 1000 patients/year three treatment areas are provided. For the first and second area the beam is delivered from horizontal beam lines similar to that used at the GSI pilot project. The beam for the third treatment place is delivered by a rotating beam transport system ('isocentric gan-

try'). All beam lines are equipped with identical horizontal and vertical scanning magnets and beam diagnostic devices for the intensity controlled rasterscan. As an option the integration of a PET monitoring system in the gantry beam line is proposed.

*f) The Gantry*

The mechanical Gantry-structure, used for HIT is shown in Fig 3 [9]. The diameter of the gantry is about 13 m; its total weight including all magnets and supports is near 600 tons. FEM calculations for this structure result in a maximum angle dependent deformation of about ±0.5 mm, which leads to an expected maximum beam position variation at the isocenter of about 1-2 mm, mainly due to a steering of the last focusing quadrupole. Although reproducable positioning errors can be handled by means of appropriate steerer settings a fast on-line position correction with the scanner magnets, that is successfully in operation at the GSI pilot project, will be used in addition.

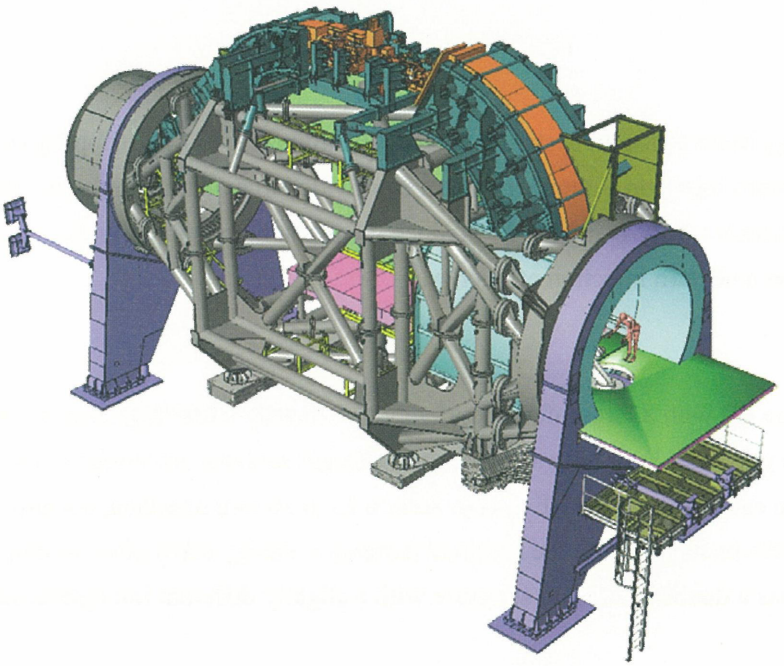

Fig. 3: View of the gantry mechanical structure
(some of the beamline elements are covered by structure elements)

In 2003 beam tests of the last gantry section, including the scanner magnets and the 90 degrees bending magnet [10] in a horizontal setup have been successfully performed within the HGF-strategy funds for investigations on 'Multifield irradiation techniques ' [11].

**Status of the facility**

After the installation of the accelerator systems, which started in Nov. 2005, the beam commissioning activities with the source and linac-branches began in March 2006. The linac commissioning was finished at the end of 2006; in 2007 the beam commissioning of the synchrotron and HEBT branches started, leading to a first extracted beam to one of the horizontal treatment places in March 2007. Until then the evaluation of the appropriate components settings is going on to achieve the requested beam properties for p- and C-beams at the horizontal treatment places, aiming to have a fixed parameter set in Nov. 2007.

Parallel to the beam commissioning procedures the installation of the isocentric gantry took place, which is

the worldwide first light ion gantry, capable to transport a 6.6 Tm beam, equivalent to a C-beam of 430 MeV/u. The first rotation of this gantry took place in April, 2007. The first delivery of a test beam through the gantry is expected for the end of 2007.

| **Time** (Year) | **Activities** |
|---|---|
| 2006 | assembly of the accelerator systems |
| 2006-2008 | Commissioning activities |
| 2008 | patient treatments (horizontal places) |
| 2009 | patient treatments (gantry place) |

Table 1: Major milestones of the HIT project

**Developments of 'treatment technique'**

*a) Rasterscan treatment method*

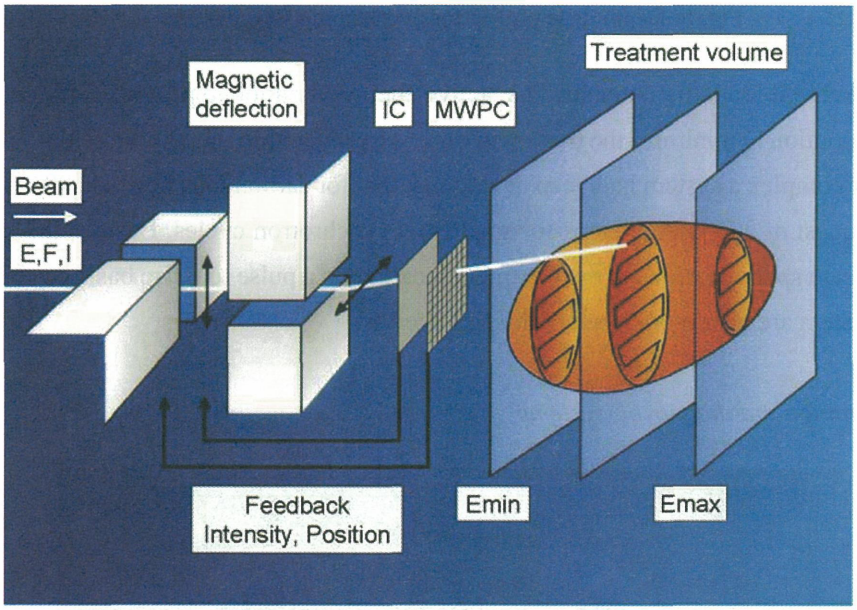


Fig. 4: Rasterscan-Method

The 'intensity controlled rasterscan' treatment modality [12] is foreseen as the only treatment method for all patient places, including the gantry.

The principle of this method, which has been developed at GSI and successfully applied to more than 350 patients within the GSI Experimental Therapy Program, is shown in Fig. 4. The tumor volume can be composed of slices ( 'isoenergy-slices' ) of different depths. These slices are irradiated with ions of specific energies, correlated to the requested penetration depth. By a sequential treatment of such slices with adequate intensities the requested dose profile for the tumor volume within the shown spread-out bragg peak is achieved. (Fig. 5).

To cover the lateral dimensions of the tumor the ion beam passes two fast scanner magnets that deflect the ions both in horizontal and vertical direction after being accelerated to the requested energy in a synchrotron and slowly extracted.

The rasterscan control system determines the excitation of the scanning magnets to deposit the requested dose profile, measuring the number of ions at a specific irradiation point by means of ionization chambers and the position and beam width at each scanning point by means of fast multiwire proportional counters in front

of the patient. When a required dose limit of an isoenergy-slice has been reached the beam extraction is interrupted very quickly (< 0.3 ms).

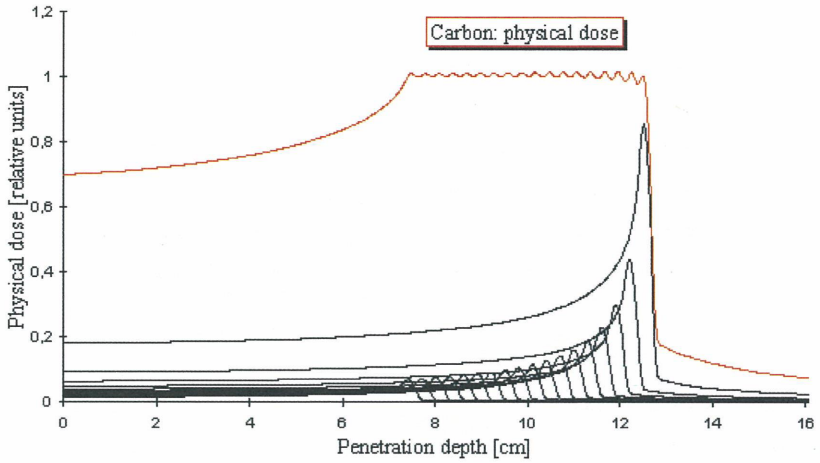


Fig. 5: Depth dose profile for overlapping Bragg peaks

The rasterscan treatment modality demands fast, active energy-variation to provide different penetration depths and intensity-variation to minimize the treatment time. Already within the Therapy Pilot Project at the existing GSI accelerator complex a system had been developed, that for carbon ions between 90 and 430 MeV/u allows the reliable request of 255 energy-steps for sequential synchrotron cycles. Besides this energy variation also intensity-and beam spot variations at the treatment location on a pulse to pulse basis can be requested. The principles of this system are also established at the HIT facility.

*b) Advanced positioning -and diagnostic-systems*

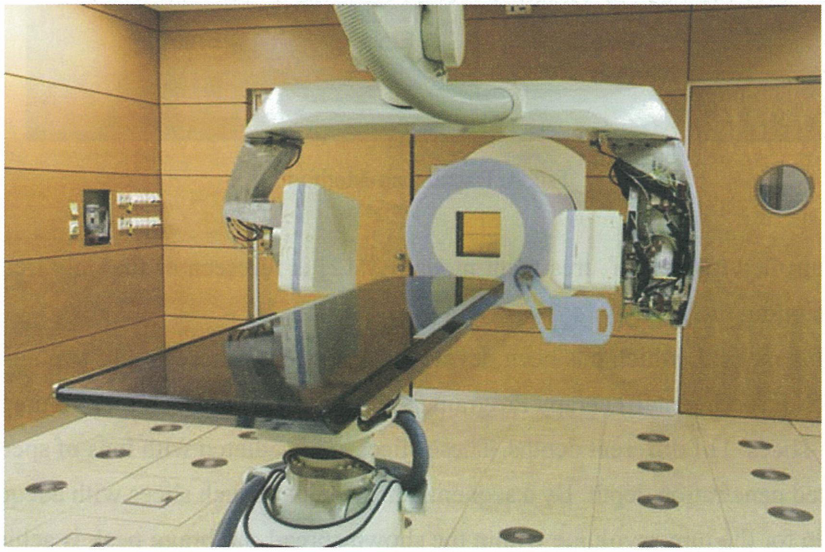

Fig. 6: Combined robotic system at the HIT treatment place

For the HIT-facility a sophisticated combined positioning and diagnostic system has been developed and commissioned by Siemens-MT on the basis of robotic technology (Fig. 6).This system allows an optimized workflow of the patient treatments and an accurate and flexible usage of patient positioning and position verifications.

c) On-line PET-diagnosis

In order to get an indication of the dose distribution during the irradiation-process an 'on-line' PET diagnostic system [13] has been implemented at GSI during the GSI Experimental Therapy program. This 'PET camera' allows to detect the position of gamma-rays of decaying positron emitters, produced either by projectile- or target-fragmentation, during the irradiation and enable the oncologists to verify the correct irradiation after each applied fraction.

*d) 'Moving' targets*

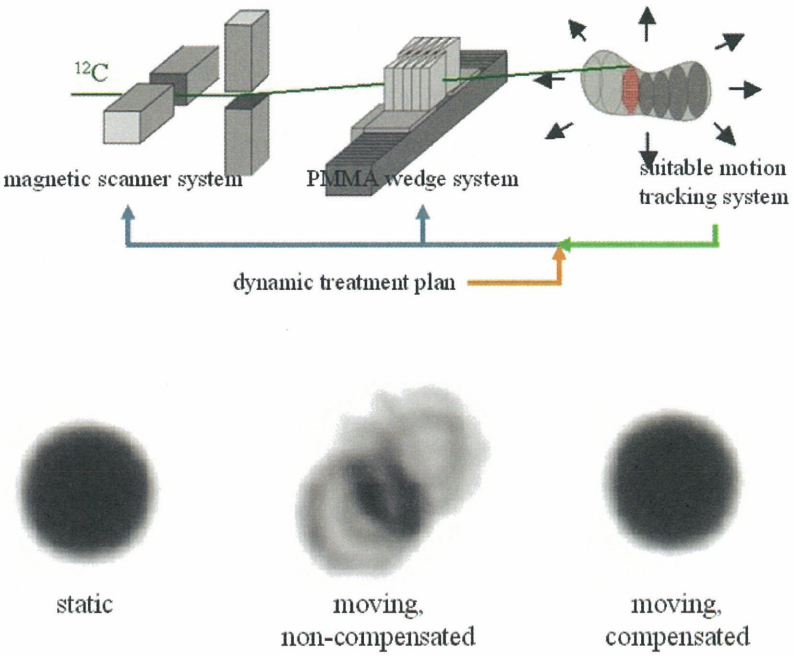


Fig. 7: '3D-online motion compensation method', schematics (upper part) and test-results for non- compensated and compensated irradiation (lower part)

As a very accurate beam delivery is mandatory for a treatment with high LET beams by means of the raster-scan method the treatment of moving organs is a challenge. At present two methods are under investigation: the (respiration) gated beam extraction and the 3D correction method. Whereas the first method is applied to patient treatments at HIMAC for many years the second method [14] '3D online motion compensation method' (see Fig. 7) has been developed at GSI and is still in a test phase.

To compensate 3D variations of a moving tumor volume the scanning magnets are used for correction in both lateral dimensions; a PMMA wedge system is proposed to realize fast particle energy variations (within certain limits) to cover variations of the penetration depth.

**References**

[1] J. Debus et al., 'Proposal for a dedicated ion beam facility for cancer therapy', 1998

[2]: H. Eickhoff et al., 'The GSI Cancer Therapy Project', PAC 1997

[3] B. Schlitt, 'Design of a Carbon Injector for a Medical Accelerator Complex', EPAC 1998

[4]: B. Schlitt at al, 'Development of a 7 MeV/u, 217 MHz Carbon Injector Linac for Therapy Facilities', Linac-Conf. 2002

[5] Y.Lu et al., 'RF Tuning of the IH Model Cavity for the Heidelberg Cancer Therapy Project', IAP internal

note: IAP-ACCC-270103
[6] B. Schlitt et al.: Commissioning of the 7 MeV/u, 217 MHz Injector Linac fort he Heavy Ion Cancer Therapy Facility at the University Clinics in Heidelberg, LINAC2006
[7] R. Cee et al.: 'Front-to End-Simulation of the Heidelberg Therapy Injector Linac' , EPAC
[8] A. Dolinskii, 'The Synchrotron of the dedicated Ion beam Facility for Cancer Therapy, proposed for the clinic in Heidelberg', EPAC 2000
[9]: U. Weinrich et al: 'The Heavy Ion Gantry of the HICAT-Facility' , EPAC 2004
[10] A. Kalimov, '3D-properties of the last gantry bending magnet', GSI-report, 1999
[11]: H.Eickhoff et al.: 'Tests of a Light-ion Gantry Section as an example of preparations for the therapy facility in Heidelberg', EPAC 2002
[12] Th. Haberer et al., Nucl. Instr. Meth. A330, 296, (1993)
[13] W. Enghardt et al.: 'Charged Hadron Tumour Therapy Monitoring by means of PET', Nucl. Instr. Meth., A525, 2004, 284-288
[14] S. Grotzinger et al: Simulations to design an online motion compensation system for scanned particle beams, Phys. Med. Biol. 2006, Jul21;51(14):3517-31

# The Status of CNAO

S. Rossi [1], E. Borloni [1] and R. Orecchia [1,2,3]

[1] CNAO Foundation, Milan, Italy; [2] University School of Milan, Italy;
[3] European Institute of Oncology of Milan, Italy

Corresponding: sandro.rossi@cnao.it

## 1. Introduction

The CNAO (Italian acronym that stands for National Centre for Oncological Hadrontherapy) is a National wide facility conceived to supply hadrontherapy treatments to patients recruited all over Italy. The CNAO is under construction in Pave, about 30 kilometres South-West of Milan. The Italian Ministry of Health, which, in the year 2001, has created the CNAO Foundation to build and run the facility, mainly finances it. The founders of CNAO are five among the largest oncological institutes in Italy: Fondazione Ospedale Maggiore (Milan), Fondazione Ospedale San Matteo (Pave), Fondazione Istituto Neurologico Besta (Milan), Fondazione Istituto Nazionale dei Tumori (Milan), Istituto Europeo di Oncologia (Milan) and the TERA Foundation (Novara, lead by U. Amaldi who was the promoter of the hadrontherapy center since 1992). Since 2003 INFN is Institutional Participant of CNAO, together with the Universities of Milan and Pave, the Polytechnic of Milan and the Town of Pave. The availability of carbon ions at CNAO will be an exclusive treatment modality for Italy and all patients with radioresistant tumours shall be addressed to the centre in Pave. To efficiently recruit patients, it will be created a network to connect the CNAO to the national health system. Pre-selection criteria will be defined on the basis of established clinical protocols and the hospitals and clinics in the network will address to the CNAO those patients that satisfy the criteria. Pathology Committees, with the participation of multidisciplinary experts, have been activated within the Scientific Committee of the CNAO Foundation to define the clinical protocols for each kind of tumour that will be treated at the centre. The contribution of experts from different disciplines (surgeons, oncologists, organ specialists in addition to radiation oncologists) will permit to best tailor the clinical modality and at the same time their participation will grow the consensus and the recruitment capability of CNAO. Three treatment rooms with four beam ports (three horizontal and one vertical) and one experimental room have been realised. At present it is foreseen to start the operation of the machine and to begin the preparation to treatments in summer 2008. The first patient treatment is expected by fall 2008 and regime operation will be fully operational within the next three years. At regime, on a double shift operation, five days per week and at least 220 days per year, the CNAO will deliver about 20 thousands sessions of hadrontherapy per year. The overall number of patients will obviously depend by the fractionation schemes adopted. The actual dimensioning of spaces and fluxes for patients, personnel and people are adequate for about 3000 patients per year. In addition is under construction a room totally devoted to physical and radiobiological researches. The site of the CNAO allows the future expansion of the facility, to add new treatment rooms and also a new research and clinical building close to the centre. The expansion in the direction of the extracted beam is potentially adequate to host two gantry rooms for carbon ions, each with the same dimensions of the present Heidelberg facility. The choice of the CNAO foundation has been to postpone the construction of the expansion in order to validate the clinical necessity of the gantry for ions and also to wait and to contribute to the technological improvements expected in this field.

## 2. Layout and buildings

The construction site is close to the internal highway of Pave and thus it is well connected by communication means. It is also located nearby the sites of three hospitals (San Matteo, Maugeri and Mondino) and the university campus and thus well placed to profit of clinical and research synergies that will be fundamental for the success of the CNAO initiatives. The buildings construction started in autumn 2005 and it is going to be completed in fall 2007.

The CNAO design is based on the following assumptions:

- the Centre will be devoted to the treatment of deep-seated tumours (up to a depth of 27cm of water equivalent) with light ion beams (proton, carbon ions and others) and to clinical and radiobiological research;
- the full-size CNAO will have 5 treatment rooms (3 rooms with fixed beams and 2 rooms with gantries) and one experimental room. For the first phase (CNAO - Phase 1) 3 treatment rooms will be equipped with 4 fixed beams, three horizontal and one vertical and one experimental room will be constructed (Figure 1).

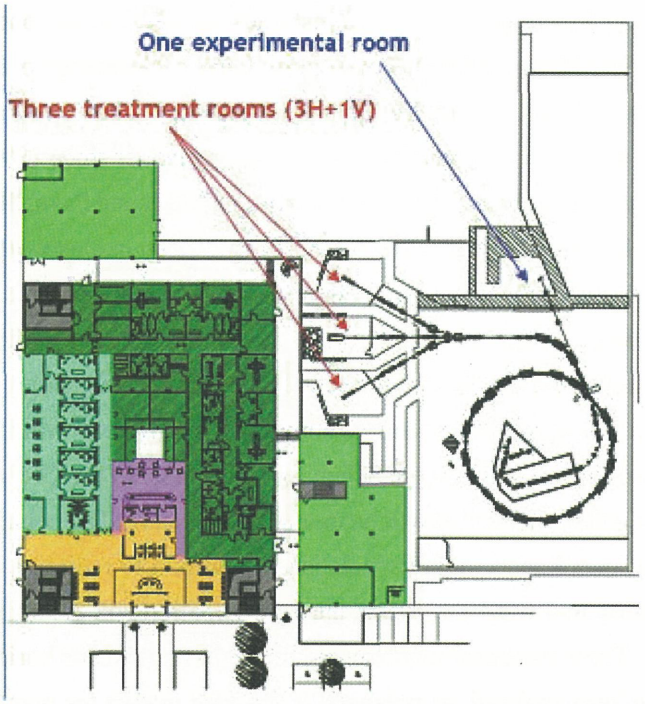


Fig. 1. Layout of the CNAO underground level - Phase 1.

The CNAO buildings develop on four levels. The underground level hosts the accelerators and the treatment rooms. The surface level hosts the ambulatories for the first visit of the patients and the medical imaging devices; two CT-PET cameras, two CTs and one NMR could be installed in the CNAO. These devices will permit the construction of the individual treatment planning for each patient. The first level is occupied by the offices of the personnel, the administration and also the spaces and the laboratories serving the experimental area. A direct connection between these areas and the experimental room is realised. The second floor occupies only half of the surface and it hosts a conference room, some smaller meeting rooms and also the direction offices. The flux of patients, personnel and public have been carefully studied in order to optimise the layout and to guarantee a quality of life that takes into account the needs of the various typology of people.

## 3. High Technology

The high technology design has been driven by the clinical requirements of the therapeutical beams, specified in Table 1.

| | |
|---|---|
| Beam particle species | p, $C^{6+}$, (possibly $He^{2+}$, $Li^{3+}$, $Be^{4+}$, $B^{5+}$, $O^{8+}$) |
| Beam particle switching time | ≤ 10 min |
| Beam range | 1.0 g/cm$^2$ to 27 g/cm$^2$ in one treatment room<br>3 g/cm$^2$ to 27 g/cm$^2$ elsewhere<br>Up to 20 g/cm$^2$ for $O^{8+}$ ions |
| Bragg peak modulation steps | 0.1 g/cm$^2$ |
| Range adjustment | 0.1 g/cm$^2$ |
| Adjustment/modulation accuracy | ≤± 0.025 g/cm$^2$ |
| Average dose rate | 2 Gy/min (for treatment volumes of 1000 cm$^3$) |
| Delivery dose precision | ≤± 2.5% |
| Beam axis height (above floor) | 150 cm (head and neck beam line)<br>120 cm (elsewhere) |
| Beam size[1] | 4 to 10 mm FWHM for each direction independently |
| Beam size step[1] | 1.0 mm |
| Beam size accuracy[1] | ≤± 0.2 mm |
| Beam position step[1] | 0.8 mm |
| Beam position accuracy[1] | ≤± 0.05 mm |
| Field size[1] | 5 mm to 34 mm (diameter for ocular treatments)<br>2×2 cm$^2$ to 20×20 cm$^2$ (for H and V fixed beams) |
| Field position accuracy[1] | ≤± 0.5 mm |
| Field dimensions step[1] | 1 mm |
| Field size accuracy[1] | ≤± 0.5 mm |

[1] At isocentre or, for fixed beam, at normal treatment distance.

Table 1. Clinical performance specifications for the CNAO.

The clinical requirements have been defined by radiotherapists and medical physicists and have been discussed in detail within the international medical community. The basic design of the CNAO accelerator and lines has been hosted at CERN in the frame of the Proton-Ion Medical Machine Study (PIMMS), from 1996 to 1999 [1].

In order to translate the clinical requirements into a machine design for high-precision scanning, several accelerator design choices have been made during the PIMMS design. Some are listed below:

- application of emittance dilution at injection;
- use of a uniform, wide momentum, medium transverse emittance beam for extraction;
- use of the momentum-amplitude selection type of extraction with the Hardt Condition;
- use of a betatron core for accelerating the beam into the resonance;
- use of an rf empty bucket to channel the beam into the resonance;
- use of the bar-like shape in phase space of the extracted beam.

This concept design has been fully engineered, first by TERA and then by CNAO/INFN (with the help of GSI for the Linac, CERN for the special magnets - septa and kickers, University of Pave and LPSC/IN2P3 Laboratory of Grenoble for the betatron core). The final design now appears as shown in Figure 2.

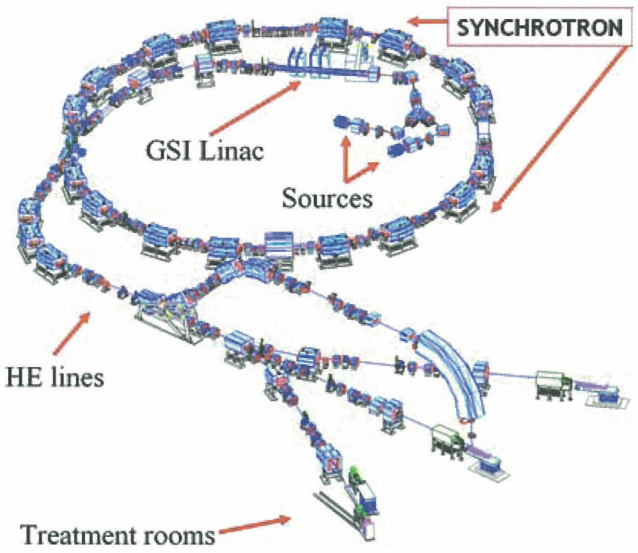


Fig. 2. Layout of the CNAO accelerators and beam transport lines.

Other important features have been added to the original PIMMS design:

• adoption of a single injector linac, designed by GSI and identical to the one used for the Heidelberg facility; the linac is suited for both protons and light ions acceleration;

• compact design of injection (inside the ring) and extraction beam transport lines (switching magnet concept);

• adoption of the multi-turn injection scheme;

• possibility to add in a second phase other treatment rooms with gantries without disturbing the routine medical activities.

A virtual tour of the beam lines and accelerator allows a brief presentation of the features of this optimised medical machine system. It has to be preliminarily underlined that the choices done for each device have taken into account the necessity to operate in a hospital based environment, the must of reaching an high operating efficiency (above 95%) and the satisfaction of basic requirements such as safety, reliability and maintainability have been the driving concepts of the CNAO design. CNAO will start activity with two identical ECR sources. The sources are already installed and preliminary measurements have been performed in May 2007. Figure 3

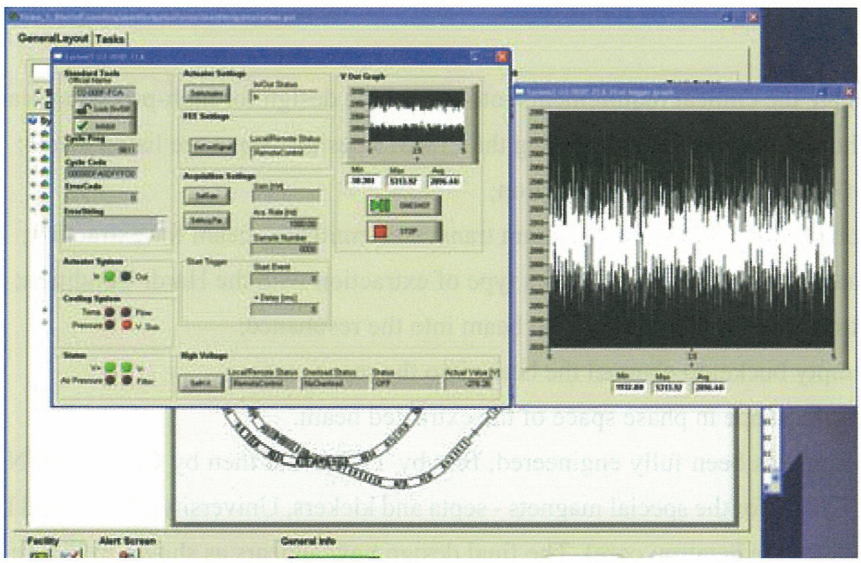

Fig. 3. First ion beam measured at the source exit with a Faraday cup.

shows the current of He3 measured with a Faraday cup.

The layout of the LEBT (Low Energy Beam Transfer) lines is designed in order to switch from one source to the other on a pulse to pulse basis. A spectrometer (90 degree bending) is placed downstream each source and a Faraday cup allows the routine setting up of the source and the related portion of LEBT before the beam utilization. This arrangement is very compact and allows the insertion of the source, LEBT and linac inside the synchrotron ring. The linac is composed of an RFQ and an IH-structure coupled together. It is identical to the one built for the Heidelberg project and it is being built under the technical supervision of GSI. The RFQ accelerates particles from 8 keV/u to 400 keV/u; the construction has been completed and it has been tested in July 2006 with the final power amplifier. The IH has been completed, vacuum tested and RF characterised at the beginning of 2007 at GSI. It accelerates the beams from 400 keV/u to 7 MeV/u.

The Medium Energy Beam Transfer line (MEBT) transports the beam from the stripping foil to the injection point in the synchrotron. In MEBT a final selection of the ion specie is made to avoid beam contamination with particles that before stripping have the same A/Q as the desired one. The CNAO synchrotron is made by two symmetric achromatic arcs joined by two dispersion free straight sections. The dispersion free sections host the injection/extraction region, the resonance driving sextupole and the RF cavity. The total length of the ring is approximately 78 m and accelerates particles till a maximum energy of 400 MeV/u, with a repetition rate of 0.4 Hz. The total bending of 360° has been divided in 16 identical dipoles powered in series. The focusing action is provided by 24 quadrupoles grouped in three families and the chromaticities are controlled by four sextupoles grouped in two families. A fifth sextupole is used for the third integer resonance excitation. Orbit correction is guaranteed by 20 steering magnets. The vacuum system, the beam diagnostics, the RF cavity, the special magnets for injection and extraction and the fast magnets for bumps and abort of the beam, the ring quadrupoles, sextupoles and correctors and the ancillary equipments (supports, cooling connections, alignment devices and so on) are already in Pave and partially installed. The four HEBT (High Energy Beam Tranfer) lines transport the extracted beam to the three treatment rooms. The HEBT dipole magnets are identical to the synchrotron magnets and this increases flexibility and reliability, reducing costs. The compact design is based on a switching magnet that is selecting the horizontal line to be used for treatment. An intrinsic safety aspect has been included in the HEBT design: interlaced with the first three dipoles of the extraction lines, a beam chopper has been installed. The chopper is composed by four fast dipoles powered in series with a +1, -1, -1, +1 scheme. This creates an orbit bump that brings the beam out of a dump at the start of the irradiation. Because of symmetry the beam stays on target also during the up and down ramps. The chopper intervention time is shorter than 260 microseconds to keep the dose delivered during intervention below 2.5% of the voxel dose. All the lines are equipped at the end with a pair of scanning magnets which allow scanning over an area of 200 mm x 200 mm.

Before the end of HEBT monitoring system is inserted that makes the link between the machine operation and the patient treatment. This device measures twice the intensity, the profile and the position of the pencil beam during the active irradiation of the target. The monitoring is the master of the treatment: it steers the scanning magnets and determine the completion of a treatment irradiation. The final version of the monitoring has been successfully tested both with protons and carbon ions. Other key features necessary to take advantage of the high spatial precision of hadrontherapy are an accurate individuation of the target and a precise and reproducible patient set-up. Treatments will be performed with patients immobilized on a couch or on a chair that will be docked to a state-of the art 6 degrees of freedom mobilization device. Set-up verification will be performed with orthogonal KV images of diagnostic quality. Additionally optoelectronic systems with markers detection and surface detection capability will be used. CNAO aims to have a high patients through-put. Design

has specifically addressed this issue and dedicated positioning rooms have been built (*Computed Assisted Positioning in Hadrontherapy*, CAPH rooms). Patients will be positioned on the couch (or on the chair) inside the CAPH rooms and then carried in the treatment room on a trolley predisposed for docking with the mobilization device, thus realizing a time optimization through a pipeline approach.

**4. Clinical Activity**

Protontherapy is considered the elective treatment for skull-base chordoma and chondrosarcoma, for uveal and choroidal melanoma and for paraspinal tumors. It has been used with promising results in a wide range of other diseases including bone and soft tissues sarcomas, HCC, NSCLC, CNS malignancies, head and neck tumors, pediatric tumors, prostatic adenocarcinoma and rectal cancer recurrence [3,4,8]. Experiences with carbon ions are still more preliminary, but results have been extremely encouraging in chordoma and chondrosarcoma, salivary gland tumors, sarcomas, HCC, NSCLC, advanced head and neck cancers, mucosal melanoma, recurrent rectal carcinoma, advanced uterine ceric carcinoma, bladder cancer, and prostate cancer [2,6,7,9]. CNAO will be able to use both protons and carbon ions [5]. At regime it will devote 80% of the time to ions and the remaining 20% to protons. CNAO activity is designed to reach regime in three years with two eight hours shifts from Monday to Friday. A workflow analysis has been performed and has shown that the facility will be able to deliver about 20 thousands treatment sessions per year. Hadrontherapy, and especially CIRT (Carbon Ion Radio Therapy), has shown a costant trend toward hypofractionation. At HIMAC (Japan) the mean number of fractions per patient is at present 13 and is still decreasing. At CNAO treatments will be carried out not only as exclusive therapy, but also as a boost after photons RT. It is estimated that about 3.400 patients per year will be treated at CNAO at regime. This number of patients is clearly inferior to the number of potential indications. There is therefore the need to define selection criteria to deliver hadrontherapy to patients that are more likely to benefit from it. To achieve this goal CNAO foundation have individuated seven groups of diseases that are considered at higher priority: lung tumours, liver tumours, sarcomas, head and neck tumours, eye tumours, central nervous system lesions and paediatric tumours. A disease specific working group has been created for each of these diseases under the leadership of a physician with recognized expertise in the field. Each working group is composed of radiation oncologists, medical oncologists, surgeons, diagnostic radiologists and organ specialists. The working groups have analyzed the literature and have produced documents with recomandations on tentative indications for trials to be conducted at CNAO. Special care has been taken to consider also alternative available treatments in the effort to propose hadrontherapy to those patients for whom it is reasonable to expect a significant advantage. A central board has been established to review documents written by the working groups and will eventually produce protocols for the trials that will start next year. Recently, two more working groups are being set-up on gynecological malignacies and on digestive cancers (pancreatic and rectal tumors). Another key issue for CNAO is to ensure a correct patient referral. CNAO will be the only carbon ion facility in Italy and therefore its basin will be the whole nation (besides foreign patients).

The clinical protocols will be submitted to the Ethical Committee and then presented to the Health Ministry in order to obtain the clinical authorizations to treat patients.

To allow a rational use of the facility it is mandatory to establish a close network with other oncological centers. For the near future CNAO will make the treatment protocols widely available to health providers, and will create specific tools for a quick patient referral (also employing approaches). A close cooperation with oncological centers and primary care provider is needed also to coordinate staging, follow-up (to be done mostly at the referring center) and treatment to be done at CNAO. An even closer cooperation will be necessary when

hadrontherapy is used within a multimodality treatment approach. An international cooperation has already started with the three European carbon ions centers foreseen (HIT, MedAustron, ETOILE) within the framework of the European project ULICE. This project aims at performing multicentric trials and at establishing a shared database of all treated patients.

**5. Acknowledgements**

The authors wish to thank the colleagues of CNAO Foundation and the collaborating institutes: thanks to their efforts the CNAO is becoming reality.

**6. References**

1. Badano L., Rossi S. et al.: Proton-Ion Medical Machine Study (PIMMS), Part I and II, CERN/PS 1999-010 DI and CERN/PS 2000-007 DR, Geneva.

2. Auberger T., Debus J., Gerard JP., Orecchia R., Potter R., Remillieux J., Ringborg U., Wambersie A.: Hadrontherapy with carbon12: radiotherapy of the near future. Radiother Oncol 2004; 73(Suppl 2):i-ii.

3. Jereczek-Fossa B.A., Krengli M, Orecchia R.: Particle beam radiotherapy for head and neck tumors: radiobiological basis and clinical experience. Head Neck 2006; 28(8):750-60.

4. Krengli M., Liebsch N.J., Hug E.B., Orecchia R.: Review of current protocols for protontherapy in USA. Tumori 1998; 84(2):209-16.

5. Krengli M., Orecchia R.: Medical aspects of the National Centre For Oncological Hadrontherapy (CNAO-Centro Nazionale Adroterapia Oncologica) in Italy.Radiother Oncol 2004; 73 (Suppl 2):S21-3.

6. Orecchia R., Fossati P.: Role of carbon ion therapy for stage I NSCLC using a regimen of four fractions over week. J Thorac Oncol 2007; 2(10): 887-8.

7. Orecchia R., Krengli M., Jereczek-Fossa B.A., Franzetti S., Gerard J.P.: Clinical and research validity of hadrontherapy with ion beams. Crit Rev Oncol Hematol 2004; 51(2): 81-90.

8. Orecchia R., Krengli M.: Number of potential patients to be treated with proton therapy in Italy. Tumori 1998; 84(2): 205-8.

9. Orecchia R., Zurlo A., Loasses A., Krengli M., Tosi G., Zurrida S., Zucali P., Veronesi U.: Particle beam therapy (hadrontherapy): basis for interest and clinical experience. Eur J Cancer 1998; 34(4): 459-68.

# New Carbon Therapy Facility at Gunma University

Satoru YAMADA*, Tatsuya OHNO, Ken YUSA and Mutsumi TASHIRO

Gunma University Heavy Ion Medical Center,
3-39-22 Showa, Maebashi, Gunma 371-8511, JAPAN.

*Corresponding; satoru@showa.gunma-u.ac.jp

## 1. Introduction

In Japan, more than 300,000 patients are killed by cancer every year, and the number is increasing rapidly year by year. It is a top priority of the Japanese Government to protect the public against the spread of cancer. Clinical trials were initiated with high energy carbon beams obtained from HIMAC1) at National Institute of Radiological Sciences, NIRS, in 1994. Accumulating clinical results of more than 3,000 patients at HIMAC, it has been made clear that carbon therapy is very much effective in curing human cancers[2].

We have six working particle therapy facilities in Japan. Only one facility, however, can provide 400 MeV/u carbon ions, whereas 4 facilities provide proton beam only and the last facility at Hyogo can accelerate both protons and 320 MeV/u carbons.

In order to expand carbon therapy throughout the country, it is strongly desired to reduce construction and operation costs of an accelerator system. NIRS has carried out design and R&D studies to respond these demands. Gunma University has been collaborating on these studies since 2004. The new therapy facility at Gunma University will be the first full scale model of the design and R&D studies.

## 2. New Facility at Gunma-University Heavy-Ion Medical Center

Based on clinical statistics at HIMAC, a new carbon therapy facility is required to accelerate carbon ions up to 400 MeV/u. The maximum energy ensures 25 cm residual range in water and permit to treat prostate cancers through patient' s pelvis. Another important requirement of the new facility is to have two orthogonal beam lines directed toward the same isocenter. This beam line configuration is required in order to realize sequential beam irradiation from different directions with single patient position. First beam course and energy switching is also required to perform the sequential irradiation. Major specifications of the facility are summarized in table 1.

An accelerator of the facility consists of an all permanent magnet ECR type ion source, an RFQ linac, an IH linac with alternating phase focusing structure and a synchrotron ring followed by a high energy beam transport system. An averaged diameter of the synchrotron is about 20 m and will accelerate fully stripped carbon ions to an energy range from 140 to 400 MeV per nucleon. The facility will have three treatment rooms equipped with fixed beam ports and another irradiation room will be prepared for future developments. A wobbling technique will be adopted to obtain a uniform irradiation field of 15 cm square at maximum. The detailed design of the facility is based on design and R&D studies performed at National Institute of Radiological Sciences, NIRS. A layout of the new facility is given in Fig. 1.

| | |
|---|---|
| Ions | Carbon ions only |
| Range | 25 cm max. in water (400 MeV/u) |
| Field size | 15 cm square |
| Dose Rate | 5 GyE/min. ($1.2x10^9$ pps) |
| Treatment Rooms | 3 (H, V, H&V), No rotational gantries |
| Fourth Room | Prepared for future developments |
| Irradiation Technique | Single & Spiral Wobbling, Respiration gated |

Table 1: Major Specification of Gunma University Carbon Therapy Facility

### 3. Design and R&D Studies at NIRS

An ion source is an ECR type and developed at NIRS[5]. Both ring and sextupole magnets are made of NdFeB type permanent magnet. Magnetic filed is as high as 1.1 T at the surface of the magnets. Microwave frequency is made variable and chosen at around 10 GHz. An ion intensity of more than 300 e?A is obtained stably for $C^{4+}$ ions with an extraction voltage and microwave power of 30 kV and 300 W, respectively.

An injector linac consists of a conventional four vane type RFQ linac followed by an interdigital H type linac with an alternating phase focusing structure, APF-IH[6), 7)]. An operation frequency of injector linac is chosen at 200 MHz, and an inside diameter of the linac tanks are about 35 cm. The maximum surface field is chosen to be 24 MV/m and 1.6 times larger than Kilpatrick' s value. This rather low value is adopted to keep electric breaking down risks to be extremely low level. During designing process of the APF-IH linac, we constructed a low power model cavity in order to check reliability of a 3-D computer code for calculation of rf characteristics of a cavity. A computer code Microwave Studio excellently reproduces experimental results.

A test stand which was designed to accelerate $C^{4+}$ ions from an ECR source up to an energy of 4 MeV/u with RFQ and APF-IH linacs was developed at NIRS and beam tests were successfully performed. A photograph of the test stand is given in Fig. 2. Measured values of a beam energy, an energy spread, beam emittances very well reproduced calculated values.

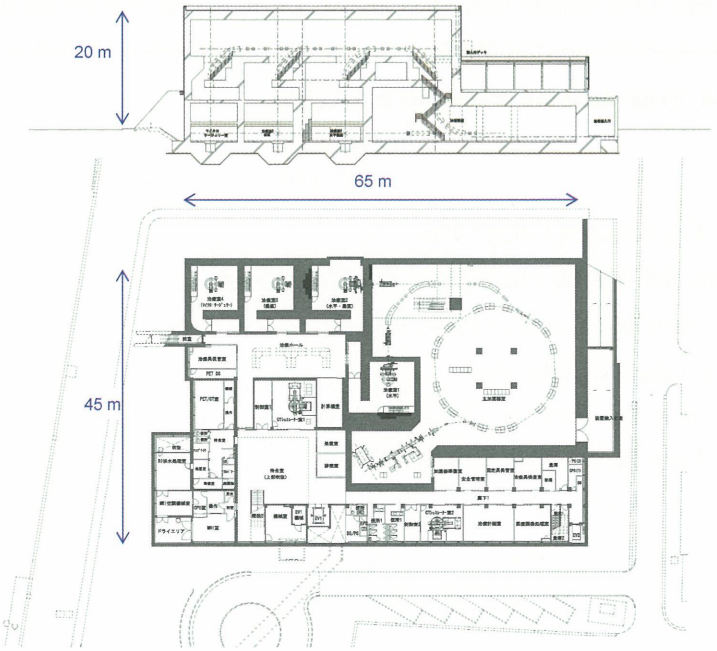


Fig. 1: A layout of the new facility.

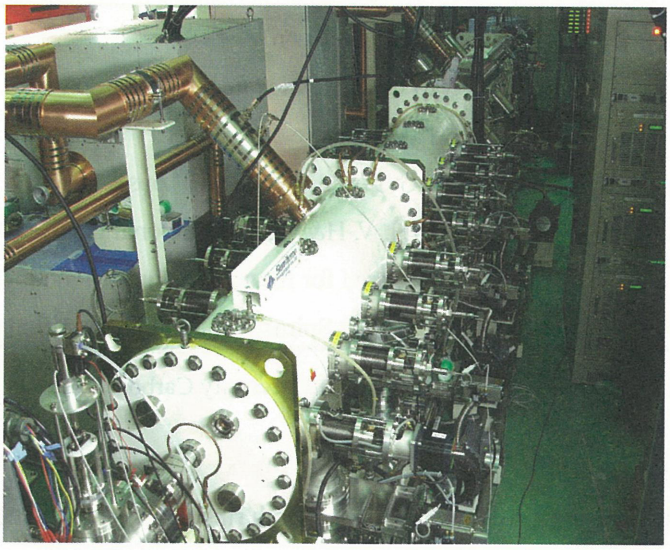

Fig. 2: A photograph of a test stand for an IH-APF linac.

An rf cavity loaded with Co based amorphous cores was developed for a synchrotron[8]. A shunt impedance of the cavity exceeded 300 Ω in a wide frequency range of 0.4 to 7 MHz without any tuning system. A new technique was applied in a cooling system of the amorphous cores: a cooling plate was adhered to only one side of the core to avoid making electric short paths across the core. The new cooling technique works very well without reducing shunt impedance of the cavity.

In order to increase beam utilization efficiency, a spiral wobbling technique was developed[9]. It requires about 1 minuet to paint whole irradiation field uniformly with rather small beam spots comparing with conventional single wobbling technique. The beam efficiency of around 45% is obtained with the spiral wobbling scheme, whereas single wobbling scheme gives only 17%. The calculated results have been reproduced very well by beam tests with high energy carbon beams from HIMAC.

## 4. Time Schedule of the Project

Based on the design and R&D studies described above, a new carbon therapy facility has been under construction at Gunma-University Heavy-Ion Medical Center. The construction started in February 2007 and will be completed in FY2008. Beam tests are scheduled in FY2009.

## 5. References


1) Y. Hirao, et al., Nucl. Phys. A538 (1992) 541c.
2) H. Tsujii, et al., Radiol. Sci. Vol.50, No.7 (2007) 5. (in Japanese)
3) K. Noda, et al., Nucl. Instr. Meth. A562 (2006) 1038.
4) K. Noda, et al., J. Rad. Res. 48 (2007) A43.
5) M. Muramatsu, et al., Rev. Sci. Instr. 76 (2005) 113304.
6) Y. Iwata, et al., Nucl. Instr. Meth. A566 (2006) 256.
7) Y. Iwata, et al., Nucl. Instr. Meth. A572 (2007) 1007.
8) M. Kanazawa, et al., Nucl. Instr. Meth. A566 (2006) 195.
9) M. Komori, et al., Jpn. J. Appl. Phys. 43 (2004) 6463.

# Application of the Local Effect Model in Treatment Planning for Carbon Ion Therapy

Michael Scholz*, PhD, Thilo Elsässer, PhD, Michael Krämer, PhD

Gesellschaft fur Schwerionenforschung Dept. of Biophysics Planckstrasse
1 D-64291 Darmstadt Germany
*Corresponding: m.scholz@gsi.de

## 1 Introduction

The relative biological effectiveness (RBE) of charged particle beams depends on several factors such as particle type and energy, dose level and the cell or tissue type under consideration[1,2,3,4]. These systematic dependencies of the RBE have to be considered when using charged particle beams for therapy. As a consequence, RBE values are expected to be patient specific and can not be adequately represented by a single number for conversion of physical/absorbed dose to the biologically isoeffective dose.

For treatment planning, RBE values have to be estimated as precisely as possible. The facilities treating cancer patients with carbon ion beams are using different strategies. At HIMAC/Chiba, an experimentally oriented approach was developed. The shape of the isoeffective depth-dose profile is based on the precise measurements of RBE in-vitro. The clinical RBE value is then determined by a link to the clinical experience with neutron beams, which show similar radiobiological characteristics as carbon beams at the end of their penetration depth[5,6]. At GSI/Darmstadt, a modeling approach is used, which will be described in more detail below[7,8,9,10].

## 2 Modelling the increased effectiveness of charged particles

### 2.1 The Local Effect Model (LEM)

The biological optimization within treatment planning for the pilot project at GSI is based on the Local Effect Model (LEM). The principal assumption of the LEM is that the local biological effect, i.e. the biological damage in a small subvolume of the cell nucleus is solely determined by the expectation value of the energy deposition in that subvolume and is independent on the particular radiation type leading to that energy deposition. This is similar to the microdosimetric approach, but is applied to much smaller volumes compared to the µm-dimensions of microdosimetry. For a given biological object, all the differences in the biological action of charged particle beams should then be attributed to the different spatial energy deposition pattern of charged particles compared to photon irradiation, i.e. on track structure. Furthermore, for a given radiation type, any difference in RBE between different cell / tissue types should correspond to a difference also in the photon dose response curve.

The energy deposition pattern of charged particles is determined essentially by the secondary electrons (δ-electrons) liberated by the primary particle when penetrating matter. The average energy deposition as a function of the distance r from the trajectory, the radial dose profile, follows a $1/r^2$-law. According to the kinematics of the secondary electron emission, the maximum transversal range of the electrons is restricted and the corresponding track radius can be described by a power law of the form[11]:

$$R_{Max} = c \cdot E^{1.7} \qquad [1]$$

where c is a constant and E is the specific energy of the projectile. Details of the particular representation of the track structure and the radial dose profile as used in the local effect model are reported by Scholz et al.[10].

For the calculation of the biological effect of a given local dose deposition within the cell nucleus, the density of lethal events ν(d) can be defined as follows:

$$\nu(d) = \frac{\overline{N_{l,X}(d)}}{V_{Nucleus}} = \frac{-\log S_X(d)}{V_{Nucleus}} \qquad [2]$$

where $V_{nucleus}$ is the volume of the cell nucleus, d is the local dose, $N_{l,X}(d)$ represents the average number of lethal events produced by photon radiation in the nucleus by a dose d and $S_X(d)$ represents the photon dose response curve.

Given the complete local dose distribution according to the impact parameters of a given set of impinging ions, the average number of lethal events induced per cell by heavy ion irradiation can then be obtained by integration of the local event density $\nu(d(x,y,z))$

$$\overline{N_{l,Ion}} = \int \nu(d(x,y,z))\, dV_{Nucleus} = \int \frac{-\log S_X(d(x,y,z))}{V_{Nucleus}}\, dV_{Nucleus} \qquad [3]$$

This formula clearly demonstrates the theoretical link between the biological effect of photon radiation and ion radiation. The integrand is completely determined by the low-LET response of the object under investigation; the particle effect is 'hidden' in the inhomogenous local dose distribution $d(x,y,z)$. For a given pattern of particle traversals, the survival probability for a cell is then given by:

$$S_{Ion} = e^{-\overline{N_{l,Ion}}} \qquad [4]$$

Eq. [3] is the most general formulation of the local effect model; it does not rely on any particular representation of the photon dose response curve. It can be applied even if only numerical values of $S_X(D)$ are available. However, for practical reasons, we take the linear-quadratic approach for the description of the low-LET dose response curve. The average number of lethal events can then be identified with:

$$\overline{N_{l;X}} = \log S_X(D) = \alpha_X D + \beta_X D^2 \qquad [5]$$

A modified version of the linear-quadratic approach is used, since for many biological objects a transition from the shouldered to an exponential shape of the dose response curve is observed at high doses. This transition is described by a parameter Dt, representing the transition dose to the exponential shape with slope , $S_{max} = \alpha + 2\beta D_t$ , so that the dose response is finally given by:

$$S_X(D) = \begin{cases} e^{-(\alpha_X D + \beta_X D^2)} & : D \le D_t \\ e^{-(\alpha_X D_t + \beta_X D_t^2 + s_{max}(D - D_t))} & : D > D_t \end{cases} \qquad [6]$$

In general, the dose $D_t$ cannot be directly derived from experimental data, since survival curves can be measured only down to $10^{-3}$ for most mammalian cell lines; $D_t$ represents thus a semi-free parameter of the model. The value of $D_t$ can be estimated, however, based on the finding, that differences in sensitivity between different

cell lines are expressed in general in a variation of the initial slope (α-term), whereas the β-term and thus the final slope $S_{max}$ are very similar. In general, values for $S_{max}$ in the order of 2 $Gy^{-1}$ and the corresponding value for $D_t$ - resulting from the particular α- and β-values - allow consistent descriptions of the experimental data.

In order to perform the numerical integration given in eq.[3] for a random distribution of particle traversals, a small grid has to be used in order to cope with the rapid, position-dependent variation according to the $1/r^2$-distribution of the radial dose profile. This leads to unacceptable computing times not compatible with the needs of treatment planning. Therefore, approximation procedures have been developed. The approximations are related to the estimation of the β-parameter of the dose response curve; the α-parameter can be always calculated exactly according to eq. [3], since the initial slope corresponds to the effect at very low doses and thus fluences. In this case, the dose response is defined by single particle effects, and no overlap of contributions from different particles has to be taken into account. A more detailed discussion would be beyond the scope of this report; details of the approximations are reported by Scholz et al.[10] and Krämer and Scholz[12].

### 2.2 Comparison with experimental data

Fig. 1 compares RBE(LET) relationships for 2 different cell lines calculated according to the original LEM as reported by Scholz et al.[10] and the optimized LEM as described by Elsässer and Scholz[13] with experimental data for carbon ion irradiation.

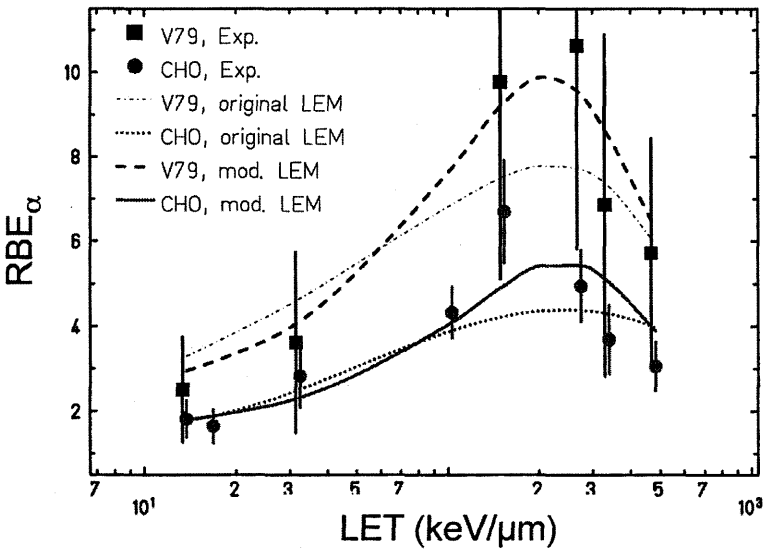


Fig. 1:The RBE is investigated for two different mammalian cell lines (V79 and CHO cells) after carbon-ion irradiation. The modified local effect model (thick lines) agrees better with the experimental data[3] than the classical local effect model (thin lines). The corresponding data for the X-ray survival curve of CHO cells are $\alpha$=0.228 $Gy^{-1}$, $\beta$=0.02 $Gy^{-2}$, $D_t$=40 Gy (old) and $D_t$ =9.5 Gy (modified). Input parameters for V79 cells are $\alpha$=0.093 $Gy^{-1}$, $\beta$=0.026 $Gy^{-2}$, $D_t$=30 Gy (old) and $D_t$=7.5 Gy (modified), respectively.

A good agreement between model prediction and experimental data is observed in particular for the modified LEM including cluster effects, and the higher RBE for V79 cells as compared to CHO cells is well reproduced. The RBE apparently correlates with the repair capacity of the cell, as reflected by the increasing width of the shoulder of the photon dose response curves.

### 2.3 Transfer to complex tissues in-vivo.

Fig. 1 demonstrates, that different cell types are characterized by different RBE values, and the same is expected to hold true also in the in-vivo and clinical situation. Therefore, normal tissues and tumor tissues might show different RBE values, but also within the groups of normal and tumor tissues a significant variation of RBE can be expected. Therefore, the question arises how to transfer the RBE values determined in-vitro to the in-vivo or clinical situation.

The local effect model as described above is based on the knowledge of the photon dose response curve. However, representative photon survival curves are not available for all tissues under consideration, and even if available, the correlation between cell survival and the clinically relevant tissue response remains unclear, at least on a quantitative level. Therefore, we have to ask which characteristic of the photon dose response curve is the most relevant for the determination of RBE.

According to eqs. [3] and [5], the nonlinearity of the photon dose response curve is a prerequisite for the prediction of RBE values greater than one. If the photon dose response curve is purely exponential, RBE is expected to be equal to one. In contrast, in the case of a shouldered x-ray dose response curve, a higher effectiveness is expected. According to that systematic, when comparing different biological systems with different photon dose response curves, for a given particle type and energy the RBE should increase with the slope ratio

$$r = s_{\max}/\alpha = 1 + 2\frac{\beta}{\alpha}D_t \qquad [7]$$

since the highest effectiveness of the very high local doses in the center of the charged particle track is determined by the final slope of the photon dose response curve.

Fig. 2 demonstrates this dependence of RBE on the slope ratio of the photon dose response curve by means of calculated RBE values as a function of dose for irradiation in an extended Bragg peak. In Fig. 2a, constant values for $\alpha/\beta$ and Dt and thus also for r are assumed, but the absolute values of $\alpha$ and $\beta$ are varied by a factor of 50. Despite this large variation, the expected RBE values only show minor differences. In sharp contrast, for a variation of the slope ratio r, expressed here through the corresponding variation of the $\alpha/\beta$-ratio and simultaneous adjustment of Dt to achieve the same final slope of $2Gy^{-1}$, an extreme variation of RBE is expected (Fig. 2b). In line with the qualitative description above, the RBE is highest in the case of a small $\alpha/\beta$-ratio.

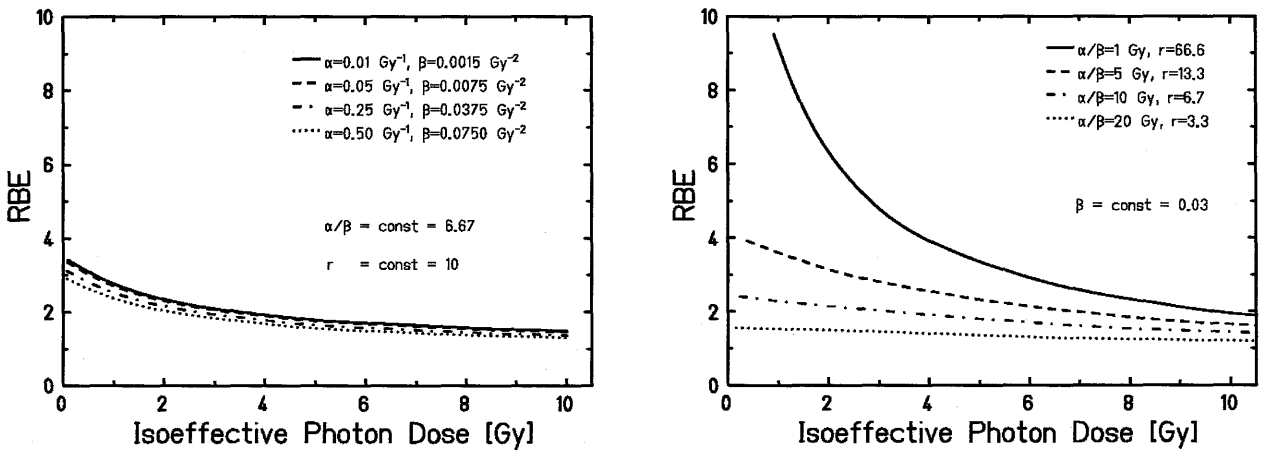


Fig. 2:Comparison of predicted RBE values in the middle of a 4cm extended Bragg peak. (a): Constant $\alpha/\beta$-ratio, variation of absolute values of $\alpha$ and $\beta$. (b): Constant $\beta$, variation of $\alpha$ and thus $\alpha/\beta$.

These findings are in agreement with other reports, suggesting that radioresistant cell lines (characterized by a small α/β ratio) in general show a more significant enhanced RBE than sensitive cell lines[14,15].

The systematic mentioned above opens the application of the LEM also to complex normal tissue effects. This is done by drawing an analogous conclusion: if two biological endpoints are characterized by the same α /β-ratio of the photon dose response curve, they should also show the same RBE for a given type of radiation. Since α/β-ratios are known for many normal tissues, these can be used to estimate the RBE. I.e., the model calculation is performed using a photon survival curve, having the same α/β-ratio as the tissue endpoint under consideration, and then assuming that both the survival curve and the tissue endpoint will show the same RBE at a given dose level. Therefore, if no detailed information about the absolute values of α and β for the tissue under consideration are available, RBE values for treatment planning are based on the α/β-ratio for the specific tissue and endpoint under consideration.

## 3 Application in treatment planning

It has been shown, that the LEM is able to predict dose response curves for endpoints in vitro, in-vivo and also for clinical data with good precision[16]. It has been implemented in the biological optimization module of the treatment planning procedure TRiP[12,17,18] for the carbon ion therapy project at GSI. Due to the tissue dependence of RBE, the biological characteristic of each tissue relevant for the therapeutic situation has to be specified. According to the principles of the model as described above, the biological characteristic with respect to radiation quality is essentially determined by the α/β-ratio for conventional photon radiation of the tissue under consideration and the value of $D_t$.

Frequently, values of α/β =10Gy are quoted for early responding normal and tumor tissues and α/β=3 Gy for late responding normal tissues. However, it is not appropriate to use these values for the purposes discussed here. In particular the value of α/β=10Gy does not reflect the situation for the tumor entities, which are expected to mostly benefit from the high-LET effect, and thus more realistic values should be used as described below.

In any case the photon parameters specific for the tissue and endpoint under consideration should be used for the estimation of RBE. Consequently, different parameters have must be applied in general for different tissues, and similarly different parameters have to be used when calculating the RBE for early and late effects in a given normal tissue, respectively. Ideally, α/β derived from clinical data would be appropriate. If these are not available, the corresponding data from representative in-vivo studies should be used, and if those are not available, *in-vitro* experiments might help to deduce the photon sensitivity parameters.

Up to now, mainly chordomas, chondrosarcomas and adenoid cystic carcinomas have been treated with carbon ions within the GSI pilot project. Since the α/β-values cannot be directly derived from clinical data for these rare tumors, the corresponding values have to be estimated based on other data. A very useful set of clinical data in that respect is the investigation of the growth characteristic of tumor metastasis in the lung as reported by Battermann et al.[19], showing a clear correlation of the photon sensitivity of the metastasis with the tumor volume doubling time. When this set of data is reanalyzed using the linear-quadratic model, it can be demonstrated that the corresponding α/β-values decrease as a function of the tumor volume doubling time. Obviously, not only the sensitivity in general, but also the α/β-ratio depends on the tumor volume doubling time. According to this analysis, the α/β-ratio of slow growing tumors is consistent with values as low as 2 Gy, and is thus con-

siderably lower than the value assumed in general for tumor tissues and early responding tissues (α/β=10 Gy) For the treatments of chordomas and chondrosarcomas, the α/β-value for the tumor tissue is thus expected to be at least very similar to that of the surrounding normal tissue. For the brain tissue, an α/β-value of 2 Gy has been chosen in accordance with the knowledge from in-vivo irradiations e.g. of the spinal cord. Consequently, although the tissues are completely different in general, a similar characteristic has been assumed with respect to their response to photon radiation in terms of their α/β-ratio.

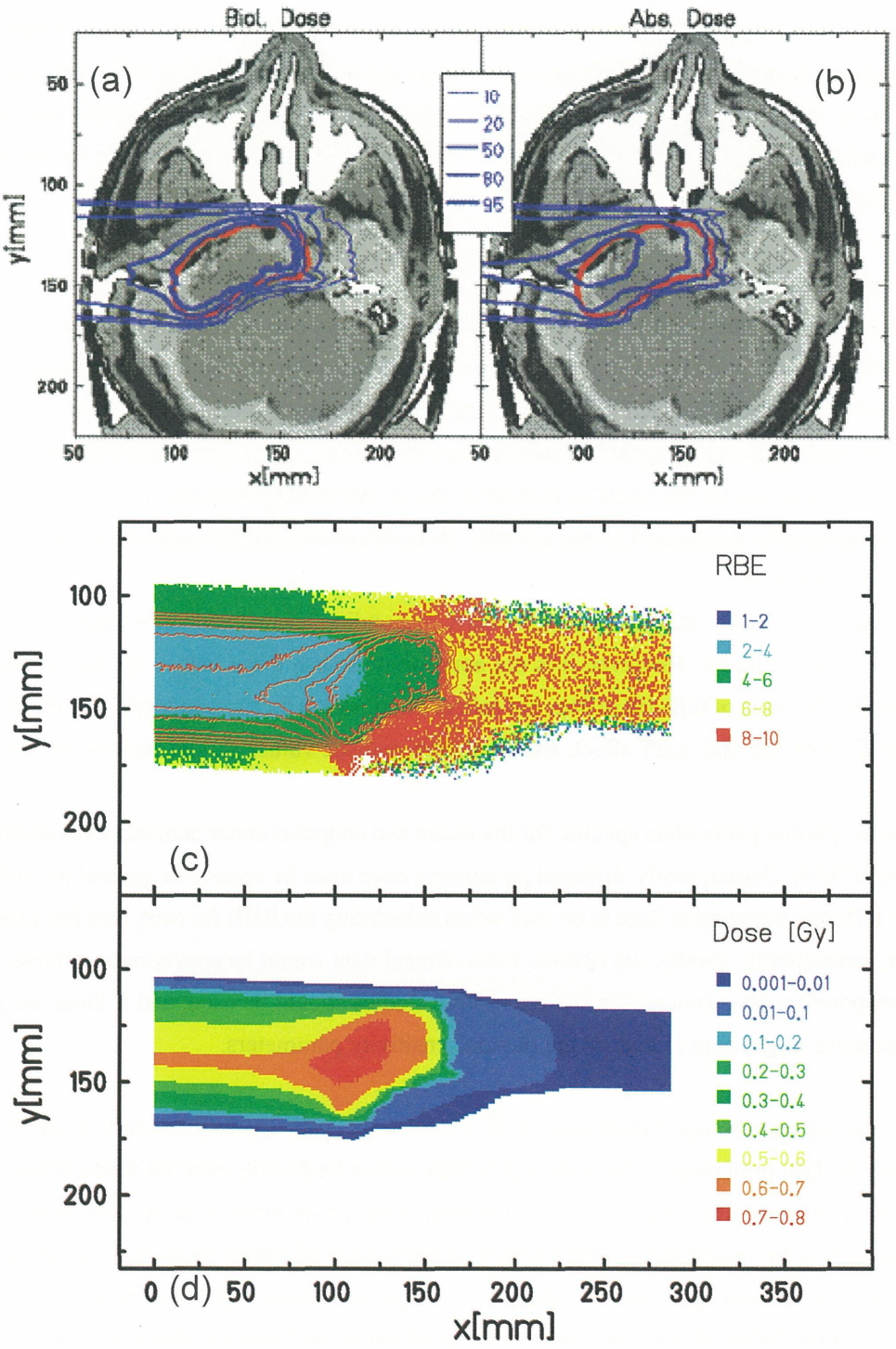


Fig. 3:Comparison of biological effective dose distribution (a) and absorbed dose distribution (b) for a typical treatment plan. The corresponding RBE-distribution in comparison to the absorbed dose distribution is shown in (c) and (d).

Fig. 3 shows an example for the distribution of RBE values for a typical treatment plan of a chordoma patient; the position dependent variation of RBE becomes clearly visible. In the TRiP treatment planning procedure also the dose dependence of RBE is fully reflected, and RBE values are always calculated exactly for the dose, which is actually applied at a given point in the treatment field. As a consequence, this dose dependence of RBE also contributes to the spatial variation of RBE: Since RBE increases with decreasing dose, comparably high RBE values are also expected at the boarder of the treatment field and beyond the distal end of the extended Bragg peak. Explicitly considering also the dose dependence of RBE represents an important difference to other approaches as they are applied e.g. at the HIMAC, where RBE values are usually considered at a fixed effect level, i.e. 10% survival.

The influence of the tissue composition is demonstrated in Fig. 4. The upper full line represents the isoeffective depth dose distribution for a homogenous biological characteristic with $\alpha/\beta$=2 Gy throughout the whole irradiated volume. The arrow on the left side depicts the isoeffective dose for the induction of acute effects in the skin at the entrance port, based an $\alpha/\beta$= 5.9 Gy; this value was derived from a reanalysis of the data reported by Hopewell[20]. According to the general systematic discussed already above, the isoeffective dose for skin reaction is significantly lower than the value for chordoma or late CNS tissue effects because of the higher $\alpha/\beta$-ratio.

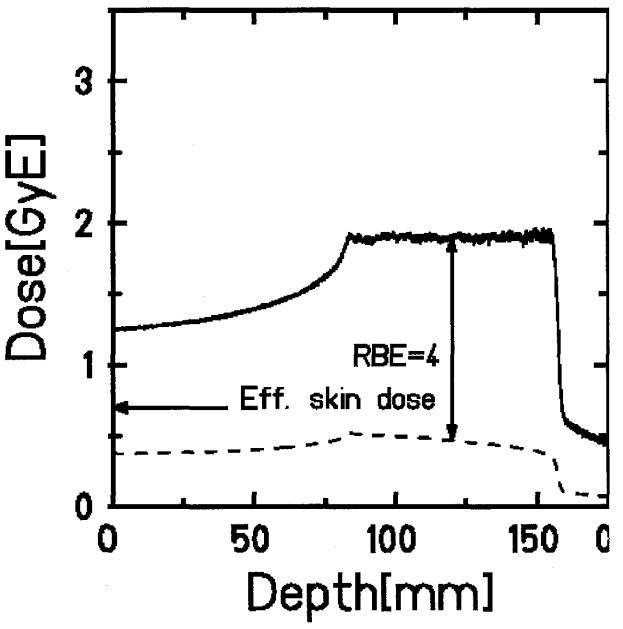


Fig. 4:Depth dose profiles (in a water-equivalent system) for a typical chordoma treatment. The full line indicates the isoeffective dose distribution based on $\alpha/\beta$=2Gy; the arrow at the left side indicates the isoffective dose level for acute skin reactions based on $\alpha/\beta$=5.9 Gy.

More precise information with respect to $\alpha/\beta$-ratios is available for other tumor entities like e.g. prostate tumor. Although the debate about the precise $\alpha/\beta$-value for prostate cancer is ongoing and the details are still under discussion, there is general agreement that the value is below 3 Gy and thus definitely lower than 10 Gy as typically assumed for other tumors. This low value makes prostate cancer a good candidate for ion beam treatment, because according to the systematic shown in Fig. 2 the RBE is expected to be high in this case.

In order to allow for a comparison with other treatment modalities like proton or advanced photon techniques like IMRT, which are mainly performed using a 2 Gy/fraction scheme, the differences in the fractionation

schedule have to be taken into account as well. So far, typical full carbon ion treatments at GSI have been performed using a 20 fraction schedule on 20 consecutive days without breaks at the weekend and an isoeffective fraction dose of 3 Gy, resulting in a total isoeffective dose of 60 Gy. (RBE values are in the order of 3 for these cases, so that the total absorbed dose is in the order of 20 Gy). The estimation of the fractionation effects requires the same $\alpha/\beta$-values which are taken for the estimation of RBE values. For example, based on an $\alpha/\beta$-value of 2 Gy, the isoeffective dose of 60 Gy in 20 fractions corresponds to a dose of approximately 75 Gy when given with a dose of 2 Gy per fraction.

## 4 Conclusions

The complex dependence of RBE on parameters such as particle type and energy, dose level and cell or tissue type require careful consideration in treatment planning for applications of charged particle beams in tumor therapy. For the precise quantitative description of these dependencies, models are required. An example of such a model, the local effect model (LEM) is described in this report. It has been tested by comparison with a wide variety of biological endpoints from in-vitro cell survival to tumor control probabilities from clinical studies.

An important feature of the approach presented here is, that it allows prediction of the response of a biological object to high-LET radiation from its response to low-LET radiation: for a given treatment field, the RBE is essentially determined by the photon sensitivity parameters $\alpha$, $\beta$ and Dt. Therefore, the experience with conventional photon treatment represents an important source for estimation of clinical RBE values.

## 5 References


1. Blakely, E.A., 'Biology of BEVALAC beams' In: Pion and heavy ion Radiotherapy: Pre-Clinical and Clinical Studies Skarsgard LD Ed. New York. (Elsevier Science Publishing Co, Inc.) 229-250 (1982)
2. Kraft, G., Radiobiological Effects of Very Heavy Ions: Inactivation, Induction of Chromosome Aberrations and Strand Breaks. Nucl. Sci. Appl., 3, 1-28 (1987)
3. Weyrather, W.K., Ritter, S., Scholz, M., Kraft, G., RBE for carbon track-segment irradiation in cell lines of different repair capacity. Int.J.Radiat.Biol., 75, 1357-1364 (1999)
4. Furusawa, Y., Fukutsu, K., Aoki, M. et al., Inactivation of aerobic and hypoxic cells from three different cell lines by accelerated 3He-, 12C- and 20Ne-ion beams. Radiat.Res. 154, 485-496 (2000)
5. Kanai T, Furusawa Y, Fukutsu K, et al., Irradiation of Mixed Beam and Design of Spread-Out Bragg Peak for Heavy-Ion Radiotherapy. Radiat. Res. 147, 78-85 (1997)
6. Kanai, T., Endo, M., Minohara, S. et al., Biophysical characteristics of HIMAC clinical irradiation system for heavy-ion radiation therapy. Int. J. Radiat. Oncol. Biol. Phys. 44, 201-10 (1999)
7. Scholz, M., Kraft, G. Calculation of heavy ion inactivation probabilities based on track structure, x-ray sensitivity and target size. Radiat. Prot. Dosim. 52, 29-33 (1994)
8. Scholz, M., Kraft, G. Track structure and the calculation of biological effects of heavy charged particles. Adv. Space Res. 5-14 (1996)
9. Scholz, M. Calculation of RBE for normal tissue complications based on charged particle track structure. Bull. Cancer Radiother. 83 Suppl., 50s-54s (1996)
10. Scholz, M, Kellerer, AM, Kraft-Weyrather, W, Kraft, G. Computation of cell survival in heavy ion beams for therapy - the model and its approximation. Radiat. Environ. Biophysics 36, 59-66 (1997)
11. Kiefer, J., Straaten, H. A model of ion track structure based on classical collision dynamics. Phys. Med.

Biol. 31, 1201-9 (1986)

12. Krämer, M. and Scholz, M. Rapid calculation of biological effects in ion radiotherapy. Phys. Med. Biol. 51 (2006) 1959?1970
13. Elsässer, T. and Scholz, M., Cluster Effects within the Local Effect Model. Rad. Res., 167:319-329 (2007)
14. Suzuki M, Kase Y, Yamaguchi H, et al. Relative biological effectiveness for cell-killing effect on various human cell lines irradiated with heavy-ion medical accelerator in Chiba (HIMAC) carbon-ion beams. Int J Radiat Oncol Biol Phys 48, 241-50 (2000)
15. Weyrather, W.K., Kraft, G. RBE of carbon ions: Experimental data and the strategy of RBE calculation for treatment planning. Accepted for publication in Radiotherapy and Oncology (2003)
16. Scholz, M., Matsufuji, N., Kanai, T. Test of the local effect model using clinical data: tumour control probability for lung tumours after treatment with carbon ion beams.Radiat Prot Dosimetry. 2006;122 (1-4):478-9
17. Krämer, M, Jäkel, O, Haberer, T. et al.. Treatment planning for heavy-ion radiotherapy: physical beam model and dose optimization. Phys. Med. Biol. 45, 3299-3317 (2000)
18. Krämer, M and Scholz, M. Treatment planning for heavy-ion radio therapy: calculation and optimization of biologically effective dose. Phys. Med. Biol. 45, 3319-3330 (2000)
19. Battermann JJ, Breur K, Hart GA, van Peperzeel HA. Observations on pulmonary metastases in patients after single doses and multiple fractions of fast neutrons and cobalt-60 gamma rays. Eur J Cancer. 17 (1981) 539-48
20. Hopewell JW, van den Aardweg GJ. Studies of dose-fractionation on early and late responses in pig skin: a reappraisal of the importance of the overall treatment time and its effects on radiosensitization and in-complete repair. Int J Radiat Oncol Biol Phys. 1991 Nov;21(6):1441-50.

# NIRS Methods of Specifying Carbon Ion Dose

Naruhiro Matsufuji*, Yuki Kase and Tatsuaki Kanai

Radiation Effect Research Team, Research Center for Charged Particle Therapy,
National Institute of Radiological Sciences

*Corresponding: matufuji@nirs.go.jp

## 1. Introduction

Many studies in the field of radiobiology have revealed that the clinical or biological effectiveness of heavy charged particles is a variable quantity. It results in that a physical dose is still a primary quantity to be controlled in carbon ion radiotherapy like as other conventional radiations, however, a kind of modification is indispensable for therapeutic purpose. Here, RBE is introduced as a tool to account for the modification. However, RBE depends on various physical parameters, as mentioned above. Primarily, RBE of a heavy ion beam gradually increases as the LET by the beam increases, reaches its maximum and then decreases. In addition, the RBE curve is known to show a different behavior for different ion species, fractionation schedules, or even dose levels. Even if these physical conditions are identical, RBE also varies as a function of biological parameters such as the type of tissue or cell, oxygenic conditions, endpoint of interest, and so on. The enormous complexity of the RBE determination hinders itself from being fully understood even at this moment. At HIMAC, unproven behaviors of factors such as dose dependency or tissue-specific response to carbon ions are kept constant in order to ascertain them from clinical outcomes.

## 2. Materials and Methods

At first, fragmentation of monoenergetic carbon ions in a patient' s body is estimated with a simulation code HIBRAC [1]. Dose-averaged LET value is deduced at each depth from the calculated LET spectra. HSG, cell line from human salivary grand tumor, was chosen as a representative of various cell lines due to its moderate radiosensitivity. Dose-survival relationships of the HSG to carbon ions of various incident energies are characterized with 2 parameters, $\alpha$ and $\beta$, by the LQ model. SOBP is designed to achieve flat survival probability (10%) on HSG entire SOBP region. Here, dose-averaging coefficients $\alpha$ and $\beta$ are used for survival calculation at each depth regarding composition of the beam.

It is assumed that carbon beam is clinically equivalent to fast neutrons at the point where dose-averaged LET values is 80 keV/μm. Our enormous neutron therapy experience tells that neutron has clinical RBE of 3.0. Then, clinical RBE of carbon is also normalized to 3.0 at the point. Clinical SOBP shape is finally deduced by equally multiplying a fixed factor, the ratio between clinical- and biological RBE value at the point where dose-averaged LET is 80 keV/μm, to entire biological SOBP.

This scheme for the designing of clinical dose results in applying universal depth-dose distributions to all patients, independent of tumor type or dose level. The universal depth dose distributions are considered to be beneficial to clarify the clinical effectiveness of carbon ion radiotherapy through clinical trials when dose dependency or the difference of radiosensitivity among tumor type is not yet proven from the viewpoint that it contributes to reduce the number of free parameters. Fig. 1 schematically shows the method for determining the RBE at the center of the SOBP for clinical situations.

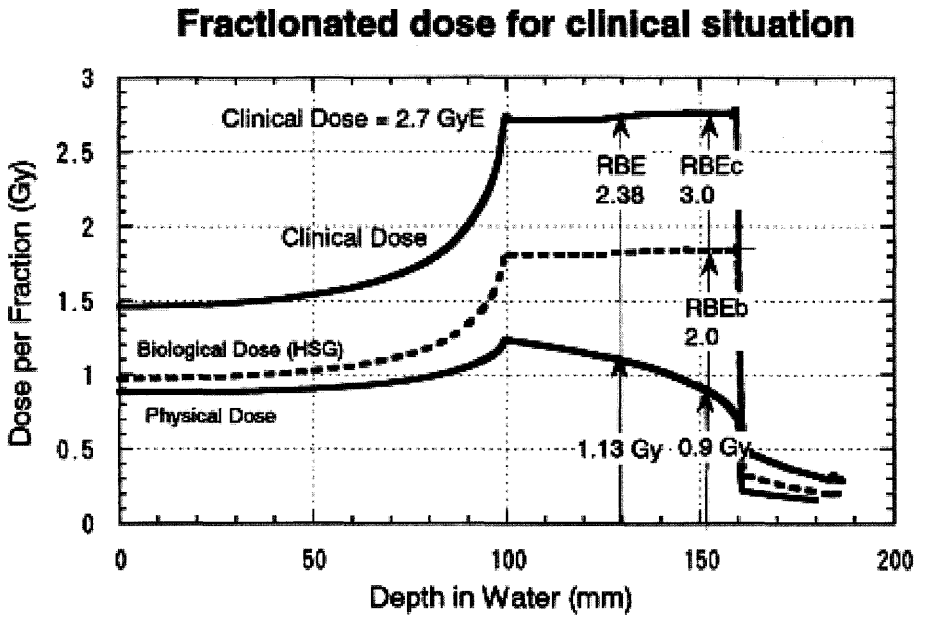


Fig. 1 Schematic method used to determine the RBE at the center of the SOBP for the clinical situation.

### 3. Results and Discussion

Verification of clinical RBE

We present here tumour control probability (TCP) analysis for non-small cell lung cancer (NSCLC) as an example of clinical results in terms of above-mentioned clinical RBE prescription scheme. Miyamoto et al. analyzed the clinical results of NSCLC treated by HIMAC beams [2]. They depict very conspicuous dose dependency of local control rate. The dose escalation study was performed with a treatment schedule of 18 fractions in 6 weeks. As to photon, Hayakawa el al. reported local control rate for NSCLC. In order to compare both results, the dose dependency of the TCP with the photon beam was fitted by the following formula [3];

$$TCP = \sum_i \frac{1}{\sqrt{2\pi}\sigma}\left\{-\frac{(\alpha_i-\alpha)^2}{2\sigma^2}\right\}\cdot\exp\left[-N\exp\left\{-n\alpha d\left(1+\frac{d}{\alpha/\beta}\right)+\frac{0.693(T-T_k)}{T_p}\right\}\right]. \quad (1)$$

α and β are coefficients of LQ model of cell survival curve. In the analysis, α and β values of HSG cells were used. σ is a standard deviation of the coefficient α, which reflects patient-to-patient variation of radiosensitivity. N is the number of clonogen in tumor (fixed value of $10^9$ was used). n and d are total fraction number and fractionated dose, respectively. T (42 days), $T_k$ (0 day) and $T_p$ (60 days) are overall time for treatment, kick off time and average doubling time of tumor cells, respectively. Values used in the analysis are shown in brackets. The result is shown in fig. 2.

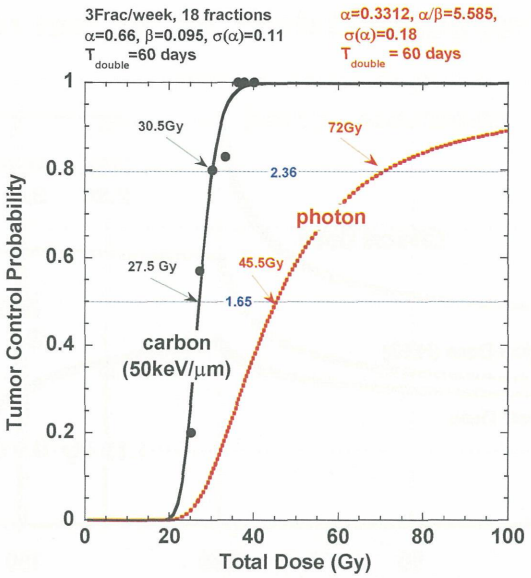


Fig. 2 TCP of NSCLC with photon (dashed, red line) and carbon (black line) beams. Circles show clinical result at HIMAC. For carbon TCP, width of SOBP and LET there were fixed as 60mm and 50 keV/μm, respectively.

Same analysis was carried out on the TCP with the carbon beam. Here, width of SOBP and dose-averaged LET in the SOBP region were both fixed as 60mm and 50 keV/μm, respectively for simplicity. The result is also shown in the figure. It is clear from the figure that the TCP curve of carbon beam is much steeper than that with photon beam. Values of s in eq. (1) is 0.18 for photon beam while for carbon beam, the value is reduced to 0.11. The result suggests that carbon beam provides equally excellent local tumor control irrelevant to individual radiosensitivity.

The difference of TCP slope shown in fig. 6 suggests that, when TCP is regarded as an endpoint, RBE value is dependent on the level of the TCP. It is found that our clinical RBE value corresponds to that at 80% TCP.

Application to hypofractionation

At HIMAC, hypofractionation study with carbon ions has been tried for some kind of tumors. Next to NSCLC, clinical trials on hepatomas will proceed into a single irradiation in no time. Before initiating a new protocol, it is desirable to estimate clinical results that correspond to prescribed dose level. The TCP analysis mentioned in the previous section is applied for this purpose. By applying σ value deduced from actual clinical result into eq. (1), it is possible to estimate TCP of different treatment schedule on NSCLC. This approach is adopted in the determination of the clinical dose to be prescribed for the single irradiation of hepatomas.

Comparison with GSI model

Different from our approach, GSI establishes and makes use of different approach named as Local Effect Model [4]. Resultant prescribed dose is apparently indicated in an identical unit GyE in both facilities; however, the value itself may differ due to the difference of the model. The difference of GyE at NIRS ($GyE_{NIRS}$) and GSI ($GyE_{GSI}$) is shown by converting $GyE_{GSI}$ into $GyE_{NIRS}$ in order to clarify required information on dose reporting.

An example of actual clinical dose distribution planned at GSI was converted into those by our scheme by the following steps.

(1) GSI clinical dose distribution (3.3$GyE_{GSI}$ to chordoma with parallel opposing irradiation)

(2) Calculate three-dimensional dose-averaged LET and physical dose distribution with TRiP, an engine of treatment planning used at GSI.

(3) Calculate $GyE_{NIRS}$ based on the physical information from (2).

The result is shown in fig. 3. It is found that $GyE_{NIRS}$ is about 20% smaller than $GyE_{GSI}$ for a typical 3.3GyE $_{GSI}$ treatment planning case.

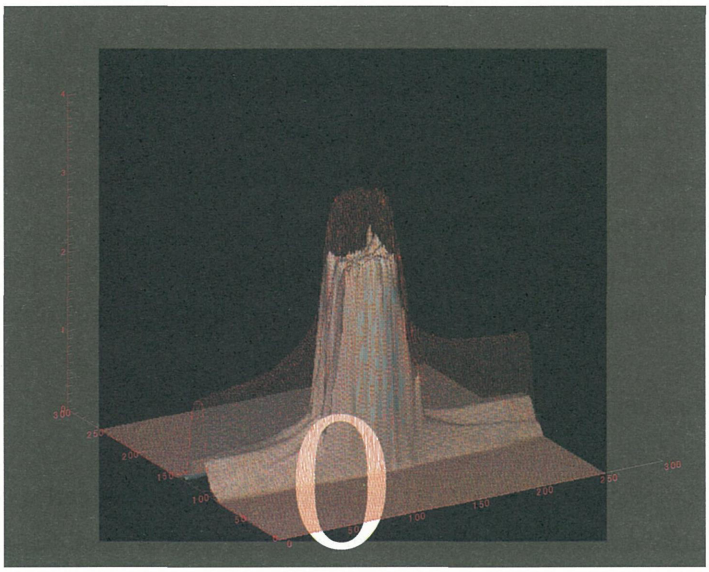

Fig. 3 Clinical dose distribution of GSI (red mesh) and NIRS (shade). The distribution was originally planned for the treatment of chordoma at GSI with parallel opposing field. At the target region, clinical GyE shows about 20% difference.

The difference is considered to be mainly due to the difference of biological system used in both model. The relationship will be affected by changing dose level, SOBP width, tumor site and so on. Hence it is too early to draw a conclusion from only one example, however, if we multiply a single factor 120% to the GSI' s physical dose distribution, the distribution agrees to ours in good precision at tumor region. Local control ratio of chordoma supports this assumption. It suggests the potential feasibility of converting GyE from one to another by multiplying single factor.

However, it is strongly required therefore to extend the comparison for various conditions and tabulate the conversion factor to make both clinical results totally comparable.

Estimation of clinical effectiveness

Currently a method has been developed in order to estimate the clinical dose from physical measurements. In this study, the microdosimetric spectra were measured with a spherical-walled proportional counter. The sensitive volume was filled with the propane-based tissue-equivalent gas from 0.5 to 6.0 micron in tissue-equivalent diameter in order to estimate the RBE value by the microdosimetric kinetic model (MKM) [5]. Actual RBE values of human tumor cells were obtained by colony assay, and compared with the model-estimated results. MKM is found to be capable of reproducing our clinical RBE values by introducing a correction that accounts for the overkill effect at high LET region [6].

## 4. Conclusion

Since 1994, more than 3,500 patients have been treated at HIMAC with the model explained in this paper. The design is found to be appropriate in contrast to the actual clinical indications.

The experience on the RBE intercomparison and the TCP analysis suggests that if the clinical results such as TCP or NTCP are expressed in terms of physical dose, it will provide good prospects to the clinical results such as the prospective estimation or the comparability among different facilities. From this point of view, it is pre-

ferable to report physical information (dose, LET and so on) together with the prescribed clinical dose. If appropriate simplifications can be introduced, the extent of physical information could be reduced.

**5. References**


1. Sihver, L., Tsao, C. H., Silberberg R, Barghouty, A. F. and Kanai, T. (1995) Calculations of depth-dose distributions, cross sections and momentum loss, Adv. Space Res. 17: 105-108.
2. Miyamoto, T., Yamamoto, N., Nishimura, H. et al. (2003) Carbon ion radiotherapy for stage I non-small cell lung cancer, Radiotherapy and Oncology 66:127-140.
3. Webb, S. and Nahum, A. E. (1993) A model for calculating tumour control probability in radiotherapy including the effects of inhomogeneous distributions of dose and clonogenic cell density, Phys. Med. Biol. 38: 653-666.
4. Scholz, M. in this proceedings.
5. Hawkins, R. ibid.
6. Kase, Y., Kanai, T., Matsufuji, N., et al. (2008) Biophysical calculation of cell survival probabilities using amorphous track structure models for heavy-ion irradiation, Phys. Med. Biol. 53, 37-59.

# A Microdosimetric-Kinetic Model Relating Mammalian Cell Killing by Heavy Charged Particles to that of Gamma and X-rays

Roland Hawkins

Department of Radiation Oncology, Ochsner Medical Institutions, 1514 Jefferson Highway, New Orleans, Louisiana, 70121, USA

Corresponding: rhawkins@ochsner.org

## INTRODUCTION

The relative biologic effectiveness (RBE) of ionizing radiation in causing the reproductive death of mammalian cells increases with increase in the linear energy transfer (LET) quality of the radiation. This property is an important consideration in determination of the schedule and dose when patients are treated with heavy charged particle radiation such as carbon ions. The microdosimetric-kinetic (MK) model (1,2) provides a relation between RBE in the limit of zero dose ($RBE_1$) and LET or, alternatively, between $RBE_1$ and a microdosimetric parameter equal to the dose average of the lineal energy spectrum ($y_D$) of the radiation (3). This relation is presented and its derivation from the MK model outlined. Experimental studies of the dependence of $RBE_1$ on radiation quality for several mammalian cell types (4-9) are examined in the context of the MK model. Some general relationships between cell killing by low and high LET radiation are suggested that may be useful in the selection of patients for treatment with high LET radiation and in the choice of dose and fractionation for such treatment.

## SUMMARY OF THE MK MODEL

The cell nucleus is conceived of as divided into $p$ compartments called domains. All domains have the same mass $m$ but may have various shapes so that, as sketched in figure 1, they fill up the space of the nucleus like pieces in a three dimensional jigsaw puzzle. The energy deposited by exposure of a population of cells to ionizing radiation of macroscopically measured average dose D is actually concentrated along the paths of high

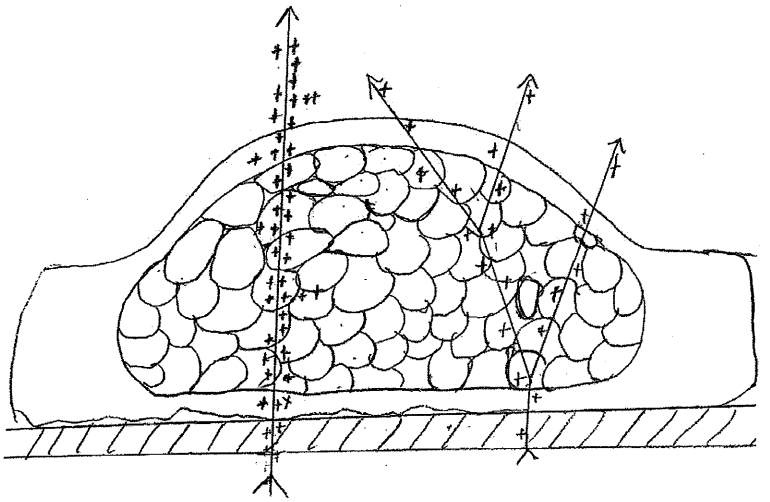

Figure 1: Nucleus of a cell spread on the surface of a culture dish and divided into compartments representing domains. On the left is sketched the track of a heavy charged particle of high LET. On the right is represented the track of a Compton electron produced by low LET X- or gamma rays.

energy charged particles of the radiation field, as depicted. As a result, the dose absorbed by individual domains varies from domain to domain and may be represented by a random variable called $z$. Note that $\langle z \rangle = D$ where the brackets indicate an average over all domains in the irradiated cell population.

It is further postulated that radiation induces potentially lethal lesions (PLL) in the DNA of the cell. The number of PLL in a domain is a random variable called $x$. The mass of DNA in a domain may also vary from domain to domain. It is a random variable called $g$. The value of $x$ averaged over the subset of domains that absorb exactly $z$ Gy and contain exactly $g$ gm of DNA is assumed to be given by:

$$(1) \qquad \langle x | z, g \rangle = k_d z g$$

Where the brackets with bar indicate a conditional average and $k_d$ is a proportionality constant. A PLL is a focus of chemical injury to the double stranded DNA where the strands may separate to form a double strand break. The value of $k_d$ is estimated from measurements of the number of double strand breaks per cell per Gy, which is called $k$, where $k_d = k/p$. The value of $k$ is about 30 to 40 per Gy per diploid human cell and is essentially the same for all mammalian cells and all values of LET up to at least about 100 $keV\,\mu m^{-1}$(10).

Figure 2 shows a single domain deformed to be a sphere of unit density, containing strands of DNA and with the path of a charged particle passing through it along a cord of the sphere. A number of PLL are shown marked on the DNA. The PLL are assumed to be confined to the domain in which they were created. They may wander about within the domain in a random flight, driven by thermal energy in a manner equivalent to Brownian motion. A pair of PLL may occasionally meet and interact to exchange strands to form what becomes a lethal exchange type of chromosome aberration. Only PLL formed in the same domain can do this. The concept of a domain incorporates in the MK model, in a simplified way, the notion that the chance of interaction between two PLL is greater the closer they are to one another. The domain acts as a surrogate for any of a number of possible restrictions on PLL travel. For instance, there may be membrane bound compartments in the nucleus or the DNA may be affixed to the nuclear membrane at multiple sites. Or, more likely, the distance a PLL on a DNA molecule can travel may be limited in a statistical sense by its half life before it disappears due to repair (11).

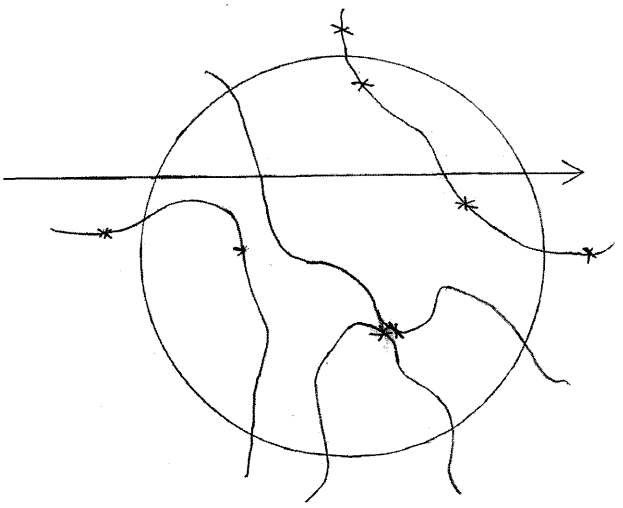

Figure 2: Sketch of a domain deformed into an equivalent sphere of the same mass and density of one gm per $cm^3$ and with the straight line path of a charged particle intersecting the domain along one of its cords. Also shown are parts of DNA strands from one or more chromosomes bearing marks representing radiation induced potentially lethal lesions.

The diameter of the sphere equivalent to a domain is called $d$. As demonstrated below, the value of $d$ is in principle measurable and is a property of the cell. Its value has been found to be of the order of 0.5 to 1.0 micrometer for several cell types (table 1). The number of domains per nucleus is of the order of several hundred to a few thousand.

Let $z_1$ be a random variable equal to the dose imparted to a domain by passage of a single high energy particle through or near it. The distribution of $z_1$ is determined by the LET quality of the radiation and the size of the domain. Unlike $z$ it does not depend on the dose D. An important quantity that contains the explicit dependence of survival on radiation quality is $\gamma = \langle z_1^2 \rangle / \langle z_1 \rangle$. It is estimated as the average length of a cord that intersects a spherical domain times the LET (1,2):

$$\gamma \simeq \frac{3d}{4m} L = \frac{0.229}{d^2} L \tag{2}$$

Where $d$ is the diameter of the domain equivalent sphere and $L$ is the LET. Alternatively, it is given by:

$$\gamma = \frac{4}{\pi d^2} y_D = \frac{0.203}{d^2} y_D \tag{3}$$

where the value of $y_D$ is the dose weighted average of the distribution of the energy deposition events recorded in a spherical tissue equivalent proportional counter divided by the average length of a cord that intersects the counter. The effective counter diameter should be equal to or near that of a domain (3). The constants make the units be such that $\gamma$ is in Gy if $d$ is in $\mu m$ and $L$ and $y_D$ are in $keV\mu m^{-1}$.

It is assumed that a PLL may undergo one of three processes. 1. It may be converted to a lethal unrepairable lesion via a first order monomolecular like process with rate constant $a$. For instance, this may be by separation of the DNA strand at the PLL to form two chromosome fragments that become a terminal deletion aberration and an acentric fragment. 2. As described above, it may combine with another PLL in the same domain to form a lethal unrepairable lesion with second order (bimolecular) rate constant $b_d$. 3. It may be repaired by a monomolecular-like process with rate constant $c$ to restore the native chromosome continuity. Finally, if a PLL undergoes none of these three processes and instead persists for a time $t_r$, it converts to a lethal unrepairable lesion. Let the number of lethal lesions that form in a domain be a random variable called $w_d$. These specifications give rise to the mass action kinetic equations:

$$\begin{aligned} \frac{d}{dt}\langle x|z,g\rangle &= -a\langle x|z,g\rangle - c\langle x|z,g\rangle - 2b_d\langle x|z,g\rangle^2 \\ &\approx -(a+c)\langle x|z,g\rangle \end{aligned} \tag{4}$$

$$\frac{d}{dt}\langle w_d|z,g\rangle = a\langle x|z,g\rangle + b_d\langle x|z,g\rangle^2 \tag{5}$$

Where the truncate approximation of equation 4 holds for dose $D \ll 150Gy$. The non linear term can be dropped because repair is by far the dominant process that eliminates PLL at doses low enough that $c\langle x \mid z, g\rangle \gg b_d\langle x \mid z, g\rangle^2$ (12). Solution of the pair of equations 4 and 5 for $\langle w_d \mid z, g\rangle$ using the truncate form of equation 4, then averaging over domains with all values of $z$ and $g$ and multiplying by the number of domains per cell gives a linear quadratic relation for the number of lethal lesions per cell (a random variable called $w$) averaged over all cells in a population instantaneously exposed to dose $D$(1,2).

(6) $$\langle w\rangle = \alpha D + \beta D^2 = (\alpha_0 + \gamma\beta) D + \beta D^2$$

The relations of the survival parameters to the kinetic constants are:

(7) $$\alpha_0 = \frac{ak}{(a+c)} + ke^{-(a+c)t_r} \quad \text{and} \quad \beta = \frac{bk^2}{2(a+c)} \frac{\langle g^2 \rangle}{\langle g \rangle^2}$$

The value of $\alpha_0$ is the average number of lethal lesions per Gy per cell originating from a single PLL. The product $\beta D$ is the average number of lethal lesions per Gy per cell originating from two PLL, each from a different particle track, when the dose is D. The product $\gamma\beta$ is the average number of lethal lesions per Gy per cell that originate from pair wise combination of PLL created by passage of a single charged particle though a cell.

If the lethal lesions are Poisson distributed among the cells of the population than equation 6 becomes the familiar linear quadratic relation for the fraction of cells $S$ that survive dose D:

(8) $$-\ln S = \alpha D + \beta D^2$$

An expression for $RBE_l = \alpha/\alpha_R$ in which the subscript $R$ indicates the value of $\alpha$ for the reference low LET radiation, usually 200 to 250 kVp X-rays or cobalt-60 radiation, can be written as:

(9) $$RBE_{1p} = \frac{\alpha_p}{\alpha_R} = \frac{\alpha_0 + \gamma\beta}{\alpha_R} = \frac{\alpha_0}{\alpha_R} + \frac{\beta}{\alpha_R} \frac{0.229}{d^2} L = \frac{\alpha_0}{\alpha_R} + \frac{\beta}{\alpha_R} \frac{0.203}{d^2} y_D$$

The subscript $p$ is added to indicate the requirement for Poisson distribution of lethal lesions. Note that if $\alpha_0$, $\beta$ and $d$ are independent of $L$ and $y_D$, than $RBE_{1p}$ is a straight line with slope proportional to $\beta_R/\alpha_R$ and $d^2$, and with intercept at zero LET or $y_D$ equal to $\alpha_0/\alpha_R$. The ratio $\alpha_0/\alpha_R$ is the fraction of lethal lesions originating from a single PLL for the reference radiation.

Particle tracks are Poisson distributed among the nuclei of the irradiated population. If passage of a single charged particle through a cell almost always causes zero or one lethal lesion and never, or hardly ever, causes two or more lethal lesions, the lethal lesions will also be Poisson distributed. As LET increases, the probability of two or more lethal lesions from a single particle passage increases. This causes grouping of lethal lesions in some cells to the exclusion and survival of others and causes $RBE_1$ to deviate downward from the $RBE_{1p}$ line. With the introduction of a parameter representing the cross sectional area the nucleus presents to the radiation beam, called $\sigma$, and assuming lethal lesion production continues to increase as indicated by equation 6 and implied by the line of equation 9, the MK model provides expressions that estimate $\alpha$ and $RBE_1$ corrected for non Poisson distribution of lethal lesions (2). These are:

(10) $$\alpha = \frac{\left(1 - \exp\left[\frac{0.16\alpha_P L}{\sigma}\right]\right)}{\frac{0.16\alpha_P L}{\sigma}} \alpha_P = \frac{\left(1 - \exp\left[\frac{0.14\alpha_P y_D}{\sigma}\right]\right)}{\frac{0.14\alpha_P y_D}{\sigma}} \alpha_P$$

$$(11)\qquad RBE_1 = \frac{\alpha}{\alpha_R} = \frac{1-\exp\left(-\frac{0.16\alpha_P}{\sigma}L\right)}{\frac{0.16\alpha_P}{\sigma}L} RBE_{1p} = \frac{1-\exp\left(-\frac{0.14\alpha_P}{\sigma}y_D\right)}{\frac{0.14\alpha_p}{\sigma}y_D} RBE_{1p}$$

The values of $RBE_{1p}$ and $\alpha_p$ are those that would be observed if, after lethal lesions are created per equation 6 they were to be magically redistributed individually and at random among the population of cells, ie, with Poisson distribution. The limiting forms of equation 11 are of interest:

$$(12)\qquad \lim_{L\to 0} RBE_1 = RBE_{1P} \quad \text{and} \quad \lim_{L\to\infty} RBE_1 = \frac{\sigma}{0.16\alpha_R}\frac{1}{L} = \frac{\sigma}{0.14\alpha_R}\frac{1}{y_D}$$

**EXPERIMENTAL STUDIES OF RBE**

Figures 3, 4 and 5 are some experiments that demonstrate the linear dependence of $RBE_1$ represented in equation 9 as well as the deviation from the line to form a maximum in $RBE_1$ as LET approaches about 100 $keV\mu m^{-1}$. Linearity implies constancy of β and the several model parameters on which it depends per equation 7. With the assumption that the production of lethal lesions continues to increase linearly as LET increases to values greater than those of the linear range and with a reasonable choice for the nuclear cross section, equation 11 may be made to fit experimental measurements of $RBE_1$ as it reaches and passes through the maximum that is found as LET increases to values greater than 100 $keV\mu m^{-1}$ (2). This implies the deviation from linearity that produces the maximum in $RBE_1$ is predominantly, if not entirely, due to the non Poisson distribution of lethal lesions and that production of lethal lesions actually does continue to increase linearly even though $RBE_1$ does not. Further, this implies the value of β and the constants on which it depends likely also do not change significantly as LET reaches and exceeds that of the maximum in $RBE_1$. Note that for LET low enough that lethal lesions are Poisson distributed, $RBE_1$ has no dependence on σ.

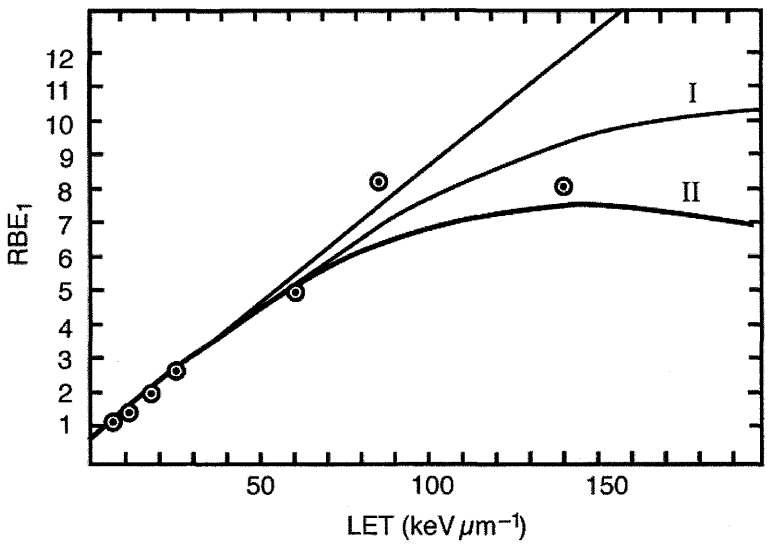


Figure 3: $RBE_1$ dependence on LET for unsynchronized human kidney cells. From data of reference 4 as plotted in reference 2. Reference radiation is 200 kVp X-rays. The straight line is equation 9, the parameters of which are listed in table 1. Curve I is equation 11 with $\sigma=100\mu m^2$ and Curve II with $\sigma=50\mu m^2$.

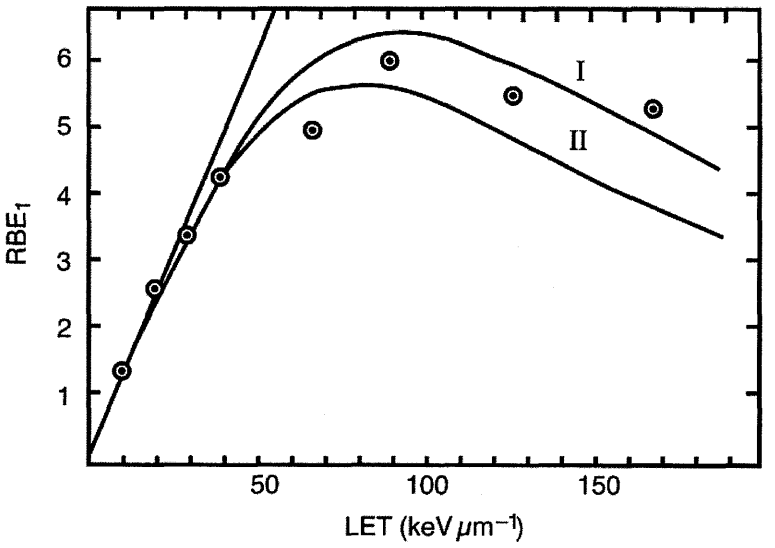


Figure 4: $RBE_1$ dependence on LET for V79 cells synchronized at G1/S transition. Data from reference 6, as plotted in reference 2. Reference radiation is 250 kVp X-rays. The straight line is equation 9, the parameters of which are listed in table 1. Curve I is equation 11 with $\sigma=32\mu m^2$ and curve II with $\sigma=24.6\mu m^2$.

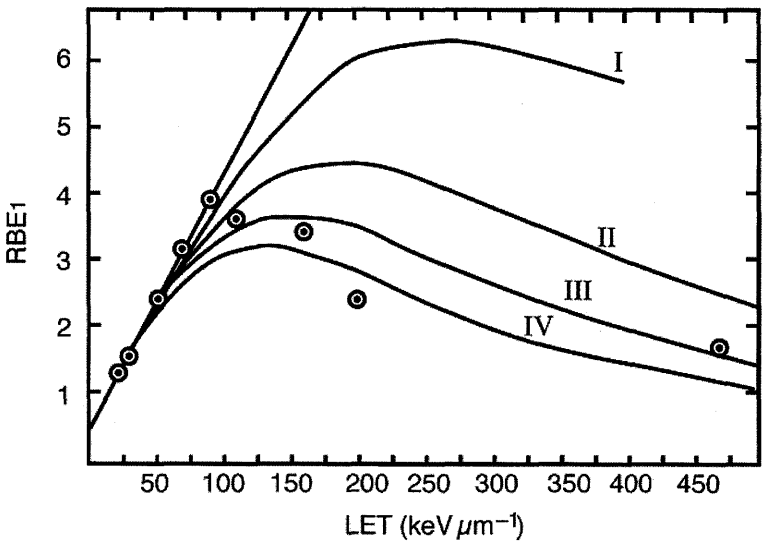


Figure 5: $RBE_1$ dependence on LET for unsynchronized HF-19 human diploid lung fibroblasts. Data from reference 5, as plotted in reference 2. Reference radiation is 250 kVp X-rays. The straight line is equation 9, the parameters of which are listed in table 1. Curve I is equation 11 with $\sigma=320\mu m^2$, curve II with $\sigma=160\mu m^2$, curve III with $\sigma=106.6\mu m^2$, curve IV with $\sigma=80\mu m^2$.

Figure 6 summarizes experimental determinations of the linear relation between $RBE_1$ and LET of equation 9 for the three cell types represented in figures 3,4 and 5 and additionally for fibroblasts obtained from patients who have the recessively inherited disease ataxia telangiectasia. All four lines are from least squares fit to data felt to be within the linear range of LET. There is uncertainty in their determination because the appropriate value of LET above which the data should be excluded because of deviation due to non Poisson distribution of lethal lesions is uncertain. This uncertainty affects the zero LET intercept more than it does the slope. By definition each line must pass through the $RBE_1$ equal one line at the LET of the reference low LET radiation, which is either 200 or 250 kVp X-rays. The appropriate value for the reference LET is uncertain. Accordingly the

$RBE_1$ equal one point was not included in the data used to determine the lines. The intersection of the lines with the $RBE_1$ equal one line suggests the reference radiation LET is in the range of about 3 to 10 $keV\mu m^{-1}$.

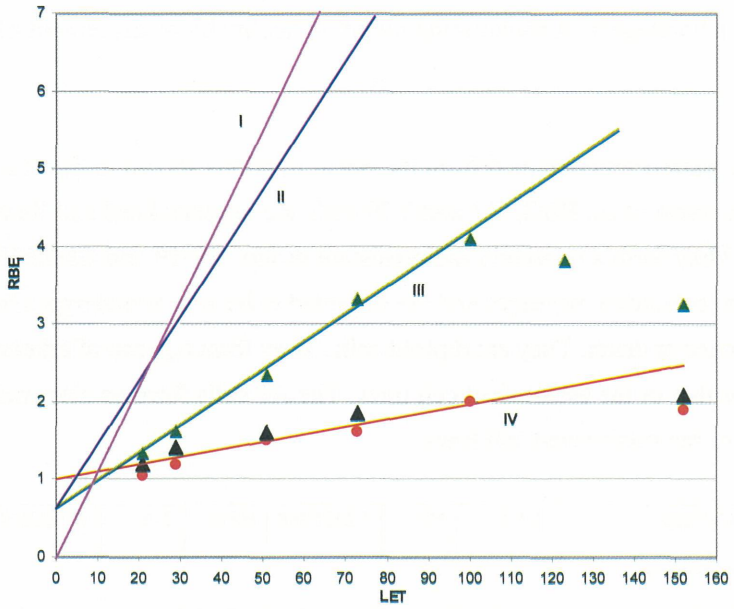


Figure 6: Composite for comparison of linear dependence of $RBE_1$ on LET per equation 9. Curve I is V79 cells from figure 4, II is human kidney cells from figure 3, III is HF-19 cells from figure 5, with data points shown. Line IV is fit to data for skin fibroblasts explanted from two patients with ataxia telangiectasia re-plotted from references 7 and 8. The reference radiation is 250 kVp X-rays.

Figure 7 shows a plot of data from Kase et al at NIRS (9) for two cell types using $y_D$ as the measure of radiation quality. The value of $y_D$ for the 200 kVp X-ray reference radiation has been measured with a tissue equivalent proportional counter with effective diameter of 0.76 and 0.97 micrometer. Its value is 4.3 $keV\mu m^{-1}$(9, 13)

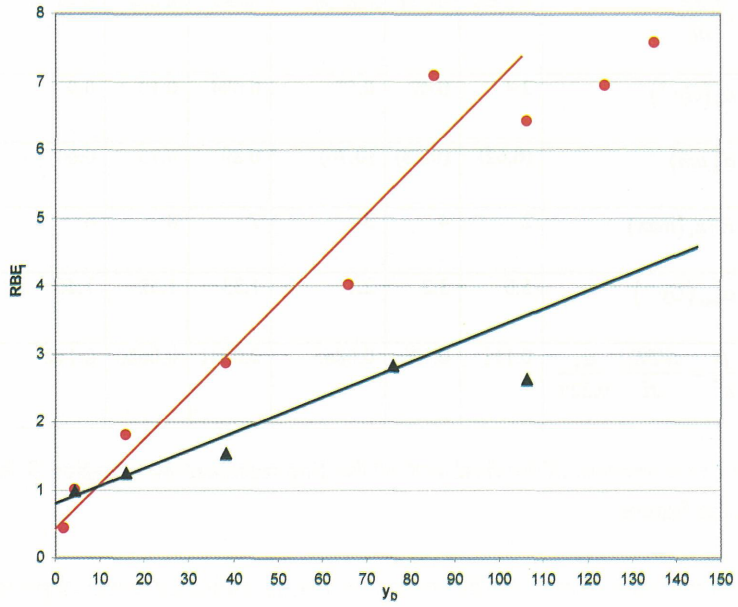


Figure 7: $RBE_1$ dependence on $y_D$. Plotted from data of reference 9. The steeper line is least squares fit to data for $y_D < 100 keV\mu m^2$ for human salivary gland cell line HSG and the less steep line similarly fit for normal human fibroblast strain GM05389. The lines represent equation 9, the parameters of which are listed in table 1.

and the $RBE_1$ equal one point is included in the data used to determine the lines in figure 7. Also included for the HSG cells is a point for cobalt 60 radiation for which $y_D$ is 1.81 $keV\mu m^{-1}$(9). Measurements of $RBE_1$ for the lower end of the range of $y_D$ are valuable as they particularly improve the accuracy of the determination of $\alpha_0/\alpha_R$. There is significant advantage in characterizing radiation quality by measurement of $y_D$ rather than by LET.

**DISCUSSION:**

Table 1 summarizes parameters obtained from the linear relations shown in figures 6 and 7. The cells sort into three groups by the value of $\alpha_R$. HSG, T-1 and V79 cells are immortalized cell lines able to be propagated indefinitely in culture. They form a relatively radioresistant group. HF-19 and GM05389 have been through a relatively low number of subculture passages and are expected to be able to undergo a limited number of future passages before senescence or death. They are diploid cells. They form a group of relatively radiosensitive cells with $\alpha_R$ about four times that of the established cell lines. The AT cells form an ultra-radiosensitive group with $\alpha_R$ about ten times that of the established cell lines.

| Cell type<br>references | AT | HF-19 | GM05389 | HSG | T-1 | V79,G1/S |
|---|---|---|---|---|---|---|
| Charged particle | $^3He$ | $^3He$ | $^{12}C$ | $^{12}C$ | $^1H$<br>$^4He$ | $^1H, ^2H$<br>$^3He$ |
| $\alpha_R\left(Gy^{-1}\right)$ | 2.5 | 0.80 | 0.70 | 0.19 | 0.19 | 0.234 |
| $\beta_R\left(Gy^{-2}\right)$ | ---- | ---- | ----- | 0.05 | 0.038 | 0.042 |
| $\lim_{L\to 0} RBE_{1P} = \alpha_0/\alpha_R$ | 0.99 | 0.59 | 0.81 | 0.44 | 0.64 | 0.018 |
| $\frac{dRBE_{1P}}{dL}$ | 0.0102 | 0.037 | 0.0251 | 0.0685 | 0.082 | 0.11 |
| $\alpha_0\left(Gy^{-1}\right)$ | 2.4 | 0.47 | 0.57 | 0.084 | 0.12 | 0.0 |
| $d(\mu m)$ | (0.62) | (0.58) | (0.76) | 0.89 | 0.75 | 0.61 |
| $RBE_1(\max)$ | 2 | 4 | 3 | 7 | 8 | 6 |
| $\alpha_{\max}\left(Gy^{-1}\right)$ | 5.0 | 3.2 | 2.1 | 1.33 | 1.52 | 1.40 |
| $\frac{\beta}{d^2} = \frac{dRBE_{1P}}{dL}\frac{\alpha_R}{0.229}$ | 0.111 | 0.129 | 0.0865 | 0.0641 | 0.0680 | 0.112 |

Table 1: Summary of parameters of survival and of the line representing equation 9 for the various cell lines referred to in the figures.

Since the experimental measurement of $RBE_1$ versus LET or $y_D$ indicates linear dependence, it is implied that $\beta$ is constant and equal to $\beta_R$. The value of $\beta_R$ is shown for the three established cell lines. There is not much variation in $\beta_R$ among the three. It is not possible to reliably measure $\beta_R$ for the more sensitive cell types and no value is listed for them. The survival relation for the sensitive cells, even for X-rays or cobalt-60 radiation, appears to be exponential, or nearly so. This is because the dominant effect of a large value of $\alpha_R$ for the dose range

accessible for colony survival measurements makes $\beta_R$ appear to equal zero. However, it can not be zero because, if it were, there would be no increase in RBE with increasing LET.

Since there is little variation in $\beta_R$ among cells for which it can be measured, the average of the three may serve as an estimate of $\beta_R$ for the other cells. The average value of $\beta_R$ for the three cell lines is 0.043 $Gy^{-2}$. Computation of the domain diameter $d$ from the slope of the line of equation 9 requires a value for $\alpha_R$ and $\beta_R$, or at least their ratio. Computed values of $d$ are listed in table 1. Those in parenthesis were computed with $\beta_R$ set equal to the average value of 0.043 $Gy^{-2}$. The computed domain diameter values show little variation suggesting that a value of $d$ equal to that of the average of those in table 1, which is 0.7 micrometers, may approximate that of many mammalian cells.

When sensitivity is expressed by the value of $\alpha_0$ the cells sort into the same sensitivity groups as for $\alpha_R$. Vulnerability to formation of a lethal lesion from a single PLL is apparently a major determinant of the magnitude of $\alpha_R$. By increasing the value of $\alpha_R$, a relatively large value of $\alpha_0$ tends to make the ratio $\beta_R/\alpha_R$ low. Per equation 9, this leads to less increase in $RBE_{1p}$ with increasing LET. This is confirmed by the entries for $dRBE_{1p}/dL$ in table 1.

The lower value of $dRBE_{1p}/dL$ leads to a lower maximum value of $RBE_1$, which is listed in table 1 as $RBE_1$ (max). This trend is not enough to reverse the order of sensitivity of the cell groups as judged by the maximum value attained by α, which is listed in table 1 as $\alpha_{max}$. However, note that whereas $\alpha_R$ of the radiosensitive diploid human fibroblasts is about 4 times that of the established cell lines, $\alpha_{max}$ is only about 1.5 to 2 times that of the established cell lines. This suggests the generalization that as LET increases to approach that of the maximum in $RBE_1$, the ratio of $\alpha$ of more sensitive cell types to $\alpha$ of more resistant cell types becomes closer to one than it is for cobalt-60 or X-rays.

**CONCLUSION:**

Since the value of $\beta_R$ shows relatively little variation among cells, the ratio $\beta_R/\alpha_R$ is largely determined by variation in the value of $\alpha_R$, which in turn is largely determined by the vulnerability of the cells to formation of lethal lesions from single PLL, as expressed in the value of $\alpha_0$. Since the rate of increase in RBE with LET is proportional to $\beta_R/\alpha_R$, a relatively large value of $\alpha_R$, and the radiosensitivity it represents, implies a lower maximum value of RBE for the more radiosensitive cells. This tends to reduce the differential in sensitivity between any pair of cell types as LET increases toward that of the maximum in RBE, as compared with the differential in sensitivity to high energy X-rays or cobalt 60. This may be particularly advantageous in treating cancers that are relatively radioresistant and in eradicating radioresistant subpopulations present in many tumors. Note for instance that the relative resistance of hypoxic cells expressed as the oxygen enhancement ratio tends to disappear as the LET approaches that of the maximum in RBE ( 14-16). This can be explained by the loss of Poisson distribution of lethal lesions (2).

Since $\alpha$ increases by several fold as LET increases up to the maximum in RBE, while $\beta$ remains essentially unchanged, the $\alpha/\beta$ ratio also increases several fold. Because of this, unlike for high energy X-rays, there is essentially no sparing of cells of normal tissues by decreasing the fractional dose in a course of radiation treatment with high LET radiation. This is particularly important to recognize in treatment that must include the brain, spinal cord or other tissues for which the $\alpha/\beta$ ratio appropriate to low LET radiation is small (2 to 5) and which are relatively spared by small fractions of the high energy X-ray radiation used to treat patients in nearly all radiation oncology clinics.

## REFERENCES


(1) R B Hawkins, A microdosimetric-kinetic theory of the dependence of the RBE for cell death on LET. Med. Phys. **25**, 1157-1170 (1998).

(2) R B Hawkins, A microdosimetric-kinetic model for the effect of non-Poissson distribution of lethal lesions on the variation of RBE with LET. Radiat. Res. **160**, 61-19 (2003).

(3) ICRU, Microdosimetry. Report 36, International Commission on Radiation units and Measurements, Appendix F, Bethesda MD, (1983).

(4) G W Barendsen, H M D Walter, J F Fowler and D K Bewley, Effects of different ionizing radiations on human cells in tissue culture III. Experiments with cyclotron-accelerated alpha-particles and deuterons. Radiat. Res. **18**, 106-119 (1963).

(5) R Cox and W K Masson, Mutation and inactivation of cultured mammalian cells exposed to beams of accelerated heavy ions III. Human diploid fibroblasts. Int. J. Radiat. Biol. **36**, 149-160 (1979).

(6) R P Bird, N Rohrig, R D kColvett, C R Geard, and S R Marino, Inactivation of synchronized Chinese hamster V79 cells with charged particle track segments. Radiat. Res. **82**, 277-289 (1980).

(7) R Cox, A cellular description of the repair defect in ataxia-telangiectasia. In: Ataxia-telangiectasia: A Cellular and Molecular Link Between Cancer, Neuropathology, and Immune Deficiency. Edited by: B A Bridges and D G Harnden (John Wiley and Sons, London), 141-153 (1982).

(8) D T Goodhead, J Thacker and R Cox, The effects of radiations of different qualities on cells: molecular mechanisms of damage and repair. Int. J. Radiat. Biol. **63**, 543-556 (1993).

(9) Y Kase, T Kanai, Y Matsumoto, Y Furusawa, H Okamoto, T Asaba, M Sakama and H Shinoda, Microdosimetric measurement and estimation of human cell survival for heavy-ion beams. Radiat. Res. **166**, 629-638 (2006).

(10) K M Prise, G Ahnstrom, M Belli, J Carlsson, D Frankenberg, J Kiefer, M Lobrich, B D Michael, J Nygren and B Sternerlow. A review of dsb induction data for varying quality of radiations. Int. J. Radiat. Biol. **74**, 173-184 (1998).

(11) R. Hawkins, A microdosimetric-kinetic model for the sensitization of V79 cells to radiation by incorporation of bromodeoxyuridine. Radiat. Res. **155**, 698-702 (2001).

(12) Hawkins, A microdosimetric-kinetic model of cell death from exposure to ionizing radiation of any LET, with experimental and clinical applications. Int. J. Radiat. Biol. **69**, 739-755 (1996).

(13) M Coppola, E Eickel, M Fitzgerald, D Pirwitz, F Porro and J Booz. Experimental evaluation of the spectral energy deposition in small volumes by low LET radiation. In Proceedings of the Fifth Symposium on Microdosimetry, Report No. EUR 5452. Edited by J Booz, H G Ebert and B G Smith. (Commission of the European Communities, Luxembourg) (1976).

(14) G W Barendsen and H M D Walter, Effects of different ionizing radiations on human cells in tissue culture. Radiat. Res. **22**, 314-329 (1964).

(15) E A Blakely, C A Tobias, T C H Yang et al, Inactivation of human kidney cells by high-energy monoenergetic heavy-ion beams. Radiat. Res. **80**, 122-160 (1979)

(16) Y Furusawa, K Fukutsu, M Aoki, et al, Inactivation o faerobic and hypoxic cells from three different cell lines by accelerated He-3, C-12 and Ne-20 beams. Radiat. Res. **154**, 485-496 (2000).

# Treatment of Skull Base Chordomas at GSI

Daniela Schulz-Ertner MD[1,2], Christian P Karger PhD[3], Alexandra Feuerhake1, Anna Nikoghosyan MD[1], Stephanie E Combs MD[1], Oliver Jäkel PhD[3], Michael Scholz PhD[4], Jurgen Debus MD PhD[1]

[1]Dept. of Radiation Oncology, University of Heidelberg, Germany
[2]Dept of Radiation Oncology, Frankfurter Diakonie Kliniken, Frankfurt am Main, Germany
[3]Dept. of Medical Physics in Radiation Oncology, DKFZ, Heidelberg, Germany
[4]Dept. of Biophysics, Gesellschaft für Schwerionenforschung (GSI), Darmstadt, Germany

Corresponding : Daniela.Ertner@fdk.info

## Abstract

**Patients and Methods:** Between November 1998 and July 2005, 96 patients with chordomas of the skull base have been treated with carbon ion RT using the raster scan technique at the Gesellschaft für Schwerionenforschung (GSI) in Darmstadt, Germany. All patients had gross residual tumors. Median total dose was 60 CGE (range 60 - 70 CGE) delivered in 20 fractions within 3 weeks. 44 Patients were treated within a clinical phase I/II trial between 1998 and 2001, and 52 further patients were treated thereafter as routine patients according to the same treatment protocol.

**Results:** Mean follow-up was 31 months (range 3 to 91 months). The actuarial local control rate was 70.0% at 5 years. Overall survival was 88.5% at 5 years. Late toxicity consisted of optic nerve neuropathy RTOG/EORTC grade 3 in 4.1% of the patients and necrosis of a fat plomb in one patient. Minor temporal lobe injury (RTOG/EORTC grade 1-2) occured in 7 patients (7.2%). Target doses in excess of 60 CGE and primary tumor status were associated with higher local control rates. A clear dose-reponse-relationship was observed when results were compared to other available data in the literature.

**Conclusion:** Carbon ion RT is an effective treatment option for skull base chordomas and is associated with acceptable toxicity. Doses in excess of 75 CGE with daily fractions of 2 CGE are likely to increase local control probability. A prospective phase III trial is needed to test the hypothesis that carbon ion RT is superior to proton RT with respect to toxicity at equieffective doses.

## Introduction

Chordomas are rare tumors which are characterized by low radioresponsiveness. About 35% of all chordomas arise in the skull base region. Complete removal of skull base chordomas is challenging due to the close vicinity to sensitive normal brain structures. After incomplete tumor resection, postoperative RT is generally recommended. Since effective tumor doses in excess of 70 Gy can hardly be reached with photons, particle therapy with protons and carbon ions has been investigated in the past for these patients [1,2,3,4,5].

At GSI, patient treatments have been carried out within a cooperative project by medical doctors of the University of Heidelberg and scientists of the GSI, the German Cancer Research Center and the Research Center Rossendorf since 1997.

Here we report our experience with carbon ion RT in patients with skull base tumors. The focus of this article is on target definition and dose prescription using active beam delivery for carbon ion RT in skull base chordomas.

## Material and Methods

### Patients

First patients with skull base chordomas were treated with carbon ion RT at GSI in 1998. Since then, more than 150 patients with skull base chordomas have been treated with carbon ion RT at GSI. The first 44 chordoma patients were treated within a clinical phase I/II trial, the following patients were treated as routine patients according to the same protocol. The most recent analysis of treatment results in skull base chordomas treated at GSI has been performed in 2006 and included 96 patients with macroscopic chordomas of the skull base. There were 54 male and 42 female patients. The median age was 47 years (range 11-80 years). Fifty-nine patients (61%) were treated for primary tumors and 37 patients had recurrent tumors. All patients had macroscopic tumors when carbon ion RT was initiated. The average follow-up period at the timepoint of the last analysis was 31 months (range 3-91 months). For detailed information on patient characteristics see Schulz-Ertner et al. [4]

### Target definition and treatment planning

Patients with skull base chordomas treated with carbon ion RT at GSI were positioned within a precision head mask and target localization was performed using stereotactic methods. The used immobilization device guarantees an accuracy of 1-2 mm [6]. The initial planning target volume (PTV1) included the gross tumor volume (GTV) plus a safety margin of 1-5mm to account for suspected subclinical disease based on clinical risk estimation. Surgical and histological reports, MRI findings and normal tissue constraints were taken into account. Even for very small tumors the entire clivus and the prevertebral muscles down to the basis of the second cervical spine were included into PTV1. Implantation metastases of skull base chordomas are reported in the literature, but the incidence of implantation metastases within the surgical pathway is reported to be as low as 5 to 10% [7,8]. Therefore, no efforts were made to completely cover the surgical pathway, thus avoiding unacceptable toxicity.

The PTV2 was defined to include the gross tumor volume (GTV) visible on the treatment planning MRI. A safety margin of 1-2mm was added to account for any movements and uncertainties in the set-up throughout the treatment course. The needed safety margin depends on the used immobilization device and was determined to be 1-2mm for the skull base region when rigid precision head masks were used. The delineation of target volumes and organs at risk was done on treatment planning CT images and coregistered MRI images according to the ICRU 50 and ICRU 62 recommendations for conformal RT. T2 weighted fat saturated and post gadolinium T1 weighted MRI sequences were found most adequate to separate the tumor accurately from normal tissues in the skull base region.

Carbon ion beams were delivered actively to the tumor using the raster scan technique [9]. Plan optimization included biologic plan optimization taking into account the local RBE (relative biological effectiveness) values. Plan optimization aimed at achieving a homogenous biologically effective dose throughout the target volume. The mean RBE for our patients was about 3 within the target volume. The local effect model (LEM), which is integrated in the TRiP software to calculate the RBE at each point, has been described in detail by Scholz et al. [10].

### Dose prescription

Target dose was prescribed to each voxel of the target volume necessitating optimization of the absorbed dose in such a way that the product of the absorbed dose and the calculated local RBE value at each voxel was the

biologically effective prescription dose. The biologically effective dose was prescribed to every scan spot throughout the dose distribution. The allowed deviances between measured and prescribed doses were kept below 5% of the prescribed dose at each point. Treatment planning aimed at covering target volumes by the 90%-isodose line and underdosage was avoided within the target volume. Dose-volume-histogram data was generated for the physical and the biologically effective dose distributions for the planning target volumes and organs at risk. PTV1 was treated to target doses between 45 and 52.5 CGE within 15 fractions. A boost dose of 15 to 17.5 CGE was delivered to the PTV2, the total target dose reached within PTV2 was therefore 60 to 70 CGE. Eighty-four patients received a target dose of 60 CGE, higher doses up to 70 CGE were delivered in 12 patients.

Late toxicity to normal brain tissue such as necrosis is assumed to be the dose limiting toxicity for radiation therapy of skull base chordomas. An $\alpha/\beta$ value of 2-3 Gy can be estimated for the biological endpoint brain necrosis. An $\alpha/\beta$ value of 2 Gy was chosen for biological plan optimization. The $\alpha/\beta$ ratio for chordoma cells is not known, but from their biological behaviour with slow tumor progression and low radioresponsiveness it can be concluded that it is also in the range of 2 Gy.

A fractionation of 7 x 3.0 to 3.5 CGE per week was applied. Using a conventional fractionation scheme of 2 CGE per day and conservatively assuming an $\alpha/\beta$ of 2 Gy for late toxicity to the brain tissue and chordoma cells, biologically equivalent doses (BED) between 75 and 96.25 CGE were reached in PTV2. The doses to optic nerves and optic chiasm were restricted to 54 CGE. The accepted maximum dose to the brainstem was 50 CGE at the center, while very small volumes of less than 1mL at the surface of the brainstem were allowed to receive up to 60 CGE. The dose to the spinal cord was constrained to 45 CGE. Taking into account the accelerated fractionation pattern used for carbon ion RT at GSI, biologically equivalent dose constraints were 63.45 CGE for optic nerves and chiasm, and 75 / 56.25 CGE for the surface / center of the brain stem, respectively. These dose constraints were similar to the dose constraints adhered to in most of the proton centers. Therefore, similar toxicity rates can be expected.

**Results**

Twenty-one patients (21.8%) showed partial remission of their tumors on follow-up MRI scans after carbon ion radiation therapy. The local control rate was 70% at 5 years. Most recurrences were located inside the former RT field. Delivery of target doses exceeding 60 CGE improved local control significantly as well as primary tumor status, while gender did not influence outcome. Three percent of the patients developed implantation metastases within the surgical pathway outside the former carbon ion RT portals. Two patients (2%) developed distant metastases. The 5-year overall survival rate was 88.5%.

Carbon ion RT was well tolerated by most of the patients. Optic nerve neuropathy RTOG/EORTC grade 3 occured in 4 patients (4.1%). Circumscribed white matter changes in the temporal lobe occurred in 7 patients (7.2%) and were much more common in patients who received target doses in excess of 60 CGE (biologically equivalent doses between 75 and 96.25 CGE). In patients who received a total dose of 60 CGE (biologically equivalent dose of 75 CGE) the temporal lobe injury rate was 3.5%. A rate of 33% was observed in patients who received doses in excess of 60 CGE. The temporal lobe lesions were associated with a perifocal edema and neurologic sequelae necessitating steroid medication (RTOG/EORTC grade 2) in 2 patients, only. The remaining 5 patients were asymptomatic and the white matter changes were reversible (RTOG/EORTC grade 1) in these patients. Soft tissue necrosis of a fat plomb inserted into the surgical pathway during surgery was observed in one patient (RTOG/EORTC grade 3).

More detailed data on outcome and toxicity can be found in Schulz-Ertner et al. [4].

**Discussion**

The oncological problem in skull base chordomas is mainly a local problem. In our carbon ion RT patient series, 11 out of 15 locoregional recurrences occured inside the former RT fields, only 4 patients developed marginal failures. No patient developed an out of field recurrence. This supports the adequateness of the target volume concept.

Distant metastases are uncommon. Incidence rates between 0 and 14% have been reported [5,7,11].This is in line with the distant metastases rate of 2% found in our series.

There is no doubt that local control is dependent on the delivery of high local doses in skull base chordomas. Particles such as protons and carbon ions offer advantages in escalating doses to circumscribed tumors while avoiding dose to critical organ structures nearby. Based on these facts, high dose proton RT has been investigated in chordomas of the skull base in the past.

Munzenrider et al. achieved a 5-year local control rate of 73% in 375 patients treated with proton RT at the Massachusetts General Hospital in Boston, USA [3].

Hug et al. report a local control rate of 59% for chordoma patients treated with protons at Loma Linda University Medical Center, USA [2].

At the Centre de Protontherapie d' Orsay, France, patients with skull base chordomas have been treated with combined photon and proton RT to doses between 67 and 71 CGE. The 4-year local control rate was 53.8% [1].

The 5-year local control rate of 70% obtained with carbon ions at GSI is somewhat higher [4], but compares favourably with the data obtained in some of the proton series with prescription doses of at least 74 CGE. The data collected at GSI as well as the data available in the literature clearly supports the assumption that particle therapy is beneficial for patients with skull base chordomas, since much lower local control rates are reported for photon RT. After conventional photon RT local control rates between 17 and 23% at 5 years have been reported [12,13]. A clear dose-response-relationship has been described for skull base chordomas taking into account all these data [4]. In congruence with this finding, prescription dose has been identified as most important prognostic factor [1,14]. Higher doses are likely to achieve higher local control rates. Strategies of combining photons and particles can therefore be considered less favourable. Highest tumor doses are reached with protons or carbon ion RT alone, because the achieved dose gradients are much steeper than with photons due to the physical properties of proton beams. Biological equivalent target doses of at least 75 CGE are recommended. Using carbon ion RT, escalation of the biological equivalent target dose to doses in excess of 75 CGE seems to be feasible in patients with small tumors in uncritical location. However, one has to be aware that the risk for temporal lobe injury will increase with higher target doses as well.

After carbon ion RT, a higher local control rate was achieved in patients with primary tumor status as compared with patients treated for recurrent tumors. Primary tumor status has been considered to be an important prognostic factor as well by others [11,15].

Female gender was found to be an unfavourable prognostic factor after proton RT in skull base chordomas [14,16]. In our series, local control and overall survival rates did not significantly differ with respect to gender.

As compared to protons, carbon ions offer the possibility to reduce overall treatment time. The overall treatment time can be reduced to 3 weeks without increasing acute and late toxicity. Acute toxicity is very mild and severe late toxicity to optic nerves and chiasm occured in 4.1% of all patients treated with carbon ion RT at GSI, only. This rate compares to the best proton series.

**Conclusions**

Carbon ion RT has been proven to be an effective treatment option for skull base chordomas with respect to local control and overall survival. Carbon ion RT minimizes severe side effects to neighboring normal tissue structures. A prospective phase III trial is needed to test the hypothesis that carbon ion RT is superior to proton RT with respect to toxicity at equieffective doses.

**References**

Noel G, Feuvret L, Calugaru V, et al. (2005) Chordomas of the base of the skull and upper cervical spine. One hundred patients irradiated by a 3D conformal technique combining photon and proton beams. Acta Oncologica 44: 700-708.

Hug EB, Loredo LN, Slater JD, et al. (1999) Proton radiation therapy for chordomas and chondrosarcomas of the skull base. J Neurosurg 91(3): 432-439.

Munzenrider JE, Liebsch NJ (1999) Proton therapy for tumors of the skull base. Strahlenther Onkol 175 (Suppl 2): 57-63.

Schulz-Ertner D, Karger CP, Feuerhake A, et al (2007) Effectiveness of carbon ion radiotherapy in the treatment of skull-base chordomas. Int J Radiat Oncol Biol Phys 68(2): 449-457.

Weber DC, Rutz HP, Pedroni ES, et al. (2005) Results of spot-scanning proton radiation therapy for chordoma and chondrosarcoma of the skull base: the Paul Scherrer Institut experience. Int J Radiat Oncol Biol Phys 63(2): 401-409.

Karger CP, Jäkel O, Debus J, et al. (2001) Three dimensional accuracy and interfractinoal reproducibility of patient fixation using a stereotactic head mask system. Int J Radiat Oncol Biol Phys 49: 1493-1504.

Fagundes MA, Hug EB, Liebsch NJ, et al. (1995) Radiation therapy for chordomas of the base of skull and cervical spine: pattterns of failure and outcome after relapse. Int J Radiat Oncol Biol Phys 33(3): 579-584.

Austin JP, Urie MM, Cardenosa G, Munzenrider JE (1993) Probable causes of recurrence in patients with chordoma and chondrosarcoma of the base of skull and cervical spine. Int J Radiat Oncol Biol Phys 25 : 439-444.

Haberer T, Becher W, Schardt D, et al. (1993) Magnetic scanning system for heavy ion therapy. Nucl Instr Meth Phys Res 330: 296-305.

Scholz M, Kellerer AM, Kraft-Weyrather W (1997) Computation of cell survival in heavy ion beams for therapy. The model and its approximation. Radiat Environ Biophys 36: 59-66.

Hug EB, Fitzek MM, Liebsch NJ, et al (1995) Locally challenging osteo- and chondrogenic tumors of the axial skeleton: results of combined proton and photon radiation therapy using three-dimensional treatment planning. Int J Radiat Oncol Biol Phys 31(3): 467-476.

Magrini SM, Papi MG, Marletta F, et al. (1992) Chordoma ? natural history, treatment and prognosis. Acta Oncologica 31(8): 847-851.

Romero J, Cardenes H, la Torre A, et al. (1993) Chordoma: Results of radiation therapy in eighteen patients. Radiother Oncol 29: 27-32.

Terahara A, Niermierko A, Goitein M, et al (1999) Analysis of the relationsship between tumor dose inhomogeneity and local control in patients with skull base chordoma. Int J Radiat Oncol Biol Phys 45(2) : 351-358.

Gay E, Sekhar LN, Rubinstein E, et al. (1995) Chordomas and chondrosarcomas of the cranial base: results and follow-up of 60 patients. Neurosurgery 36(5): 887-896.

Thieblemont C, Biron P, Rocher F, et al. (1995) Prognostic factors in chordoma: role of postoperative radiotherapy. Eur J Cancer 31A(13-14): 2255-2259.

# Carbon Ion Radiotherapy for Skull Base Tumor

Jun-etsu Mizoe*, Azusa Hasegawa, Ryo Takagi, Hiroki Bessyo, Takeshi Onda and Hirohiko Tsujii

Research Center Hospital for Charged Particle Therapy,
National Institute of Radiological Sciences

*Corresponding: j_mizoe@nirs.go.jp

## Introduction

It is clear that the charged particle therapy is more appropriate radiotherapy for the skull base tumor than conventional XRT because of excellent dose distribution[1-2]. Clinical evidence of proton therapy, alone or combined with photon therapy, showed excellent tumor control and minimized normal tissue morbidity[3-5]. There are only few reports from GSI/Heidelberg of carbon ion radiotherapy for skull base tumor[6-7]. This paper describes the NIRS experience of carbon ion radiotherapy for skull base tumors.

## Result of Pilot study

Pilot study for skull base tumor was started on May 1995. Till the April of 1997, a total of 8 patients were enrolled into this study. They consisted of 4 cases of chordoma, 3 cases of memingioma and one case of metastatic adenocarcinoma. Their age ranged from 38 to 69 years with median age of 52 years. There were 4 male and 4 female patients. All of 8 cases were treated by 48 GyE through 16 fractions for 4 weeks.

Observed acute reactions were mild. There were only 2 patients with grade 1 acute reaction of the mucosa. There were no other acute reactions of the skin, the brain and the spinal cord. Also observed late reactions were mild. There were one patient with grade 2 late reaction of the brain and one patient with grade 1 late reaction of the spinal cord. There was no other observed late reaction of the skin and the mucosa.

One patient with chordoma showed PR and other seven patients showed SD (Fig. 1). Except one meningioma patient showed local recurrence at 6 months, other seven patients showed no evidence of re-growth till now.

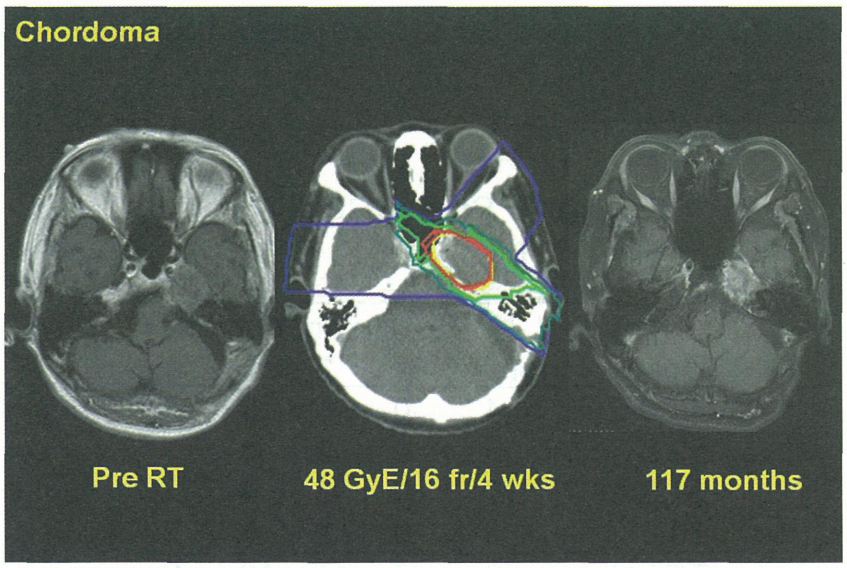


Fig. 1: Chordoma patient treated by 48 GyE/16fractions/4 weeks. The tumor shows no change in size 117 months after therapy.

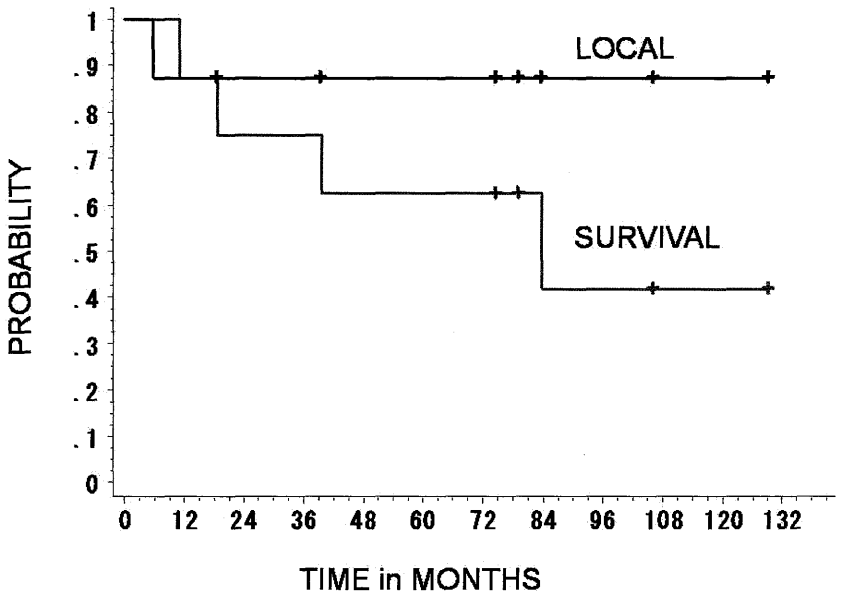


Fig. 2: Local control and survival curves of 8 patients in pilot study.

The 5 years and 10 years local control rate was 87.5% (S.E.: 11.7%) and 87.5% (S.E.: 11.7%)(Fig. 2). One meningioma patient died of local relapse at 11.1 month, one chordoma patient died of multiple lung metastases at 18.6 month, one metastatic adenocarcinoma patient died of multiple lung metastases at 39.5 month and one chordoma patient died of skip lesion of cervical bone at 83.9 months. The 5 year and 10 year survival rate was 62.5% (S.E.: 17.1%) and 41.7% (S.E.: 20.5%)(Fig. 2).

**Result of Phase I/II Dose Escalation Study**

The phase I/II dose escalation study for skull base tumor was started on April 1997. Till the August of 2003, a total of 29 patients were entered into the study. They were consisted of 16 cases with chordoma, 6 cases of meningioma, 5 cases of chondrosarcoma, one case of olfactory neuroblastoma and one case of giant cell carcinoma. Their age ranged from 21 to 68 years with median of 47 years. There were 11 male and 18 female patients. All patients were treated by 16 fractions for 4 weeks and total dose was 48.8 GyE for 4 patients, 52.8 GyE for 6 patients, 57.6 GyE for 10 patients and 60.8 GyE for 9 patients. Used number of ports was 2 ports for 11 patients, 3 ports for 16 patients and 4 ports for 2 patients (Table 1).

In acute skin reaction, one patient, who had 492.6 cm3 CTV and was treated by 48.0 GyE, showed grade 3

Phase I/II Study (Skull Base)

| | | Number of Port | | | |
|---|---|---|---|---|---|
| Dose | total | 1 | 2 | 3 | 4 |
| 48.0 GyE | 4 | 0 | 1 | 3 | |
| 52.8 | 6 | 0 | 2 | 4 | |
| 57.6 | 10 | 0 | 6 | 4 | |
| 60.8 | 9 | 0 | 2 | 5 | 2 |
| TOTAL | 29 | 0 | 11 | 16 | 2 |

Table 1: The number of ports in carbon ion radiotherapy for skull base tumor (phase I/II study).

reaction (Fig. 3). There was no other grade 3 or higher acute skin reaction (Table 2). In acute mucosal reaction, one patient, who had 345.6 cm3 CTV and was treated by 57.6 GyE, showed grade 3 reaction. There was no other grade 3 or higher acute mucosal reaction (Table 3). There was no observation of acute brain and spinal cord. In late reactions, observed maximum reactions were 1) grade 1 skin reaction in 4 patients, 2) grade 1 mucosal reaction in 2 patients, 3) grade 2 brain reaction in 2 patients, and 4) no reaction in the spinal cord.

Five year local control showed 79% in 16 chordoma patients, 80% in 6 meningioma patients and 100% in 5 chondrosarcoma patients (Fig.4). Five year over all survival showed 87% in chordoma, 83% in meningioma and 60% in chondrosarcoma (Fig. 5).

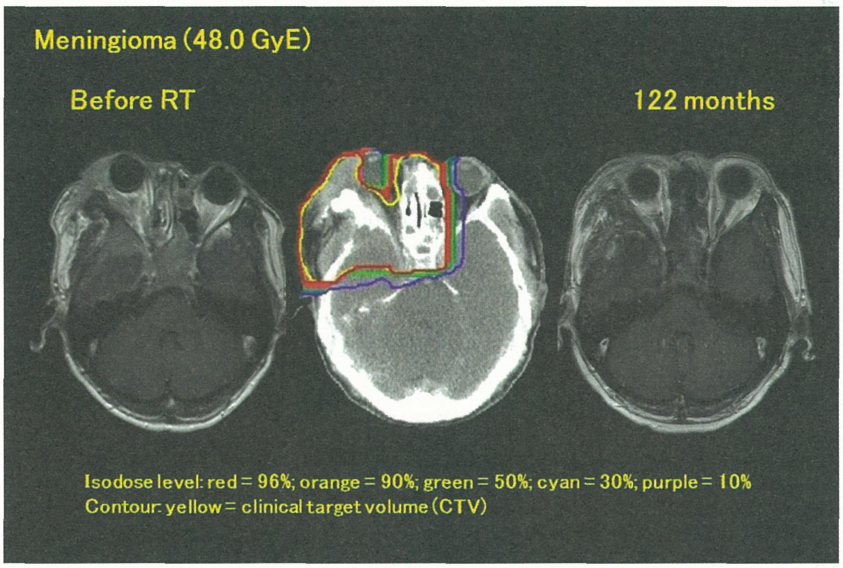


Fig. 3: Meningioma patient treated by 48 GyE/16fractions/4 weeks. The patient had 492.6 cm3 CTV and showed grade 3 skin reaction.

Phase I/II Study (Skull Base)

Acute Reaction (Skin)

| | | Grade | | | | |
|---|---|---|---|---|---|---|
| Dose | total | 0 | 1 | 2 | 3 | 4 |
| 48.0 GyE | 4 | 1 | 2 | 0 | 1 | |
| 52.8 | 6 | 2 | 2 | 2 | | |
| 57.6 | 10 | 4 | 6 | | | |
| 60.8 | 9 | 1 | 7 | 1 | | |
| TOTAL | 29 | 8 | 17 | 3 | 1 | 0 |

Table 2: Acute skin reaction in phase I/II study for skull base tumor.

Phase I/II Study (Skull Base)

Acute Reaction (Mucosa)

| | | Grade | | | | |
|---|---|---|---|---|---|---|
| Dose | total | 0 | 1 | 2 | 3 | 4 |
| 48.0 GyE | 4 | 4 | 0 | 0 | | |
| 52.8 | 6 | 4 | 0 | 2 | | |
| 57.6 | 10 | 4 | 5 | 0 | 1 | |
| 60.8 | 9 | 4 | 5 | | | |
| TOTAL | 29 | 16 | 10 | 2 | 1 | 0 |

Table 3: Acute mucosal reaction in phase I/II study for skull base tumor.

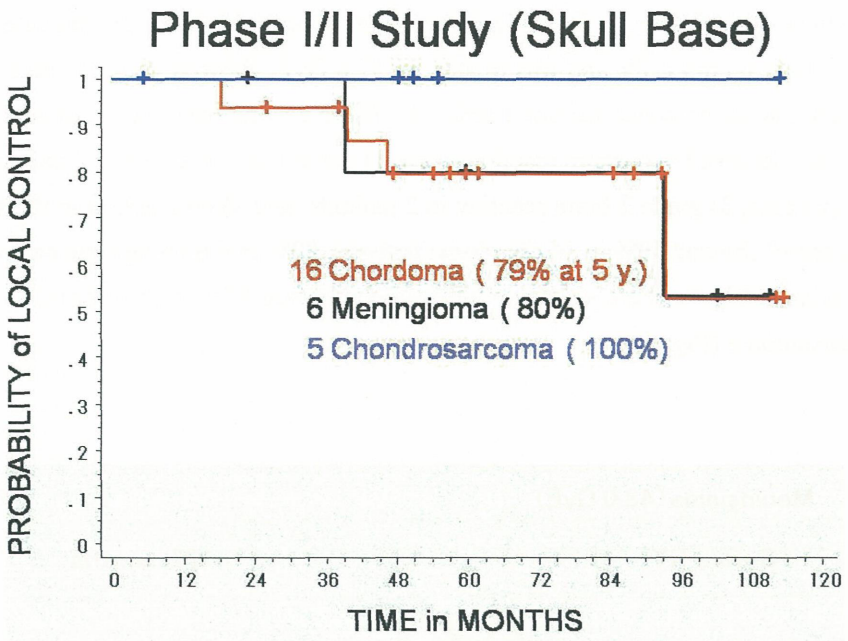


Fig. 4: Local control curves of 16 chordoma, 6 meningioma and 5 chondrosarcoma patients (Phase I/II study).

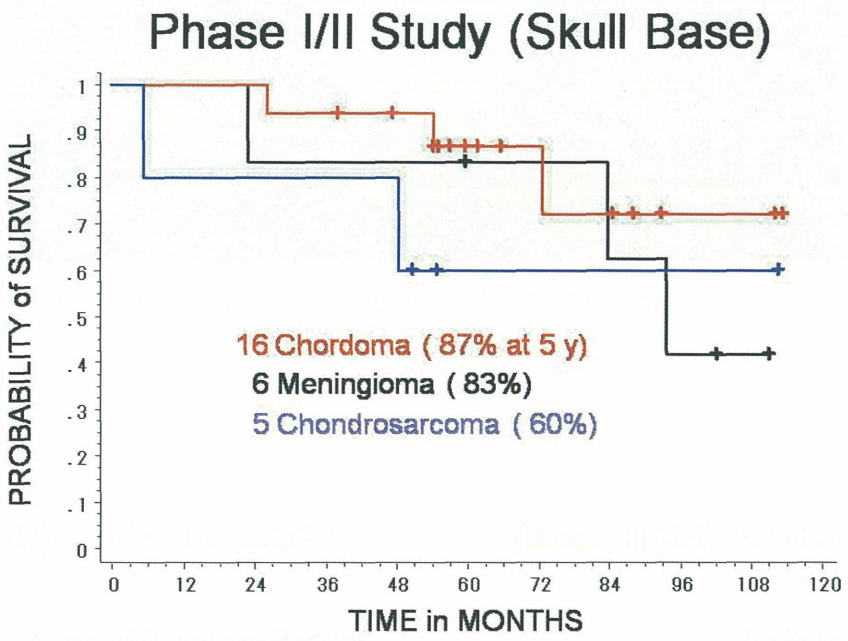


Fig. 5: Survival curves of 16 chordoma, 6 meningioma and 5 chondrosarcoma patients (Phase I/II study).

**Preliminary Results of Phase II Study**

From the April of 2004, a phase II study has been started for the skull base tumor. Till the July of 2007, a total of 18 patients were treated by a fractionation method of 60.8 GyE (3.8 GyE fraction dose) through 16 fractions for 4 weeks. Adding the patients who were treated by 60.8 GyE in the phase I/II study between the September of 2002 and the August of 2003, a total 27 patients were analyzed in this sesstion There were 19cases of chordoma, 5 cases of chondrosarcoma and 2 cases of olfactory neuroblastoma. Their age ranged from 16 to 78 years with median age of 52 years. There were 13 male and 14 female patients. Twenty out of 27 patients were treated by shrinkage field after 38 GyE through 10 fractions. CTV1 for initial 10 fractions ranged from 4 to 247 cm3 with median volume of 73 cm3 and CTV2 for followed 6 fractions ranged from 4 to 187 cm3 with

median volume of 53 cm3.

In the acute reactions, observed maximum reactions were one patient with grade 2 skin reaction and 3 patients with grade 2 mucosal reaction. There were no reactions of the brain and the spinal cord. In the late reaction, only one patient showed grade 1 brain reaction and there were no other grade 1 or higher normal tissue reactions.

Follow up periods of 27 patients ranged from 7 to 63 months with median of 38 months and there was no local relapse till the time of analysis (Fig. 6). One out of 19 chordoma patients died of liver dysfunction at 8.7 month. Three out of 5 chondrosarcoma patients died of 1) metastasis of the distant cervical vertebrae at 4.2 month, 2) bleeding from tumor bed at 5.4 month and 3) pneumonia at 48.4 month. All of these 4 patients were confirmed as having no local relapse at the expired time. Overall survival curves are shown in Figure 7.

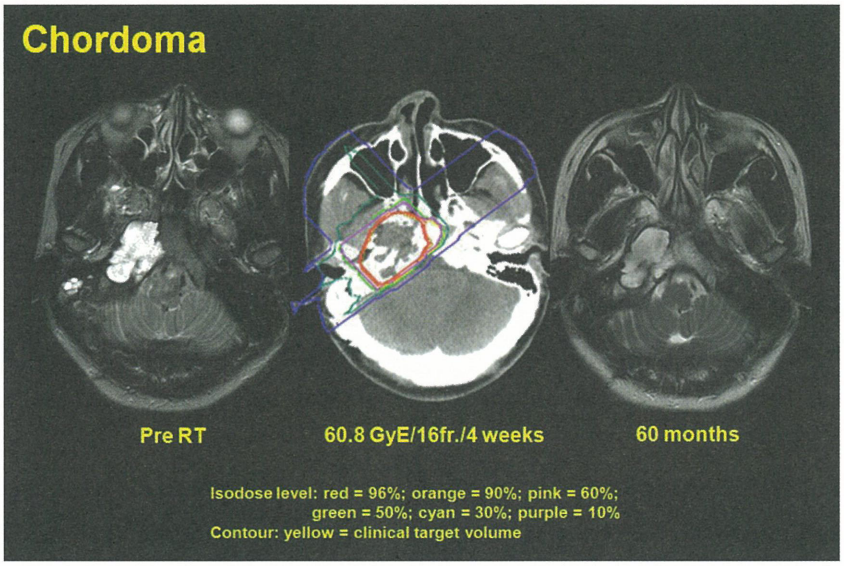


Fig. 6: Chordoma patient treated by 60.8 GyE/16 fractions/4 weeks. There is no re-growth of the tumor 60 months after therapy.

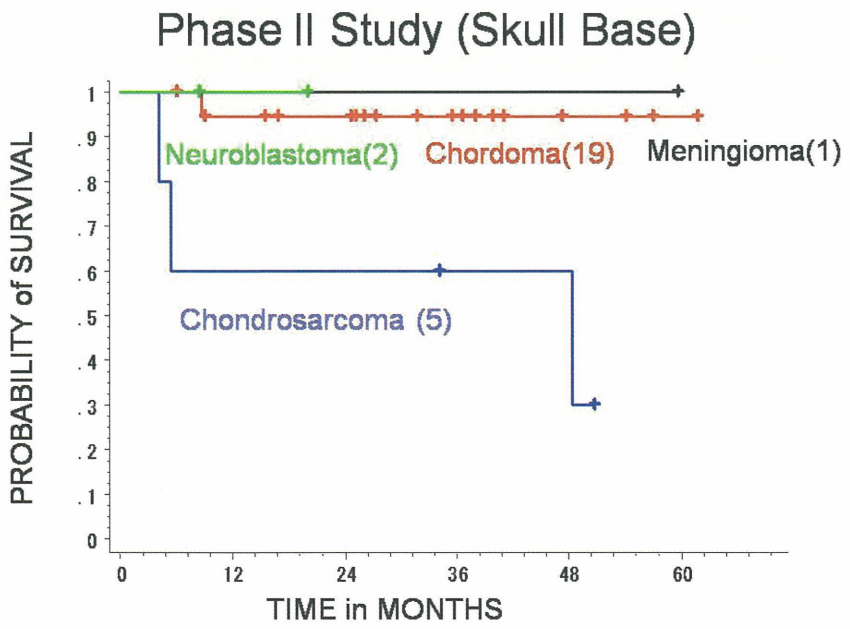


Fig. 7: Survival curves of 19 chordoma, 5 chondrosarcoma, 2 neuroblastoma and one meningioma patients (treated by 60.8 GyE in phase I/II + II study).

**Discussion**

Observed normal tissue reaction of phase II study is acceptable. Therefore, there will be some possibility of higher total dose than 60.8 GyE in NIRS study. Even if local control rate is 100% at present time and follow up periods is short, there will need careful and reliable follow up study of skull base patients for future total dose alternation.

**Conclusion**

Dose escalation study for skull base tumor concluded that 60.8 GyE/16 fractions/4 weeks is recommended dose for skull base tumor because of good local control rate.

With multi portal irradiation, normal tissues showed mild reaction and there is no severe morbidity of important organs.

**References**


1. Mendenhall WM, Mendenhall CM, Lewis SB, et al. Skull base chordoma. Head Neck. 2005; 27: 159-65.
2. Jereczek-Fossa BA, Krengli M, Orecchia R. Particle beam radiotherapy for head and neck tumors: radiobiological basis and clinical experience. Head Neck. 2006; 28:750-60.
3. Debus J, Hug EB, Liebsch NJ, et al. Brainstem tolerance to conformal radiotherapy of skull base tumors. Int J Radiat Oncol Biol Phys. 1997; 39:967-75.
4. Noel G, Feuvret L, Calugaru V, et al. Chordomas of the base of the skull and upper cervical spine. One hundred patients irradiated by a 3D conformal technique combining photon and proton beams. Acta Oncol. 2005;44:700-8.
5. Weber DC, Rutz HP, Pedroni ES, et al. Results of spot-scanning proton radiation therapy for chordoma and chondrosarcoma of the skull base: the Paul Scherrer Institut experience. Int J Radiat Oncol Biol Phys. 2005; 63: 401-9.
6. Schulz-Ertner D, Nikoghosyan A, Hof H, et al. Carbon ion radiotherapy of skull base chondrosarcomas. Int J Radiat Oncol Biol Phys. 2007; 67: 171-7.
7. Schulz-Ertner D, Karger CP, Feuerhake A, et al. Effectiveness of carbon ion radiotherapy in the treatment of skull-base chordomas. Int J Radiat Oncol Biol Phys. 2007; 68: 449-57.

# Inter-comparison between GSI and NIRS for Biological Effectiveness of Carbon Ions

Akiko Uzawa [*1], Koichi Ando[*1#], Sachiko Koike [*1], Yoshiya Furusawa [*1], Yoshitaka Matsumoto [*1], Nobuhiko Takai [*1], Ryoichi Hirayama [*1], Masahiko Watanabe [*1], Michael Scholz [*2], Thilo Elsässer [*2] and Peter Peschke [*3]

[*1]: Research Center of Charged Particle Therapy, National Institute of Radiological Sciences, Chiba, Japan
[*2]: Biophysics, Gesellschaft für Schwerionenforschung, Darmstadt, Germany
[*3]: Radiation Oncology, Deutsches Krebsforschungszentrum, Heidelberg, Germany

[#] Corresponding author: ando@nirs.go.jp

## INTRODUCTION

A phase I/II clinical study on carbon ion radiotherapy started at National Institute of Radiological Sciences (NIRS), Chiba, Japan in 1994. A total of nearly 3000 patients have been treated with HIMAC synchrotron by Year 2006, and are analyzed for toxicity and local tumor response (1). Clinical studies of carbon ion radiotherapy using SIS synchrotron also started at Gesellschaft für Schwerionenforschung (GSI), Darmstadt, Germany in 1997, and large effort has been paid to treat chordoma of the skull base (2). Clinical outcome of these two institutions has been well recognized and attract a lot of attention from worldwide. Therapeutic effectiveness of carbon ion beams depends on factors including physics and biology. Different from photon beams, carbon ion beams are biologically heterogeneous along with the beam path, due to change of linear energy transfer or LET. This heterogeneity is most prominent at Spread-Out Bragg peak or SOBP that targets deep-seated tumors in the patient body. As the SOBP of Chiba/HIMAC therapy is provided by use of a scatterer (3), projectile particles should be more fragmented within the SOBP than that of GSI/SIS which is made by changing beam energy and do not use any scatterer (4). It is therefore important to compare biological effectiveness of carbon ion beams between NIRS/HIMAC and GSI/SIS. We here have intercompared between the two beams using gut crypt survivals, and reported that the two beams are biologically identical to each other after single and daily-fractionated irradiation as well.

## MATERIALS and METHODS

Animals:

C3H/He female mice 10 to 12 weeks old were used. Mice were produced in specific pathogen free facilities at NIRS, and moved 2-3 days before start of irradiation to conventional environment in either NIRS or GSI. Anesthesia with ketamine and xyladine was used during irradiation. Mice were kept in a Lucite jig especially designed for gut irradiation, and they received horizontal beams. For each dose, either 3 or 4 mice were used.

Irradiation:

Carbon ions were accelerated to 290 MeV/u by HIMAC and SIS synchrotrons, and spread out to 6-cm width. The SOBP profile for the SIS synchrotron used in the experiment was adjusted to be the same as the SOBP profile being used for therapy at Chiba (3), and was different from that being used for therapy at Darmstadt. Using different thickness of tissue-equivalent absorbers, mouse jejunum was placed at 3 different positions within the 6-CM SOBP, i.e., middle position, 2-cm upstream form the middle position and 2-cm downstream form the middle position. Dose rates for HIMAC and SIS beams depended on irradiation position, and were

approximately 3 Gy/min and 1 Gy/min, respectively. Mice received either single dose irradiation or 3 fractionated doses with a fixed interval of 24 hr for 3 days.

Endpoint:

Crypt survivals were histologically measured. Jejunum was removed and fixed in formalin 3.5 days after irradiation. Histology preparations were made, and H&E staining was used to count microscopically the number of crypts surviving and regenerating. For non-irradiated control, the number of crypts per circumference section was between 120 and 145. Experiments were repeated 2 or 3 times for each synchrotron facilities, and the data obtained from each were combined for use. Obtained on survival curves were two iso-effect doses of D30, and D10, the doses required to reduce survivals to 30 and 10 crypts, respectively. Isoeffect doses were used to compare biological effectiveness between the two facilities.

## RESULTS

Figure 1 shows physical depth dose distribution of carbon ion beams used in the present study. Jejunum was irradiated at 3 positions indicated by arrows. Jejunum located 7 mm depth from abdominal skin surface, which was measured by a range absorber method. As shown in figure 2, mice were placed in a Lucite jig and received

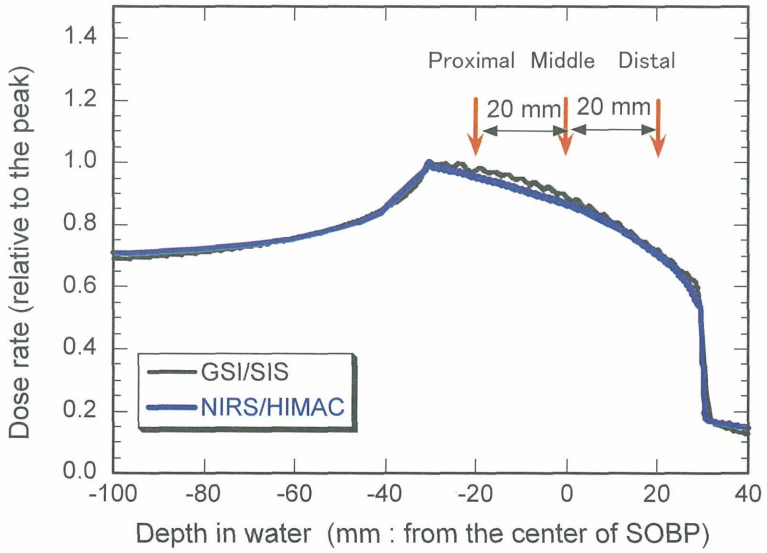


Figure 1 Depth dose distribution of Carbon-ion beams with a 6-cm SOBP
Arrows indicate three positions of gut irradiated with carbon ions.

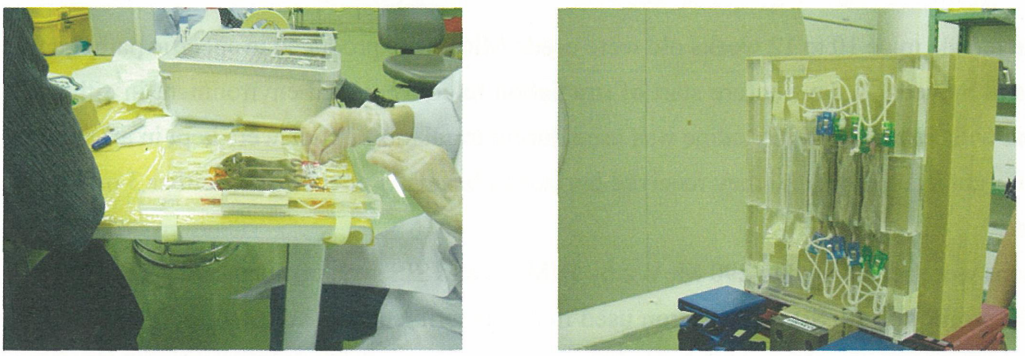

Figure 2 Mice immobilized in a jig.
Left panel: Receiving an IP injection of ketamine and xylazine, mice were placed in a Lucite jig. Hands and feet were picked by clothespins with strings. Right panel: Horizontal beams passed through a Lucite plate (4 mm thick) and abdominal wall before reaching to jejunum.

horizontal beams. Carbon ions pass through a 4-mm thick Lucite plate and abdominal wall before reaching to jejunum. First, physical doses of carbon 6-CM SOBP at various positions were measured (figure 3 A). Changing thickness of binary filters, doses sharply drop at the distal fall-of of the SOBP. Within 2 mm from the initial drop, doses decreased to nearly 1/10. The middle position of this drop was made by a use of 129 mm thick of binary filter. Second, jejunum crypt survivals were measured at various positions within the same 6-Cm SOBP. After a fixed dose of 10 Gy at a position made by 109 mm thick of binary filter, number of crypt survived this dose was 1.0 (figure 3B). Number of crypts gradually increased when thickness of binary filter increased from 114 mm, and reached to 130, almost an unirradiated level , at 123 mm thick. This increase is due to decrease of physical doses at the distal fall-off. What was different from physical fall-off was that the range of crypts increase was 9 mm and wider than the range of dose decrease. This indicates that jejunum was not flat to the horizontal beam, and partly bending back and forth in body. The middle position of the crypt drop was made by a use of 118 mm thick of binary filter. Subtracted 118 mm form 129, resulting 11 mm includes thickness of both the 4mm thick Lucite and abdominal wall, thickness of which could easily be calculated as 7 mm ( the water equivalent thickness of 4 mm Lucite is 4.64 mm) .

Figure 4 shows crypt survivals after single and fractionated dose of carbon-ion irradiation. The left panel is for proximal positions at NIRS and GSI, and indicates very similar dose response relationship between the two facilities. This similarity is also observed fort the middle (middle panel) and the distal (right panel) positions.

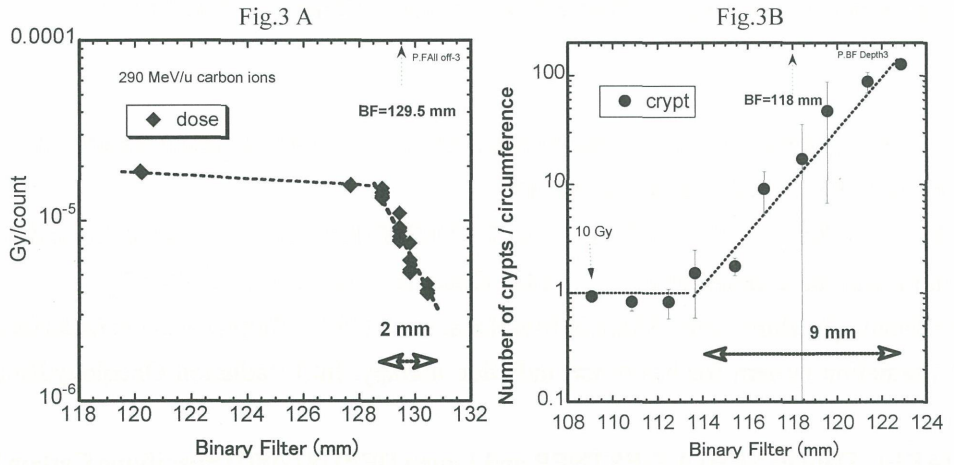


Figure 3 A method used to determine depth of jejunum in body.
290 MeV/u Carbon-ion beams with 6-cm SOBP were used. Left panel: Physical dose fall-off, right panel: Crypt survivals at the fall-of.

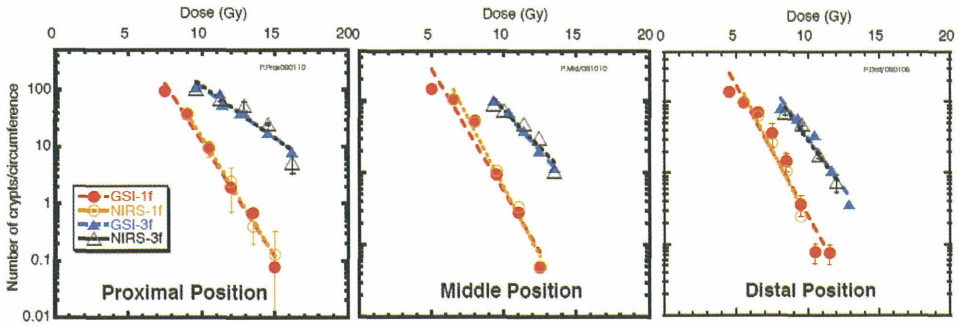


Figure 4 Crypt survivals after irradiation with carbon ions
Single doses for GSI were shown as red, closed circles, while single doses for NIRS as orange, open circles. For 3 fractions, GSI data were shown as blue, closed triangles, while NIRS data as open black triangles. Bar is standard deviation.

## DISCUSSION and CONCLUSION

We here presented and compared between GSI and NIRS for gut crypt survivals after irradiation with 6-cm carbon-ion SOBP profiles. Comparing isoeffect doses for single irradiation, a ratio of GSI to NIRS (GSI/NIRS) of carbon ions at $D_{30}$ were 1.02, 1.05 and 1.01 for proximal , middle and distal position, respectively. , while the ratio of GSI/NIRS at $D_{10}$ were 1.02, 1.03 and 1.00 for proximal , middle and distal position, respectively. Comparing isoeffect doses for fractionated carbon ions, the ratio at $D_{30}$ were 1.02, 1.00 and 0.99 for proximal , middle and distal position, respectively, while the ratio at $D_{10}$ were 0.98, 0.98 and 0.99 for proximal , middle and distal position, respectively. When we averaged these values, difference between GSI and NIRS beams is 1 %. We conclude that no difference between the two synchrotron facilities of carbon-ion beams was detected by the gut crypt survivals method, an in vivo dosimetry.

## ACKNOWLEDGEMENTS

We are grateful to Prof.Gerhard Kraft, Dr.Sylvia Ritter, Dr.Suo Sakata and Dr.Ryonfa Lee for their help to conduct experiments. The animals involved in these studies were procured, maintained and used in accordance with the Recommendations for Handling of Laboratory Animals for Biomedical Research, compiled by the Committee on the Safety and Handling Regulations for Laboratory Animal Experiments, NIRS. This report is partly supported by the Special Coordination Funds for Research Project with Heavy Ions at the National Institute of Radiological Sciences-Heavy-ion Medical Accelerator in Chiba (NIRS-HIMAC).

## References

1. Hirohiko TSUJII, Junetsu MIZOE, Tadashi KAMADA et al. (2006) Clinical Results of Carbon Ion Radiotherapy at NIRS, J.Radiat, Res. 48: A1-A13.
2. Schulz-Ertner D, Karger CP, Feuerhake A, et al. (2007) Effectiveness of carbon ion radiotherapy in the treatment of skull-base chordomas, Int J Radiat Oncol Biol Phys. ;68(2): 449-57
3. Tatsuaki Kanai, Masahiro Endo, Shinichi Minohara, et al. (1999) Biophysical characteristics of HIMAC clinical irradiation system for heavy-ion radiation therapy, Int.J.Radiation Oncology.Biol.Phys. 44(1), 201-210,
4, Oliver JAKEL, Daniela SCHULZ-ERTNER and Jurgen DEBUS (2007) Specifying Carbon Ion Doses for Radiotherapy: The Heidelberg Approach , J.Radiat, Res. 48: A87-A95

# Relative Biological Effectiveness (RBE) of Carbon Ions in the Normal Central Nervous System (CNS).

Peter Peschke[1], Christian P. Karger[2], Michael Scholz[3], Juergen Debus[4], Peter Huber[1,4]

[1] Clinical Cooperation Unit Radiation Oncology, DKFZ Heidelberg, Germany
[2] Dept. of Medical Physics in Radiation Oncology, DKFZ Heidelberg, Germany
[3] Dept. of Biophysics, GSI Darmstadt, Germany
[4] Dept. of Clinical Radiology, University of Heidelberg, Germany

## Introduction

Higher precision and an improved biological effectiveness were the main driving forces in experimental radiotherapy for the past 100 years. Particle radiotherapy using protons and carbon ions closely meet these demands, because ion beams have millimeter precision and an inverse depth-dose profile with an increase of the dose with depth. In addition to these physical advantages, heavy charged particles such as carbon ions exhibit an increased relative biological effectiveness (RBE) in the Bragg peak relative to the plateau region. While several medical facilities exploit energetic protons to treat deep-seated tumors, the use of carbon ions is limited to two hospital based facilities in Japan and a pilot project in Germany at GSI. The first dedicated European clinical heavy-ion therapy (HIT) facility in Heidelberg (Germany) will soon be open for patient treatment. In Europe, an active beam scanning technique is used for dose delivery. Compared with passive beam delivery techniques favored in Japan, beam scanning allows for dose conformation not only at the distal but also at the proximal edge of the tumor for each field [1]. An important consequence of the beam scanning technique with heavy ions is the necessity to calculate tumor and normal tissue RBEs separately for each point within the complete treatment field. Yet, one has to keep in mind that although ion beams exhibit a previously unattained precision in dose delivery, there will always be small volumes of normal tissue in the high-dose volume. These might be normal tissue in the beam entrance channels, especially those close to the target volume, as well as normal tissue in the target volume itself which cannot be spared for various reasons.

The determination of biological effective doses is done by use of the local effect model (LEM). Such biophysical models are required, because the RBE of ion beams exhibits a complex dependence on many physical and biological parameters such as beam energy and LET, penetration depth, dose level and the repair capacity of the tissue as well as on the selected biologic endpoint [2]. The LEM is implemented in the treatment planning system and enables the assignment of "individual" RBEs to each of the millions of voxels in a patient CT [3]. Pilot studies at GSI focused on radioresistant skull-base tumors, locally advanced adenoid cystic carcinomas and paraspinal tumors, which are difficult to treat, because a sufficient high dose often cannot safely be delivered in general with conventional radiation, due to the tolerance doses of neighboring radiosensitive normal tissues. Unfortunately, in most cases the radiation tolerance of these critical normal structures are not known precisely, because of uncertainties in the RBE of the carbon ions ($^{12}C$). To exploit the role of carbon ions for late complications in the normal central nervous system (CNS), normal rat brain as well as the rat spinal cord was used as a late effect model to determine the radiotolerance of photon and carbon ion irradiations.

**Response of the normal rat brain.**

In 1997 we have started our investigations with a study applying single doses of carbon ions and photons to the right frontal lobe of the normal rat brain. Animals were irradiated stereotactically at the right frontal lobe using an extended Bragg-peak with maximum doses between 15.2 and 29.2 Gy. Late changes in the normal brain, detected by T1- and T2-weighted magnetic resonance imaging (MRT) were taken as basis to calculate dose-response curves. For follow up, two biological end points were selected at 12, 14, 16 and 20 months: (A) any contrast enhancement in the brain after injection Gd-DTPA in T1-weighted MRI, and (B) any hyperintense signal in the brain in T2-weighted MRI.

Radiation-induced tissue alterations of the normal rat brain monitored by MRI exhibited a time-dependent progression up to 17 month post irradiation and remained stationary after that time. At 20 months the tolerance doses at the 50% effect probability level were 20.3 ± 2.0 Gy and 22.6 ± 2.0 Gy for changes in T1- and T2-weighted MRI, respectively [4]. The RBE, as calculated on the basis of a previous identical animal study with photons was 1.95 ± 0.2 and 1.88 ± 0.18 for T1- and T2-weighted MRI [5].

This study represented the first published quantitative analysis of carbon ion-induced late effects in the normal brain. Remarkable was the differential behavior of the selected biological endpoint: Beyond 17 months the MRI changes remained in a progressive state for photons, whereas the tolerance dose for carbon ions was already stationary. This situation lead to decreasing tolerance doses for photons and hence to some extend time-dependent RBE-values. No significant difference in RBE was found for the two MRI end points. Although the tolerance doses for the two MRI techniques were quite different, the RBE-values are nearly the same. Moreover, the comparison of our results with a parallel performed single dose study on carbon ion-induced myelitis of the rat spinal cord yielded a rather good agreement with respect to RBE. This holds in spite of the different tissue architecture and the different biological endpoints. The labor intensive treatment procedures with individually positioned animals in a stereotactic frame, the elaborative follow-up by MRI and the suboptimal biological endpoint supported the decision that for systematic measurements of normal-CNS complications the spinal cord might represent the more suitable model.

**Tolerance of the rat spinal cord.**

The cranial part of the spinal cord of the rat was irradiated with 1, 2, 6 or 18 fractions of photons or $^{12}$C-ions, respectively. Plateau irradiations were performed in the entrance region of a 270 MeV/u Bragg-peak, while for the peak irradiations a 10 mm spread-out-Bragg-Peak of 140 MeV/u. was used. Animals were followed up for 300 days after irradiation for the onset of paresis grade II. Dose response curves were calculated for each irradiation experiment and $D_{50}$-values (dose at 50% complication probability) were determined. Based on these $D_{50}$-

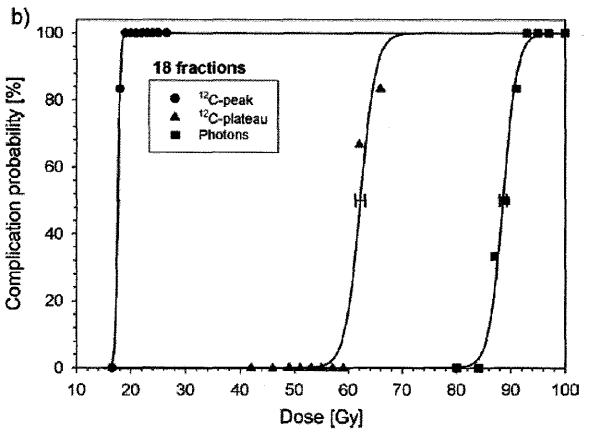


Fig. 1. Dose-response curves for late complications of the rat spinal cord after 18 consecutive fractions of carbon ions in a 10 mm spread-out Bragg peak (circles), in the entrance channel of 12C-ions (triangles) and photons (squares). (reprinted from [7] with permission from Elsevier)

values, the RBE and the related α/β-parameters were calculated. The measured RBE-values were compared with predictions of the local effect model (LEM).

The experimentally determined RBE-values for 1, 2, 6 and 18 fractions were 1.44±0.08, 1.37±0.05, 1.33±0.02 and 1.42±0.02 for the plateau- and 1.77±0.06, 2.17±0.06, 2.97±0.05, and 5.04±0.08 for the peak-irradiations. The respective predictions by the LEM were 1.14, 1.19, 1.37, and 1.72 for the plateau- and 1.28, 1.61, 2.35, and 3.80 for the peak irradiations. The α/s-values derived by logistic regression were 2.8±0.4 Gy for photons, 2.1±0.4 Gy for the plateau and 37.0±5.3 Gy for the peak-irradiations, respectively [6,7].

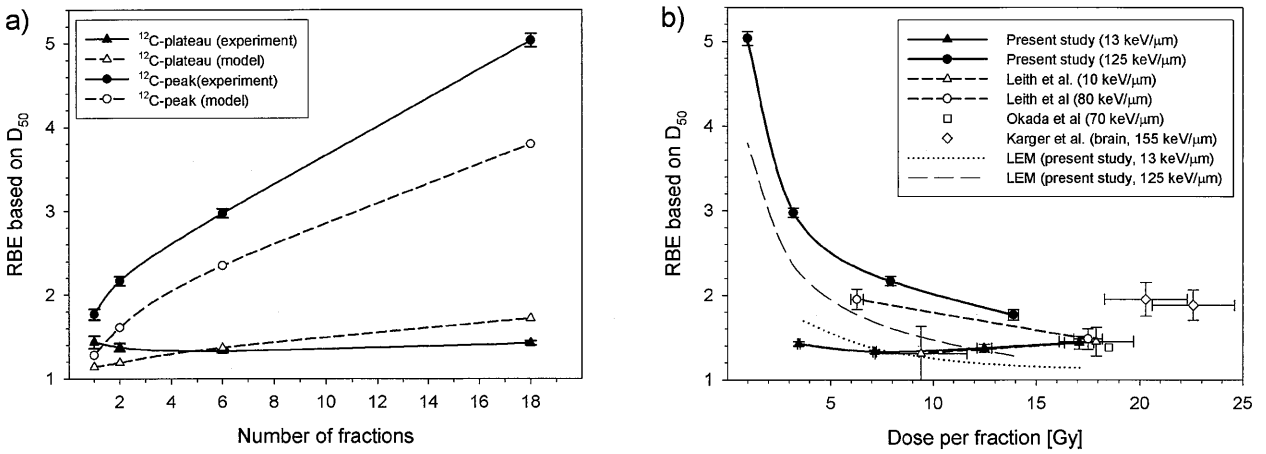


Fig. 2. Radiation-induced myelitis in the rat spinal cord: Dependence of the relative biological effectiveness (RBE) on fraction number (a) and dose (b). (reprinted from [7] with permission from Elsevier).

Carbon ion irradiations of the spinal cord are significantly more effective in the peak than in the plateau region. A significant fractionation effect was only found for the plateau-irradiations. For the peak irradiations, the LEM correctly describes the dose dependence of the RBE, although it generally underestimates the RBE by 25%. In the plateau region, overestimations of up to 20% were found for the clinically applied low doses per fraction. The experimental data contribute to the validation of the LEM and quantify the involved uncertainties

**Discussion and Conclusion**

As a complementation to experiments performed at NIRS focusing on early reacting normal tissues, we have directed our interest to late complications in the normal tissue of the CNS. In our hands, the spinal cord tissue model turned out to be a reliable system to exploit different radiation qualities, especially with respect to their role in late radiation effects. Up to now, only few experimental data on the RBE of carbon ions were available for the CNS. Morphological parameters were in the focus of normal brain studies. The effects of carbon-ion irradiation and X-irradiation on the development of rat brain were compared on the histological level showing that the effects of both carbon-ion irradiation and X-irradiation on the development of rat brain are similar in character. The effect of 1.5 Gy carbon-ion irradiation compares to that of 2.0 or 2.5 Gy X-irradiation [8]. Impact of heavy ions on postnatal mouse cerebella development have been described [9] showing in vivo evidence of more pronounced apoptotic cell death after carbon ion treatment. The pathogenesis of delayed encephalopathy in cats induced by carbon ions was characterized by a long-standing edema of the white matter due to vascular hyperpermeability, and the vascular dilatation seemed to be caused by a reduction in the vascular bed and/or hemoconcentration due to hyperpermeability [10].

The latency interval for the development of limb paralysis after the irradiation of the rat spinal cord with fractionated doses of charged particles in the plateau and Bragg-peak regions was first examined by Leith et al. and

Rodriguez et al. [11-13]. Their results showed a distinct decreased tissue tolerance in the high-LET Bragg-peak region. The RBE of high-LET beams of charged particles, for spinal cord injury, is known to be in the range of 1.2 to 3.0 [14, 15] with the RBE being lower for single compared to fractionated doses [12]. This database is significantly extended by the present study, especially in the clinically relevant region of low doses per fraction. Moreover, the results clearly demonstrate that in vivo studies with well characterized biological endpoints are helpful contributions to better define the tolerance doses needed for normal tissues. The experimental data contributed to the validation of the LEM and helped to quantify the involved uncertainties.

In the course of the clinical pilot studies at GSI only a few tumor types have been treated, mostly brain, head-and-neck, and spinal cord cancers. One of the challenges for the upcoming new medical facilities, will be to verify if the rasterscan-based treatment can be successfully extended to a number of other tumor sites. As normal-tissue tolerance remains the limiting factor for a general extension to new tumor sites, it is for these sites that more information on normal-tissue response is urgently needed to minimize the risk associated with the treatment. Likewise, as a consequence of the physical and biological enhanced effectiveness, hypofractionation (large fraction sizes) is taken in consideration and in a number of cases patients have been treated with better tumor control than conventional therapy [16]. Systematic in vivo measurement combined with an radiobiology modeling of fractionation effects should help to answer the question to what extent a fractionation scheme remains its advantage in reducing the risk to normal tissue. Last but not least, studying the molecular mechanisms underlying carbon ion irradiation on normal tissues effects might not only help to understand clinical response but also might open new avenues for the development of interventional strategies for patients undergoing carbon ion therapy.

**Acknowledgements:**

We thank Alexandra Tietz, Uschi Schierbaum, Karin Leotta and Rainer Kuhnlein (DKFZ) for their excellent technical support. We also thank Dr. Rita Sanchez-Brandelik, University of Freiburg, Germany, Prof. Albert van der Kogel, Univ. Nijmegen, NL and Prof. Eric W. Hahn, U.T. Southwestern Medical School at Dallas, TX, USA for their help with the experimental set up and design of the study.

**References**

1. Kraft G. (2000) Tumor therapy with heavy charged particles. Prog. Part. Nucl. Phys. 45: S473.S544.
2. Scholz M., Kellerer A.M., Kraft-Weyrather W., Kraft G. (1997) Computation of cell survival in heavy ion beams for therapy. The model and its approximation. Radiat. Environ. Biophys. 36: 59-66, 1997.
3. Kramer M, Weyrather WK, Scholz M. (2003) The increased biological effectiveness of heavy charged particles: from radiobiology to treatment planning. Technol Cancer Res. Treat. 2: 427-436.
4. Karger CP, Munter MW, Heiland S, Peschke P, Debus J, Hartmann GH. (2002) Dose-response curves and tolerance doses for late functional changes in the normal rat brain after stereotactic radiosurgery evaluated by magnetic resonance imaging: influence of end points and follow-up time. Radiat. Res. 157: 617-625.
5. Karger CP, Debus J, Peschke P, Munter MW, Heiland S, Hartmann GH. (2002) Dose-response curves for late functional changes in the normal rat brain after single carbon-on doses evaluated by magnetic resonance imaging: influence of follow-up time and calculation of relative biological effectiveness. Radiat. Res. 158: 545-555.
6. Debus J., Scholz M., Haberer T., Peschke P., Jakel O., Karger C.P., Wannenmacher M. (2003) Radiation

tolerance of the rat spinal cord after single and split doses of photons and carbon ions. Radiat. Res. 160: 536-542.

7. Karger C.P., Peschke P., Sanchez-Brandelik R., Scholz M., Debus J. (2006) Radiation tolerance of the rat spinal cord after 6 and 18 fractions of photons and carbon ions: experimental results and clinical implications. Int. J.Radiat. Oncol. Biol. Phys. 66: 1488-1497.
8. Inouye M, Takahashi S, Kubota Y, Hayasaka S, Murata Y. (2000) Similarity between the effects of carbon-ion irradiation and X-irradiation on the development of rat brain. J Radiat Res (Tokyo).41: 303-311.
9. Kinoshita C., Yaoi T., Nojima K., Fushiki S. (2003) The effects of heavy ion particles on the developing mirine cerebellum, with special reference to cell death. Acta Histochem Cytochem. 36: 145-151.
10. Okeda R, Okada S, Kawano A, Matsushita S, Kuroiwa T. (2003) Neuropathology of delayed encephalopathy in cats induced by heavy-ion irradiation. J Radiat Res (Tokyo). 44: 345-352.
11. Leith,T., Woodruff K.H., Howard J., Lyman T., Smith P., Lewinsky B.S. (1977) Early and late effets of accelerated charged particles on normal tissue. Int. J. Radiat. Oncol. Biol. Phys. 3: 103-108.
12. Leith J.T., McDonald M., Powers-Risius P., Bliven S.F., Howard J. (1982) Response of rat spinal cord to single and fractionated doses of accelerated heavy ions. Radiat. Res. 89: 176-193.
13. Rodriguez A., Alpen E.L., DeGuzman R.J. Irradiation of rat thoraco-lumbar spinal cord with fractionated doses of helium and neon ions. In Proceedings of the 8th International Congress of Radiation Research, Vol. 1, pp. 249.
14. Geraci J.P. and Mariano M.S. (1994) Relationship between dose and the latent period for radiation myelopathy in rats. Radiat. Res. 140: 340-346.
15. Okada S., Okeda R., Matsushita S. Kawano A. (1998) Histopathological and morphometric study of the late effects of heavy-ion irradiation on the spinal cord of the rat. Radiat. Res. 150: 304-315.
16. Tsujii H, Mizoe J, Kamada T, et al. (2007) Clinical Results of Carbon Ion Radiotherapy at NIRS. J Radiat Res (Tokyo). 48 Suppl A: A1-A13.

Corresponding Author:
Peter Peschke, Ph.D.
Department of Radiation Oncology German Cancer Research Center Im Neuenheimer Feld 280
69120 Heidelberg, Germany
Email: P.Peschke@dkfz.de

# 産総研における線量標準の現状と今後

独）産業技術総合研究所計測標準研究部門量子放射科
放射線標準研究室　黒澤　忠弘

Corresponding: tadahiro-kurosawa@aist.go.jp

## 1．はじめに

当所では、X線・γ線の線量標準として、空気カーマ・照射線量を供給している。線量の強度としては、環境・防護・診断・治療領域をカバーしている。また放射線防護のために、β線による組織吸収線量標準も設定を行い、2006年度から校正を開始した。本報告では、これらX線・γ線・β線の線量標準に関して概説し、最後に今後の計画について簡単に紹介する。

## 2．X線標準

産総研ではX線照射施設として、管電圧10kV～50kVの軟X線照射室、管電圧40kV～300kVの中硬X線照射室の二つを有している。X線の線質を表す指標として次式に示すQI値（Quality Index）を用いている。

$$QI = \frac{E_{eff}}{E_{tube}} \qquad (1)$$

ここで、Etubeは管電圧（kV）、Eeffは実効エネルギー（keV）で、実効エネルギーは基準電離箱による電流測定によって得られた半価層から求めている。中硬X線では、管電圧が40, 50, 60, 75, 100, 125, 150, 175, 200, 225, 250kV、QI値は0. 4, 0. 5, 0. 6, 0. 7, 0. 8, 0. 9が、また軟X線では管電圧10, 15, 20, 30, 40, 50kV、QI値が0. 4, 0. 5, 0. 6, 0. 7, 0. 8の条件で照射場を設定している。

照射線量の絶対測定を行うために、軟、中硬X線とも自由空気電離箱を用いている。自由空気電離箱の概略図を図１に示す。軟X線では空気による減衰の影響が大きいことから、小型の自由空気電離箱を用いている。自由空気電離箱で照射線量を測定する場合に基準となる位置は規程面と呼ばれ、電離箱のX線入射口の絞りの内側に設定されている。規程面の面積と集電極のビーム軸方向の長さとの積を空気体積といい、この容積が感度に比例する。

測定した電流に対して以下に上げる様々な補正等を行い、照射線量を求めている。[1]

1）空気質量の算出：測定時における気温、気圧による空気密度の補正
2）湿度補正：空気中の湿度による電離量の補正
3）再結合補正：イオン再結合により飽和電流が得られないための補正
4）空気減衰補正：規程面と電流を測定している集電極中心との間の空気層によるX線の減衰を補正
5）電子損失補正（Kel）：電離箱内で生じた高速電子が電極等にエネルギー付与した分の補正
6）散乱線補正（Ksc）：電離箱内で生成された二次光子による電離量の補正
7）入射口散乱・透過補正:入射口側面によって生成された散乱線による電離量の補正、またエッジ部分を透過した光子による電離量の補正

上記の５）、６）、７）に対する補正係数は測定から求めることは非常に困難であることから、シミュレーションによる計算によって補正係数を評価している。図２にEGSコード［2］によって求められた補正係数の例を示す。[3]

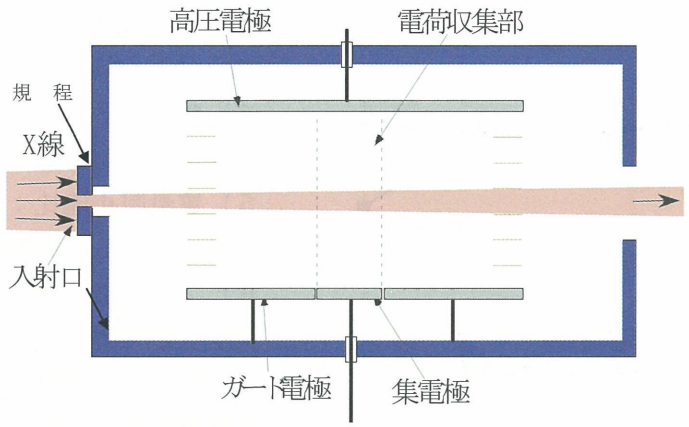


**図１　自由空気電離箱の構造**

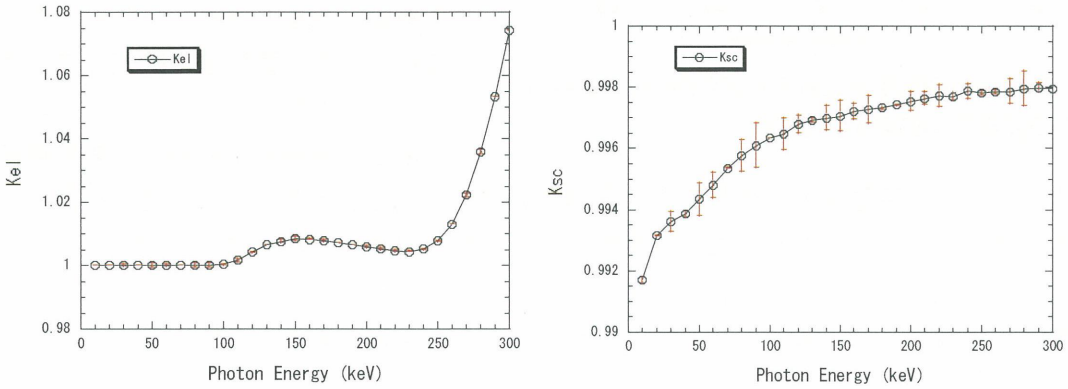


**図２　中硬Ｘ線用自由空気電離箱の電子損失、散乱線補正係数。単色エネルギー光子に対する結果である。**

## ３．　γ線標準

γ線照射施設として、小γ線源照射室及び大γ線源照射室の二つがある。照射に使用している線源は以下のものである。

小γ線源照射室：Cs-137--- 222GBq,　18.5GBq,　1.85GBq
Co-60---- 185GBq,　18.5GBq,　3.7GBq

大γ線源照射室：Cs-137--- 34TBq
Co-60---- 134TBq

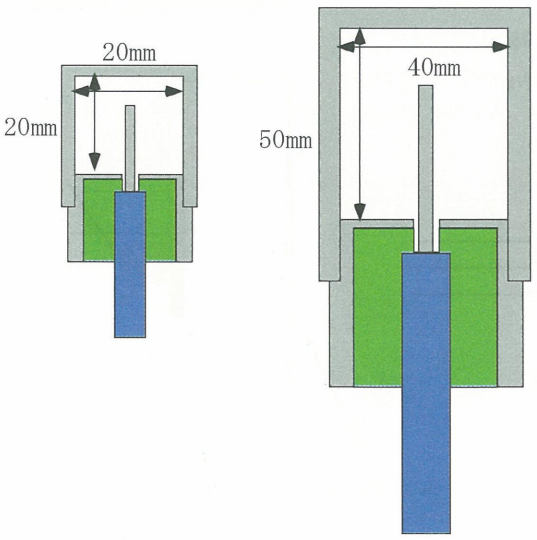


**図３　グラファイト壁空洞電離箱の概略図。右側の空洞容量は約60ml，左側は約6ml。**

γ線照射線量の測定には、グラファイト壁空洞電離箱を用いている。これはBragg-Grayの空洞理論を基にしている。線量率の違いにより、図３に示すような空洞容積の異なる２種類の円筒型空洞電離箱を用いて絶対測定を行っている。[4, 5]

空洞電離箱の場合も、測定された電離電流に様々な補正、換算を行って照射線量を求めている。

１）空気質量の算出:測定時における気温、気圧による空気密度の補正

２）湿度補正：空気中の湿度による電離量の補正

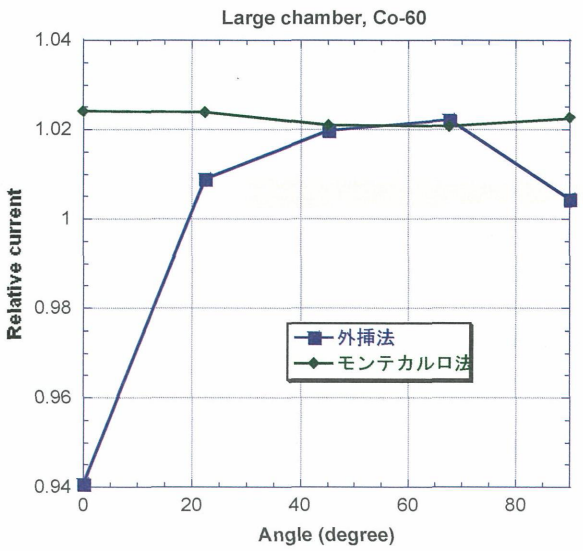


図４　電離箱の電離電流に対する外挿法とEGSコードによる壁補正後の照射角度依存

３）再結合補正：イオン再結合により飽和電流が得られないための補正

４）質量エネルギー吸収係数比：壁材のグラファイトから空気への換算

５）質量阻止能比：空洞内物質の空気からグラファイトへの電子阻止能の換算

６）ステム散乱補正：電離箱を支えているステムからの散乱線の寄与を補正

７）壁補正:電離箱壁によるγ線の減衰、また壁内で生成された散乱線を補正

１）～６）は、測定または評価されている物理定数から求めているが、７）に関しては、従来の測定法に問題があることが分かり、現在はシミュレーションによる計算によって評価している。その計算例として図４を示す。これは電離箱の設定角度を０度から90度まで変化させた場合の、従来の壁補正手法であった外挿法とシミュレーションによる壁補正を行った後の比較である。図からも明らかなように、電離箱の照射角度を変えると外挿法では補正が十分ではなく補正後の値が一定ではない。これは壁による減衰が角度によって異なるためで、シミュレーションによる補正を行うことによって値が一定となることが分かった。[6]

## ４．β線標準

β線組織吸収線量標準は旧電総研時に一度設定されたが［7]、照射装置、測定器とも老朽化し、近年では使用されていなかった。そこで、β線標準に関するISO規格［8］に準拠した照射装置、また絶対測定を行うための外挿電離箱を製作し、再設定を行った。

β線源としてはPm-147，Kr-85，Sr-90/Y-90の三種類で、照射場を均一にするために線源と基準位置の間にフラッタリングフィルターを設置している。図５に照射装置及び外挿電離箱の概略図を示

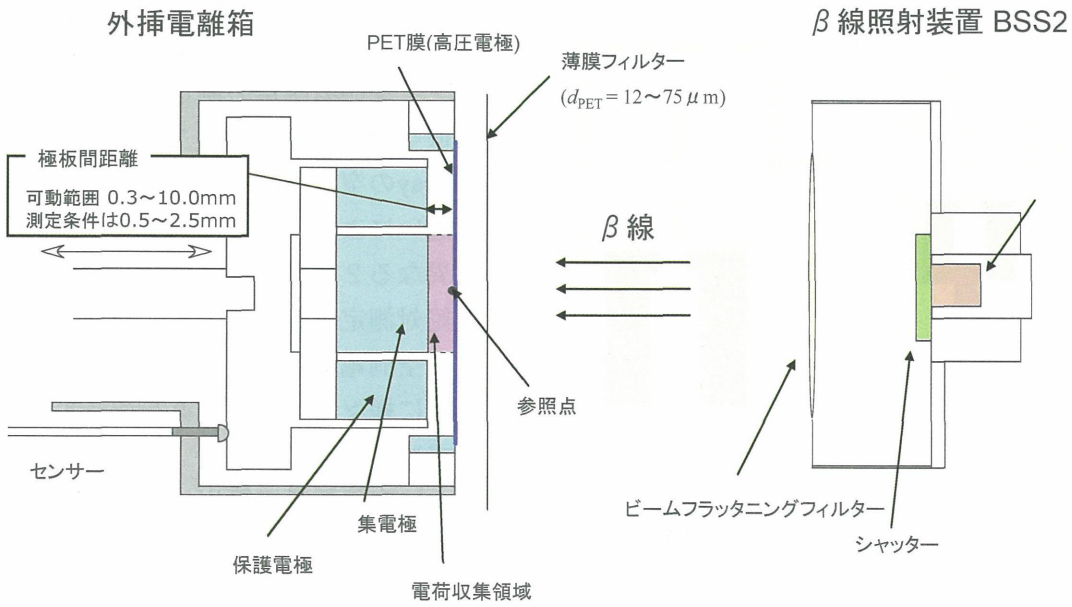


図５　外挿電離箱及び照射装置概略図

す。検出器前面はアルミコーティングされたPET膜で、電離箱の高電圧極となっている。集電極及び保護電極は可動式となっており、電極間隔を0.3mm～10mmまで変化させながら電離電流値を測定することが可能である。

外挿電離箱による7mg/cm$^2$深部の組織吸収線量率$\dot{D}$（0.07）は、電極間隔$l$の関数としての電離電流値$I(l)$を用いて、次式により求める。

$$\dot{D}(0.07) = s_{t,a}\frac{\overline{W_0}}{e}\frac{1}{\rho_{a0}a}\left[\frac{\mathrm{d}}{\mathrm{d}l}KI(l)\right]_{l=0} \qquad (2)$$

ここで$s_{t,a}$は、$\beta$線に対する組織と空気の平均質量阻止能比で、外挿電離箱で計測される電離箱内の空気吸収線量を、組織吸収線量に換算するための係数である。$(\overline{W_0}/e)$は、参照条件（気温20℃、大気圧1013hPa、相対湿度65％）における空気の平均の$W$値と素電荷の比で、電離箱で計測される電離電荷量を吸収エネルギーに変換するための係数である。$a$は集電極の実効的な面積で、$\rho_{a0}$は標準状態の空気の密度である。

$\left[\frac{\mathrm{d}}{\mathrm{d}l}KI(l)\right]_{l=0}$は電流値増加量を極板間隔増加量で割った商の極板間隔0における極限であり、$K$は各種の補正係数の積を表している。補正された電流値$KI(l)$は電極間隔$l$に対して大まかには比例関係を示す。測定により得た$KI(l)$に対して二次式でフィッティングを行い、得られた二次式に基づいて$\left[\frac{\mathrm{d}}{\mathrm{d}l}KI(l)\right]_{l=0}$を求める。

## 5．　放射線標準の今後の計画について

### 5．1　水吸収線量標準の開発

医療、特に放射線治療分野の基準となっているCo-60に対する水吸収線量標準の開発を進めている。水吸収線量の定義としては、単位質量あたりの水に吸収されるエネルギーであり、J/kg (=Gy)である。本研究では、吸収されるエネルギーを測定するためにグラファイトカロリーメータ［9］を用いている。図６にその概略図を示す。熱量測定部となるコアと、その周りを覆うジャケット、シールドからなる。コア、ジャケット、シールドとも温度測定用サーミスター、温度調整用ヒーターが内臓されている。外部からの熱雑音を小さくするために、各領域の間には真空層を設けている。Co-60γ線による温度上昇率は、一分の照射で約1m℃と非常に小さいため、サーミスターの微小な抵抗の変化を測定する必要がある。本システムでは、交流ブリッジ回路による変化量の測定を行っている。

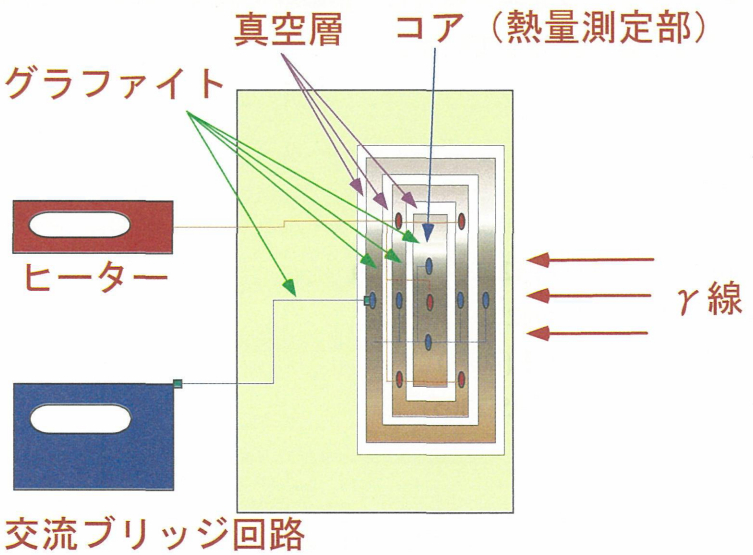


図６　グラファイトカロリーメータ概略図

カロリーメータによって測定される量はグラファイト吸収線量であり、水吸収線量への変換が必要となる。図７に変換のための概念図を示す。グラファイトカロリーメータで評価したグラファイト吸収線量を、一度仲介器である空洞電離箱に同一のファントム中で値付けする。これを水中のファントムに移し、水中でのグラファイト吸収線量を評価する。グラファイトから水吸収線量へは、質量エネルギー吸収係数によって換算を行い、最終的に水中のある深さにおける水吸収線量を評価することができる。校正を行う際には、水ファントム中に被校正機器を設置し測定を行うことになる。

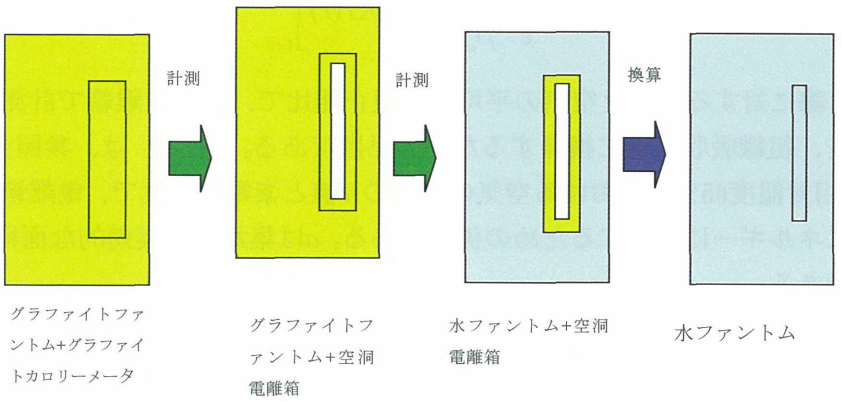


**図７　グラファイトカロリーメータから水吸収線量評価のためのステップ概念図**

５．２　マンモグラフィ線質の開発

マンモグラフィを用いた乳癌検診が急速に普及しており、その品質管理のためにその線質に対応した標準の供給が重要となっている。産総研では低エネルギーのＸ線発生装置としてはタングステンターゲットの管球を所有しているのみであったが、社会のニーズに合わせるため、新たにモリブデンターゲットのＸ線管球を導入した。現在は照射装置の特性評価を行っており、2008年度中にはIEC61267に示されている線質を開発し供給を開始したいと考えている。

５．３　I-125小線源空気カーマ

小線源治療に用いられているI-125の基準線量は、線源から1m離れた位置での空気カーマ率となっている。線源はおよそ15MBqであることから、微小電流を測定する困難さがある。将来的には外挿型の自由空気電離箱による絶対測定を予定しているが、この治療の急速な普及により迅速な標準供給のニーズが高まっている。そこで日本アイソトープ協会と協力し、産総研の軟Ｘ線場において校正された大型の空洞電離箱を用いて校正する手法を開発している。

参考文献

[1] 松本健、直井次郎、電総研彙報, 47, 28(1983)
[2] H. Hirayama et.al., SLAC-R-730(2005)
[3] T.Kurosawa, N.Takata, Y.Koyama, J. Nucl., Sci. Technol., 42, 1077(2005)
[4] 高田信久、黒澤忠弘、小山保二、医用標準線量、7, 11(2002)
[5] Kurosawa T., Koyama Y., Takata N., 医用標準線量、6-2, 1 (2001)
[6] T.Kurosawa, N.Takata, Y.Koyama, Appl., Rad., Isot., 62, 805(2005)
[7] 松本健、崎原克彦、小山保二、電総研彙報、11, 73(1992)
[8] ISO 6980-2 (2004)
[9] Domen S.R., Lamperti J.P., A Heat-loss Compensated Calorimeter: Theory Design and Performance, J. Res. Nat. Bur. Stand. 78A, 1974

# 水吸収線量の標準線量計測

# Dosimetry standards of absorbed dose to water

首都大学東京大学院　齋藤秀敏

Corresponding: saitoh@hs.tmu.ac.jp

## 1．はじめに

投与線量の変化に対して、腫瘍の局所制御率および正常組織の障害発生率は急峻に変化する。したがって、放射線治療において吸収線量は重要な管理項目の一つであり、５％[1] あるいは3.5％[2] の合成標準不確かさが目標値とされている。このことから、AAPM Report 13では５％の合成標準不確かさの要素として、ファントムを使用した吸収線量計測において2.5％、体内吸収線量計算において4.3％の標準不確かさを与えている[3]。

すべての放射線治療施設において正確な吸収線量評価を実施し、その線量評価が正しいことを保証するためには、

ａ）吸収線量の国家標準が確立していること。

ｂ）国家標準にトレーサブルな線量校正サービスが提供されていること。

ｃ）吸収線量計測のための標準プロトコルが提供されていること。

ｄ）第三者による線量評価体制が整備されていること。

が、必須となる。

本項では、日本の放射線治療施設の現状を紹介し、線量校正および標準プロトコルの現状と今後などについて述べる。

（第三者評価については、峯村氏のページを参照いただきたい。）

## 2．日本の放射線治療の現状

日本における放射線治療の現状は、日本放射線腫瘍学会（JASTRO）データベース委員会放射線治療施設構造調査が２年に一度行うアンケート調査によって明らかにされている[4]。

図１は、1990年からの放射線治療を施行された全新患数および１治療施設あたりの新患数の平均値の年次変化を示している。1995年の調査では約73,000であった全新患数が、2005年の調査では約

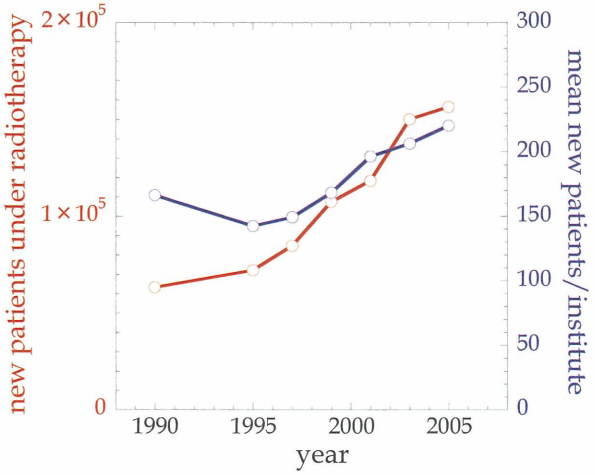


**図１　放射線治療を受けた全新患数および一治療施設あたりの新患数の平均値の年次変化**

Fig. 1 Change of new patients under radiotherapy

162,000と10年間で２倍以上に増大している。これに伴い、１治療施設当たりの平均新患数も1995年の142人から2005年の220人と、10年間でおよそ1.5倍に増加している。

図２は、治療施設数の年次変化であり、グラフ右の縦軸は構造調査アンケートへの回答率の変化を示している。全放射線治療施設数は調査年度によって変動が大きいように見えるが、増減がアンケート回答率と連動していることから、2000年代では700～730施設程度で放射線治療が実施されていると推定することができる。JASTROの2005年調査の推定施設数は735である。

図３は、地方別の治療施設数の推定値である。北海道31、東北60、関東191、甲信越52、東海88、近畿115、中国54、四国31および九州90の施設が点在している。県別で見ると人口1,000人当たりの施設数が最小４、最大70、１施設当たりの人口は全国平均179に対して、最小は101人、最大は353人と地域差があることが報告されている。

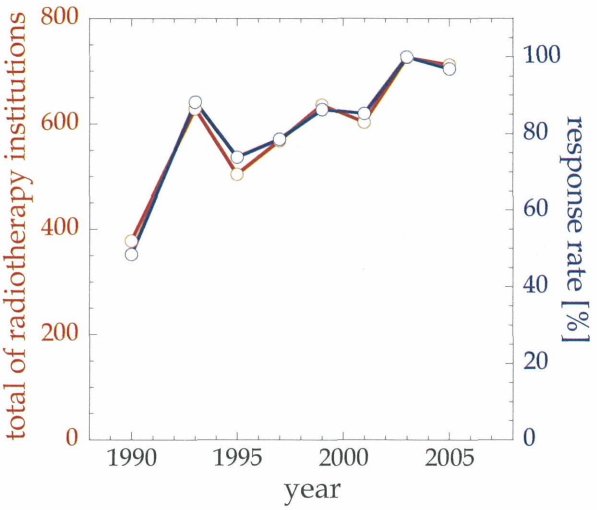


**図２　国内の全放射線治療施設数とJASTRO構造調査アンケートへの回収率の年次変化**

Fig. 2 Change of total radiotherapy institutions

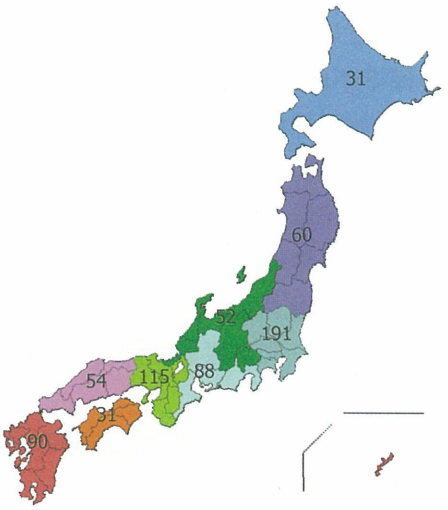


**図３　地方別の治療施設数の推定値**

Fig. 3 Regional distribution of radiotherapy institutions in Japan

表１は、放射線治療のために導入されている装置の種類と台数である。全世界で使用されているリニアックのおよそ１割の台数に相当する765台が日本国内に設置されている。このうち、X線エネ

**表１　外部放射線治療装置の種類と台数**

Table 1 Equipments for external radiotherapy

| equipment | number |
|---|---|
| Linac | 765 |
| with dual energy | (498) |
| with 3D-CRT function | (462) |
| with IMRT function | (170) |
| Microtron | 24 |
| Telecobalt (actual use) | 11 |
| GammaKnife | 48 |
| CyberKnife | 12 |
| Tomotherapy | 1 |
| Synchrotron | 6 |

ルギーを２種類以上発生できる装置が498台、3D-CRT治療が可能な装置が462台、IMRT機能を持つものが170台である。リニアックのほかに、Microtron 24、GammaKnife 48、CyberKnife 12、Tomotherapy 1およびSynchrotron 6が2005年において設置されている台数である。一方、実際に治療に利用されている$^{60}$Co遠隔照射装置の台数は11という調査結果となっている。

以上から、日本における放射線治療患者数は高齢者人口の増加、地域差の縮小、放射線治療を選択する患者の増大によって、増加傾向がしばらく継続すると考えられる。この増加傾向の患者を治療する外部照射装置は、安定した出力が得られる$^{60}$Co遠隔照射装置が衰退し、ほとんどが加速器へと移行している現状が明らかになった。このことは、加速器による治療で投与線量を監視するモニタ線量計の校正に関わる国家標準、線量計校正サービス、そして多様な線質に対応する線量計測の標準プロトコルが品質保証にとって重要な要因となっていることを示している。

## ３．線量標準と線量校正

物理量の計測では、より高位の標準によって校正され、国際標準あるいは国家標準につながる経路、すなわち計測のトレーサビリティが確立されている必要がある。

図４は、ユーザ施設のリファレンス線量計が二次標準（Secondary Standard Dosimetry Laboratory；SSDL）によって校正され、さらにSSDLの線量計が国家の標準である一次標準（Primary Standard Dosimetry Laboratory；PSDL）によって校正される線量校正の体系を示している[5]。日本の放射線治療におけるPSDLは産業技術総合研究所（産総研、Advanced Industrial Science and Technology；AIST）であり、グラファイト壁空洞電離箱によって$^{60}$Coγ線照射場の照射線量が校正されている。SSDLに相当する医用原子力技術研究振興財団（財団、Association for Nuclear Technology in Medicine; ANTM）の空洞電離箱式の二次標準線量計は、産総研のγ線照射場で置換法によって照射線量の校正定数、コバルト校正定数$N_c$が与えられている。同様にユーザのリファレンス電離箱線量計は、財団の線量計校正センターがある放射線医学総合研究所（放医研）の$^{60}$Coγ線照射場において置換法によって校正され、コバルト校正定数$N_c$が与えられている。

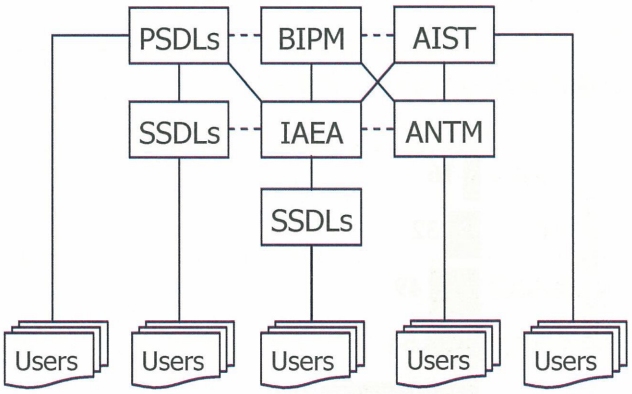


**図４　ユーザのリファレンス線量計から一次標準線量へのトレーサビリティの経路**

Fig. 4 Traceability of user's reference dosimeters to Primary Standard

現在、財団は照射線量のJCSS校正事業者登録を申請している。JCSSとはJapan Calibration Service Systemの略称であり、登録事業者は校正方法、不確かさの見積もり、設備が適切であるかなどが審査され、登録が許可された事業者のことである。これによってISO/IEC17025に適合した品質システムで校正できる能力を持った事業者として、日本で始めて放射線治療レベルの照射線量についてJCSS標章の入った校正証書を発行が可能となると同時に、IAEAが定義する本来のSSDLの条件を満たすことになる。

## 4．線量計校正の現状

財団の線量計校正センターが行っている治療用電離箱線量計の校正サービスの現状について統計的データを示す[6,7]。

表２に財団の線量計校正センターが行った電位計、電離箱数を示した。同表内の数値は、同一年度内に重複して校正した数を除外した値である。校正を依頼した施設数は、治療用線量計の校正サービスが財団に移行した2004年度483施設、2005年度507施設、2006年度595施設であった。2006年度の単年度で見ると、全治療施設数のおよそ８割が校正サービスを受けたことになる。また、2006年度には、電位計695、円筒形電離箱1,013本、平行平板形電離箱597本が校正され、円筒形と平行平板形電離箱の本数の比率は63％対37％であった。さらに、１台の電位計当たりおよそ2.3本の電離箱を所有している状況が読み取れる。

**表２　線量計校正センターによる校正線量計校正の年次変化**

Table 2 Calibrated electrometers and ionization chambers at ANTM as SSLD

| | 2004 | 2005 | 2006 |
|---|---|---|---|
| Institutions | 483 | 507 | 595 |
| electrometers | 535 | 571 | 695 |
| cylindrical chambers | 743 | 798 | 1,013 |
| plane-parallel chambers | 411 | 474 | 597 |

校正された電離箱の73.4％は過去に校正履歴があり、そのコバルト校正定数の変化を追跡することができる。また、20.2％は新規に購入された電離箱であり、校正履歴が不明な電離箱はわずかに6.4％であった。

校正歴のある電離箱について直前の校正から次の校正までの期間の度数分布を図５に示した。同図は、69％の電離箱が1.5年以内、85％が２年以内の間隔で校正されていることを示している。現在の外部放射線治療の吸収線量計測の標準プロトコルである標準測定法01では、リファレンス線量計の定義として、少なくとも１年に１度は校正を受けることが望ましいとしている。全電離箱のおよそ$1\sigma$がプロトコルに従った校正を行っていることになる。

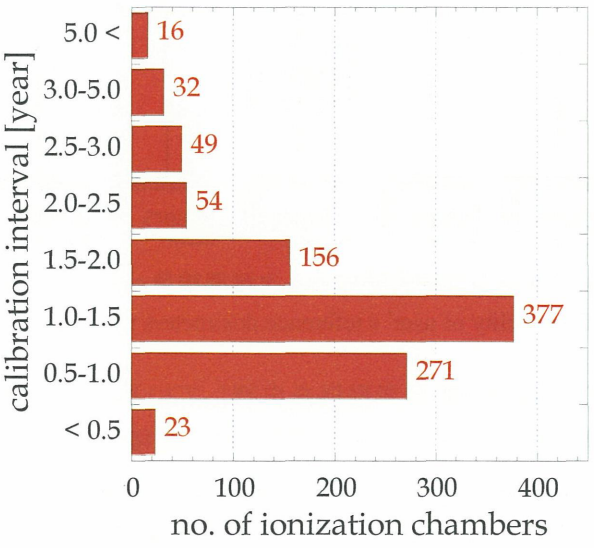


**図５　直前の校正からの期間の度数分布（2005年度）**

Fig. 5 Interval from the previous calibration (2005)

図６は前回の校正で与えられたコバルト校正定数からの変化の度数分布である。全電離箱の95％の電離箱が±１％以内の変化であることが示されている。このデータから、およそ$2\sigma$に相当する電離箱が$N_c$校正の不確かさ[8]の範囲内にあると考えられる。

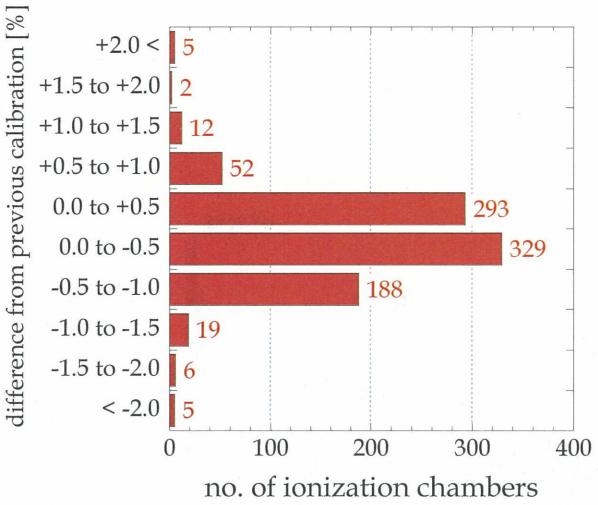


**図６　直前の校正からのコバルト校正定数の変化量の度数分布（2005年度）**

Fig. 6 Difference from previous $N_c$ calibration (2005)

## ５．外部放射線治療のための吸収線量計測の標準プロトコル

外部放射線治療のための吸収線量計測のための標準プロトコルであるAAPM Report 67[9]およびIAEA　TRS-398[10]では、水吸収線量$D_w$を放射線治療装置の出力の評価に採用している。また、吸収線量計測には$^{60}$Co γ線で値付けられた水吸収線量校正定数$N_{D,w}$をもつ電離箱線量計を使用し、電位計の指示値$M$から、次の簡潔な式で$D_w$を算出する。

$$D_W = M N_{D,w} k_Q \quad (1)$$

ここで$k_Q$は、校正で使用する$^{60}$Co γ線に任意線質での電離箱線量計の感度を補正する係数であり、TRS-398では*100 kV*以下のX線から、MV X線、電子線、陽子線、さらにAr粒子までに対応する線質決定法と線質変換係数算出法を提供している。粒子線の水吸収線量計測の詳細については、Vatnitsky氏のページを参照いただきたい。

水を媒質とすること、および電離箱線量計の校正を水吸収線量で行うことは、吸収線量評価が放射線治療分野において重要であり、水が人体のおよそ70％を占め、軟部組織と等価だからである。さらに、照射線量によって校正された電離箱を使用する場合に対して、電離箱壁およびビルドアップキャップの吸収、散乱の補正、電離箱およびビルドアップキャップの$^{60}$Co γ線に対する空気との制限質量阻止能および質量エネルギー吸収係数の相違、空気のW値など、不確かさの要因を減少させることができる。

図７は、同一の電離箱線量計に与えられたカーマ校正定数$N_k$ ($N_c$) に対する$N_{D,w}$の比を、電離箱ごと、形式ごとに示している[10]。直接的に水吸収線量に対する感度を評価できる$N_{D,w}$に対して、同一の形式であっても個々の製品ごとに、壁、ビルドアップキャップの材質および厚さなどのばらつきがカーマ（照射線量）評価の不確かさを拡大させていることが明らかである。

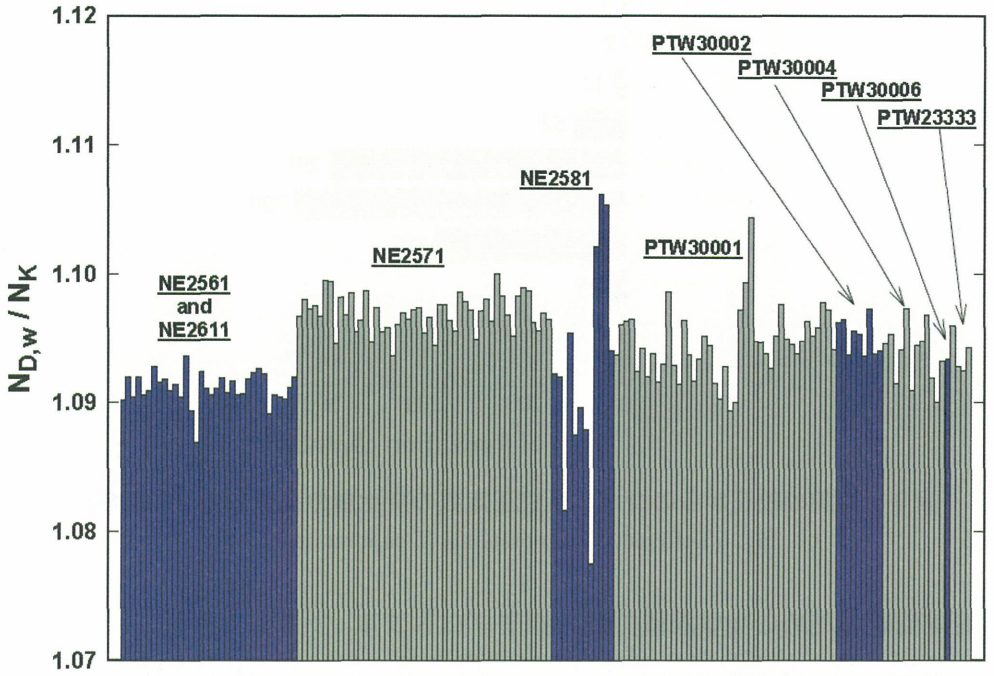


**図７　電離箱線量計個別のカーマ校正定数に対する水吸収線量校正定数の比[10]**

Fig. 7 Chamber to chamber variations of the ratio of $^{60}$Co calibration factors $N_{D,W}$ /$N_K$[10]

日本医学物理学会でも、この不確かさの要因を減少させた$N_{D,w}$を使用し、式（1）で水吸収線量を評価する外部放射線治療における吸収線量の標準測定法（標準測定法01）[11] を2002年に発刊し、５年が経過した。しかし、水吸収線量の国家標準が未整備であるため、$N_{D,w}/N_c$を理論的に求めた校正定数比$k_{D,x}$を与えて、次式で$D_w$を算出しているのが現状である。

$$D_w = M N_c k_{D,x} k_Q \quad (2)$$

したがって、同一形式の電離箱であっても製品ごとのばらつきが水吸収線量評価の不確かさを大きくしている状況は未だに改善されていない。

## ６．水吸収線量標準の今後

2007年現在、放射線治療における線量標準は照射線量であるが、2009年度を目標に水吸収線量の国家標準を確立する計画が進んでいる。これによって、2010年台早々にはグローバルスタンダードである$N_{D,w}$による水吸収線量評価が可能になる予定である。（１次標準については、黒澤氏の「産総研における線量標準の現状と今後」のページに詳しい。）

図８は2006年度に校正された円筒形電離箱の防水への対応の比率である[7]。$N_{D,w}$ベースの水吸収線量計測プロトコルが周知され、耐水性電離箱の比率が44％まで増大している。防水鞘などの使用によって必ずしも耐水性の電離箱である必要は無いが、耐水性の製品が主流になり、今後も比率は増大すると予想される。

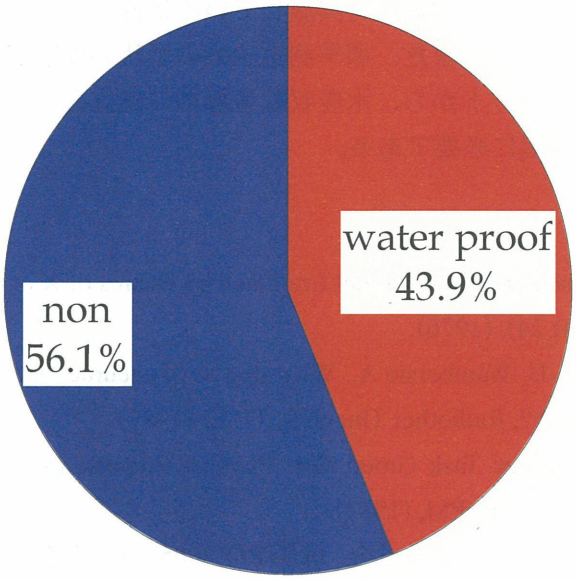


**図８　耐水性、非耐水性円筒形電離箱の比率（2006年度）**

Fig. 8 Ratio of water proof to non-water proof cylindrical ionization chambers (2006)

表３にIAEA TRS-398での水吸収線量評価と、標準測定法01による$N_c$および$k_{D,x}$を使用した現在の水吸収線量評価の不確かさの要因と合成標準不確かさを比較して示した。IAEA TRS-398では、$N_{D,w}$、$k_Q$、$M$それぞれの不確かさを0.6、1.0、0.9％と見積もり、合成標準不確かさを1.5％と評価している[10]。これに対して標準測定法01では、$N_c$および$k_{D,x}$の不確かさがそれぞれ0.74、1.3％であるため、$N_{D,w}$に相当する不確かさが1.5％、合成標準不確かさが2.0％と評価されている[8]。数年後の$N_{D,w}$校正サービスの開始によって、ファントム中での吸収線量評価の不確かさの改善が期待されるところである。

**表３　光子に対するFarmer形電離箱での水吸収線量評価の不確かさの比較**

Table 3 Uncertainties of absorbed dose to water for photon using Farmer type

| components of uncertainty | | IAEA TRS-398 | JSMP01 (situation in 2007) |
|---|---|---|---|
| $N_{D,W}$ | calibration factor in terms of absorbed does to water | 0.6 | (1.5) |
| $N_c$ | calibration factor in terms of exposure | - | 0.74 |
| $k_{D,X}$ | conversion factor in terms of $N_c$ to $N_{D,w}$ | - | 1.3 |
| $k_Q$ | beam quality correction factor | 1.0 | 1.0 |
| $M$ | measurement at calibration point | 0.9 | 0.9 |
| combined standard uncertainty [%] | | 1.5 | 2.0 |

## 6．おわりに

国内の放射線治療施設のほとんどが加速器使用して治療を実施している現在、線量標準、線量計校正サービス、そして多様な線質に対応する線量計測プロトコルは品質保証にとって重要である。線量計校正サービスの現状から、全電離箱のおよそ$1\sigma$に相当する電離箱が標準測定法01に従って年に１度、さらに$2\sigma$近くが２年に１度の校正を実施している状況が示され、ユーザの線量計校正に対する認識の高さが明らかとなった。また、標準測定法01の現状の問題点と、グローバルスタンダードである水吸収線量評価のメリットから、水吸収線量標準の確立と、評価の不確かさを改善するための$N_{D,w}$供給体制の確立が早期に必要である。

## 参考文献


1) Determination of Absorbed Dose in a Patient Irradiated by Beams of X or Gamma Rays in Radiotherapy Procedures (ICRU Report 24), (1976).
2) Mijnheer BJ, Battermann JJ, Wambersie A.: What degree of accuracy is required and can be achieved in photon and neutron therapy?, Radiother. Oncol. 8, 37?52 (1987).
3) Radiation Therapy Committee Task Group #24: Physical Aspects of Quality Assurance in Radiation Therapy (AAPM Report 13), AAPM, (1984).
4) 日本放射線腫瘍学・データベース委員会: JASTRO 2005年定期構造調査解析結果(第1報), http://www.jastro.jp/report/topic/070419.pdf, (2007).
5) Andreo P, Burns DT, et al.: Absorbed dose determination in external beam radiotherapy: An international code of practice for dosimetry based on standards of absorbed dose to water (IAEA TRS-398), IAEA, (2000).
6) 佐方周防, 秋山芳久、他: 医用原子力技術研究振興財団による線量計校正実績(平成17年4月～平成18年3月), 医用標準線量 11(2), 7-15, (2006).
7) 佐方周防: 私信, (2007).
8) 福村明史, 遠藤真宏, 他: 新しい治療用線量計校正トレーサビリティと校正定数の不確かさ, 医用標準線量9(1), 1-9, (2004).
9) Almond PR, Biggs PJ, et al.: AAPM7S TG-51 protocol for clinical reference dosimetry of high-energy photon and electron beams, Medical Physics 26(9), 1847-1870, (1999).
10) Andreo P, Burns DT, et al.: Absorbed dose determination in external beam radiotherapy: An international code of practice for dosimetry based on standards of absorbed dose to water, IAEA TRS-389, (2000).
11) 日本医学物理学会編: 外部放射線治療における吸収線量の標準測定法, 通商産業研究社, (2002).

# 第三者評価による品質保証・品質管理(QA・QC)について
## － 米国RPC研修報告 －
# Quality Assurance and Quality Control by Third-party Evaluation
## － RPC training report －

国立がんセンター　がん対策情報センター　峯村　俊行

Corresponding: tminemur@ncc.go.jp

### 1．はじめに

近年、がん患者の増加に伴い、より高度な治療が必要とされている。特に放射線治療に関しては、人口の高齢化による高齢がん患者の増加が顕著で、こういった患者の多くに非切除治療の中核として放射線治療がなされている。

放射線治療計画でも照射野という２次元的な考え方から標的体積という３次元放射線治療（3D-CRT）に移行することで、より複雑な治療計画が行われるようになった。また、強度変調放射線治療（IMRT)、定位放射線照射（SRI：SRS, SRT, SBRT)、イメージガイド下放射線治療（IGRT)、永久挿入密封小線源治療などの新しいタイプの放射線治療の開発と導入が、結果的に放射線治療の現場での仕事量を増加させ、通常の作業も複雑にしている。このように放射線治療には、治療計画、放射線治療装置等々で新しい知識と高度な技術が求められている。この高精度な治療を保証する体系的な活動としては、放射線治療の品質保証（Quality Assurance：QA)、品質管理（Quality Control：QC）が不可欠である。最近、わが国でも、このQA・QCに対して活発な動きを見せているが、欧米と比較するとやはり十分な活動を行っているとは言えない。

欧米では、QAを円滑に運用するために、各施設内にQA委員会を設置してそれぞれのプログラムを実行するのが一般的である。また、諸外国では、第三者評価機関が物理技術のQA面において、出力線量に関してのさまざまな調査を郵送、訪問で行っている。

郵送調査に関して代表的な組織としては、IAEA / WHO（International Atomic Energy Agency / World Health Organization)、EQUAL（ESTRO-QUALity assurance network)、RPC（M. D. Anderson Cancer Center Radiological Physics Center）の３組織が活動を行っている。

この３組織の中でもRPCは郵送調査だけでなく、訪問調査に関しても高度な技術と豊富な経験を持ち合わせている施設である。この度３ヶ月間、RPCで研修を受ける機会が得られたので、その内容について報告する。

### 2．Radiological Physics Center (RPC) とは？

RPCは、AAPM（American Association of Physicists in Medicine）とCRTS（Committee on Radiation Therapy Studies）の後押しを受けて、1969年にNCI（National Cancer Institute）の財政的援助で設立され、物理学的技術支援を約40年間行っている施設である。また、RPCはRTOG（Radiation Therapy Oncology）、ITC（Image-Guided Therapy Center）等のQAグループと連携を持ちながら、全米放射線治療施設の2/3（約1500施設、約3000放射線治療装置、約7500ビーム）の臨床試験参加施設に対して放射線治療のQA・QCプログラム支援活動を行っている。スタッフ数は総勢30名ほどの物理スタッフのみでこれらの施設を支援している。

RPCの使命としては、以下の３つが挙げられる。

（1） 臨床試験参加施設の処方線量の正確性を保証し、
それをNCIやQAグループに報告する。
（2） 臨床試験参加施設において誤った箇所がある場合、
それを修正してその情報を施設にフィードバックする。
（3） 施設の匿名性を保持し、有益と思われる情報を社会に提供する。

## 3．RPCの活動内容

主な活動内容は、臨床試験参加施設を中心に物理学的技術支援を行っている。具体的には、郵送調査や訪問調査を行うことで、放射線治療で使用された線量データ、放射線治療計画で使われる計算アルゴリズム、各施設の品質管理施策、小線源治療の線源強度などをモニタリングしている。RPCの医学物理士は、上記のさまざまな事柄に対して物理学的な立場から現在の高精度化した放射線医療を支援している。

### 3－1．郵送調査

RPCでの主な業務の１つに、熱蛍光線量計（TLD：Thermo Luminescent dosimeter）による郵送調査がある。この調査活動は開始してから約30年間継続されている。このTLDによる郵送調査は世界的にも広く実施されており、IAEAの報告[1)]によれば、全世界に約5700の放射線治療施設があるが、このうち過去５年間にTLD郵送調査に協力した施設はIAEA/WHOで約630施設、EQUALで約450施設、それ以外の臨床試験グループや、国単位の枠組みによる調査に対して合計約1100施設が参加し、これにRPCの調査施設数を考慮すると、全世界の約60％の施設が協力していることになる。今まで、このIAEAの調査で我が国は非協力国として扱われていたが、2007年11月より財団法人医用原子力研究振興財団において、ガラス線量計による郵送測定が行われるようになり、ようやく世界の基準に達する見込みである。

RPCでの郵送調査は、郵送したTLD-100（LiF：Mg, Ti）パウダーを施設側の放射線照射装置で照射した後、それを返送してもらうことで、TLDの特徴である退行現象（フェーディング）、非直線性、感度のエネルギー依存性を考慮して出力線量やエネルギーを求めている。写真１、２で示すようにRPCから送られてくる測定キットの中には、TLDパウダーを挿入したアクリルファントムと設置用の台が入っているだけであり、郵送に対する軽量化が考えられている。アクリルファントムはＸ線用と電子線用で、セットアップ用の台が異なり、また、測定するエネルギーによってファントムの大きさも分類されている。

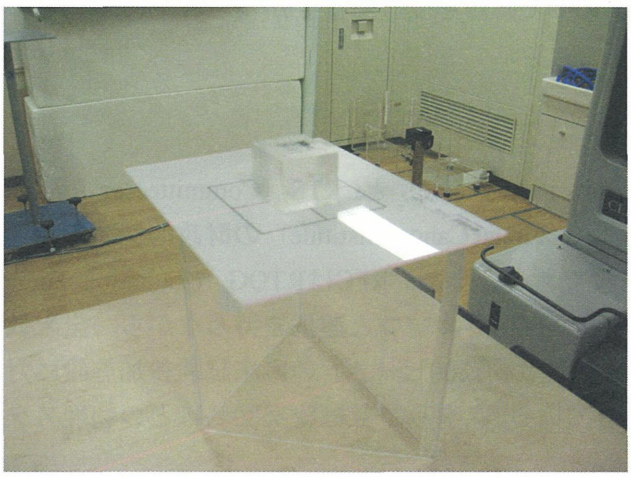

写真１：Ｘ線用の測定キット

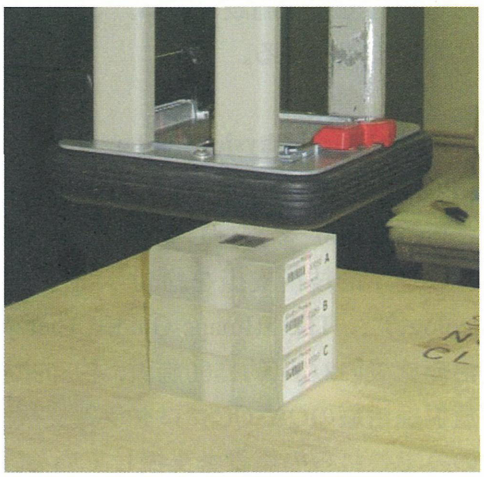

写真２：電子線用ファントム

この郵送調査は約30年間続けられていて、その活動で得られた過去の情報と現在の結果を比較することにより診療試験参加施設の出力線量状況を把握している。この他にもTLDを使用した郵送調査では、放射線治療装置の発展に伴い、フィルム（Gafchromic film）も合わせて装備可能なIMRT用ファントム（頭頚部、前立腺）、SRS用、SBRT用ファントム（肺および肝臓）等を用いて、各種照射法に合わせた郵送調査を行っている。また、 Tomotherapy用の円柱状ファントムや小線源治療用のファントムなどの開発も行っている。

このTLD郵送調査の許容基準は測定のバラつき、電離箱との絶対値評価による不確定度、セットアップなどの許容誤差を見積もることでその値を５％と定めている。[2)]

１回目の調査で５％以上の相違があれば２回目の調査を行い、それでもさらに５％以上の相違があるときは、RPCと施設の間で電話による改善策が話し合われ、場合によってはRPCスタッフによる訪問調査が行われる。

## ３－２．訪問調査

訪問調査の主な目的は、施設の線量計算、測定方法の誤りがる場合、改善策を提言し、QA施策等についての助言を行うことである。また、患者さんに適正な線量が照射されているかを確認し、その線量データを保証するためにモニタリングを行う。実際の調査内容は、放射線照射装置の出力線量チェック、温度計・気圧計などの機器チェック、放射線治療計画装置（RTPS）の計算アルゴリズムチェック、RTPS計算による線量チェック、小線源治療の線源強度チェック、放射線治療装置のQAプログラム施策の支援、施設のQA担当者に対してのアンケート調査などを行う。

RPCでの測定に関してのガイドラインは、Ｘ線と電子線のキャリブレーション・プロトコルにおいてAAPM TG-51[3)]、電子線の電離箱を使用したときの線量測定においてAAPM TG-25[4)]、小線源治療においてAAPM TG-43[5)]、そしてQAの基準に対してはAAPM TG-40[6)] に準拠して測定、線量計算を行っている。

訪問調査による測定方法は、施設で治療に使用しているRTPSの計算結果とRPCスタッフによる施設での測定結果を比較することにより、投与線量が適正であることを確認する。測定項目は、以下のとおり。

（１）幾何学的位置を確認する
- 線源からの光学距離（Light distance-indicator）と機械的距離（Mechanical pointer）の相違を確認する
- 機械的距離とレーザーローカライザー（laser localizer）との相違を確認する
- 実照射野と光照射野の相違を確認する

（２）Ｘ線の線量調査（水吸収線量測定）
- 最大深（$d_{max}$）での線量DMU（Dose/MU）を求める
- 深部量百分率（PDD）を求める
- %dd（10）xから線質を求める
- イオン再結合補正係数$P_{ion}$、極性効果補正係数$P_{pol}$を求める
- 出力係数（OutPut Factor : OPF）を求める
- くさび係数（Wedge Factor : WF）を求める
- MLC（Multi Leaf Collimator）を使用したときの線量を求める
- 非対称な上下の絞り（Asymmetric-jaws）に対する線量を求める
- 投与線量を求める

（４）電子線の線量調査

・最大深における電位計の最大値$I_{max}$と線量の最大値$d_{max}$を求める
・勾配補正係数$P_{grad}$、$P_{ion}$、$P_{pol}$を求める
・Cone factorを求める
・SSDの広がり（SSDを100cmから110cmにする）による相違を確認する

（５）小線源治療の線源強度調査
・Well型電離箱を使用して線源強度を確認する

上記の測定結果は、AAPM TG24[7]を参考に評価される。AAPM TG24[7]では標的に対する吸収線量の決定精度は、±５％以内（線量分布で－５％～＋７％以内）と示されているので、RPCではこれに準拠して、ビームの校正値±３％以内、各種ファクター値（OPF, WFなど）±２％以内、幾何学的位置の相違±３mm以内と定めている。

臨床試験参加施設で患者登録数の多い施設に対しては、郵送調査の結果によらず訪問調査が行われており、年間20～40施設、これまでに700施設余りに実施されている。なお、訪問調査で３％～５％の相違であれば改善を勧め、５％以上であれば積極的に原因追究をするとしている。

訪問調査においては１施設あたり数日から１週間をかけて調査を行う。具体的には、X線２ビーム、電子線６～８ビームに対して6時間ほどで測定し、同時に解析も行う。この他にも、小線源治療の線源強度、施設のQAプログラムのチェックを行うので、放射線照射装置が２台ある施設に対しては、平均３日間で調査を終了する。

RPCでは問題のある施設に対して、その施設の状況を把握し、問題の解決に向けて施設とのコミュニケーションを図ることも訪問調査においての重要項目の１つとされている。

## ４．おわりに

放射線治療の安全性を保証するには、第三者による評価が不可欠である。特に高品質、高精度な放射線治療においては、様々な測定や検証を行うための機材、装置の開発は必須であり、そしてまた、基礎的な物理学現象を理解し、発想力、応用力を兼ね備えた人材も求められている。RPCでは上記のような装置が開発されており、人材も医学物理士として存在している。IAEAの調査にもあったように今まで非協力国として扱われていた日本も、今後は第三者による評価体制を整え、安全な治療が行えるように放射線治療施設に対して知識と技術の支援を行う必要がある。


１） J. Izewska, H. Svensson, et al.: Radiation Dosimetry Audits, IAEA Volume2 (IAEA-CN-96/76), 139-157 (2003).

２） T. H. Kirby, W. F. Hanson, et al.: Uncertainty Analysis of Absorbed Dose Calculations from Thermoluminescence Dosimeters, Medical Physics 19, No6, 1427-1433 (1992).

３） P. R. Almond, P. J. Biggs, et al.: AAPM' s TG51 Protocol for Clinical Reference Dosimetry of High-Energy Photon and Electron beams, Medical Physics 26, 1847-1870, (1999).

４） American Association of Physicists in Medicine, RTC Task Group 25, "Clinical Electron-Beam Dosimetry,: Report of AAPM Radiation Therapy Committee, Task Group 25," Medical Physics 18, 73-109, (1991).

５） R. Nath, L. L. Anderson, Dosimetry of Interstitial Brachytherapy Sources: Recommendations of the AAPM Radiation Therapy Committee, Task Group 43, Medical Physics 22, 209-234, (1995).

６） Task Group 40, Radiation Therapy Committee, American Association of Physicists in Medicine: "Comprehensive QA for radiation oncology", Medical Physics 21, 581-618, (1994)

7） AAPM Report 13: Physical Aspects of Quality Assurance in Radiation Therapy, American Institution of Physics for American Association of Physicists in Medicine, (1984).

# Dosimetry of proton beams - recommendations of new ICRU/IAEA report.

Stanislav Vatnitsky

International Atomic Energy Agency, IAEA, Vienna

Correponding: s.vatnitsky@iaea.org

## Introduction

In recent years, there has been an increased interest in the medical community throughout the world to establish dedicated hospital-based facilities employing proton and light-ion beams for radiotherapy. However, at present there are no recognized uniform standards for dose prescription, dosimetry and treatment techniques for these beams. Such standards are essential for the design of new facilities, for the evaluation of clinical data from the various facilities, and for assessing the efficacy of proton and light-ion beam radiation therapy relative to photons or other modalities. To fill this gap the ICRU and IAEA prepared a common Report 78[1)] where the concepts and recommendations of ICRU reports concerning radiation therapy are extended to proton therapy and the necessary information is given on techniques, procedures and harmonization the clinical descriptions of proton treatments. The planning of proton therapy requires accurate dosimetry and beam calibration in order to ensure the exact delivery of the prescribed dose. On the other hand, the extensive exchange of clinical experience and medical treatment protocols needs to be based on consistent and harmonized dosimetry procedures. This paper reviews the recommendations given in new ICRU report 78 for standardization dosimetry and QA procedures of therapeutic proton beams.

## 2. Materials and methods

### 2.1. Reference dosimetry

The lack of national and international dosimetry standards for proton beams, and the lack of understanding of details of the relevant physics, historically made calorimeters and Faraday cups (FC) become the dosimetry instruments of choice for the reference calibration of these beams. ICRU 78 provided thoughtful review of the current status of application of these instruments in proton beam calibration. It was recognized that the major difficulties with both water and graphite calorimetry are currently understood and have largely been solved. ICRU 78 recommended when available, calorimeters should be used as primary standards or, alternatively, to confirm the proton calibration coefficient of the reference ionization chamber. Due to the large differences frequently observed between FC-dosimetry and calorimeters or ionization chamber dosimetry, but not sufficiently understood, it was not recommended the sole use of fluence-based techniques for calibration of clinical proton beams.

Currently, air-filled thimble ionization chambers with $^{60}$Co calibration factors are recognized as the most practical and reliable reference instrument for proton dosimetry. The publication of the ICRU Report 59[2)] represented the first attempt to harmonize clinical proton dosimetry worldwide and included both $^{60}$Co air-kerma and absorbed-dose-to-water based formalisms for ionization chamber dosimetry. Upon the adoption of ICRU 59 in multiple proton centres, international dosimetry using ionization chambers with $^{60}$Co calibration showed a considerable improvement in homogeneity, and a comparison among various institutions described in ref[3)] resulted

in agreements within 1% for all participants in the calibration of a common beam using their own instrumentation.

The International Code of Practice IAEA TRS-398[4], based on standards of absorbed dose to water for external radiotherapy beams, was published in 2000. For protons, TRS-398 differed substantially from ICRU 59. A detailed comparison of the two recommendations has been done in ref[5], providing a discussion of the source of the differences. As it was indicated above, ICRU 78 minimized the role FC and calorimeters in proton dosimetry, favouring the use of ionization chambers and adopting IAEA TRS-398 as a Code of practice for practical beam calibrations. The adoption of TRS-398 was supported with the careful analysis of the basic physics data and provided recommendations were given for passively modulated and scanned proton beams. A comparison of recent recommendations for dosimetry in reference conditions of proton and ion beams is given in Table 1.

| | ICRU 59[2] | IAEA TRS-398[4] | ICRU/IAEA 78[1] |
|---|---|---|---|
| Particle type | protons | Protons, ions | Protons |
| Beam type | Passive modulation | Passive modulation | Passive modulation and scanned beams |
| Reference phantom material | water | water | water |
| Reference dosimeter | Ion chamber: *thimble* | Ion chamber: *thimble or parallel plate* | Ion chamber: *thimble or parallel plate* |
| Calibration quality | $^{60}$Co | $^{60}$Co | $^{60}$Co |
| ic calibration factor | $N_X$, $N_K$, $N_{D,w}$ | $N_{D,w}$ | $N_{D,w}$ |
| ic wall material | No restriction | No restriction | No restriction |
| Beam quality specifier | Effective energy | Residual range | Residual range |
| Stopping powers | ref [7] | ref [8] | ref [8] |
| $W_{air}$ | 34.8±2% | 34.2±0.4%<br>34.5±1.5%- ions | 34.2±0.4% |
| Use of chamber specific factors | yes | yes | yes |
| $u_c(D_w)$, 1σ | 2.8% | Protons:<br>2.0% - *thimble*<br>2.3% - *parallel plate*<br>Ions:<br>3.0% - *thimble*<br>3.4% - *parallel plate* | Protons:<br>2.0% - *thimble*<br>2.3% - *parallel plate* |

Table 1. Main features of the Codes of Practice and protocols for dosimetry in reference conditions of proton and ion beams

Knowledge of $(w_{air}/e)$ - the mean energy to form an ion pair in the ionization chamber gas for protons - is required for conversion of the charge collected in an ionization chamber to deposited energy. As seen from Table 1 the values recommended in the two most recent protocols, ICRU 59 and IAEA TRS-398 differ by more than 2%. A re-analysis of available data should be performed in order to explain any differences and correct in new ICRU report any inadvertent errors in the $(w_{air}/e)$ -values used in the two most recent protocols. The analysis published by Jones[6] and included into ICRU 78 report showed that only $(w_{air}/e)$ -values deduced from the comparison of all available calorimetry and ionometry data should be evaluated to determine the appropriate w-value to use for ionization chamber dosimetry. The value thus determined is 34.2 J $C^{-1}$ ± 0.4 %, which is consistent with the TRS-398 recommended value. As it is given in Table 1, ICRU 59 and TRS-398 use proton

stopping powers given in ICRU Report 49[7] but TRS-398 includes secondary electron transport and nuclear interactions [8]. The stopping power data from TRS-398 are recommended by ICRU 78 and a table of beam quality correction factors from TRS-398 is reproduced in ICRU 78 Report. Plastic phantoms should not be used for reference dosimetry in proton beams since the fluence correction factors, for scaling absorbed dose to water in plastic to absorbed dose to water in water at the same water equivalent depth are not very well known. Nevertheless, when accurate chamber positioning in water is not possible or when no waterproof chamber is available, their use is feasible for the measurement of depth dose distributions for low energy proton beams[4]. The recommendations of ICRU 78 for reference dosimetry in scanned beams are based on the experience at the Paul Scherrer Institute (PSI)[9].

2.2. Measurements in non-reference conditions

Relative dose measurements or measurements in non-reference conditions are performed for routine daily clinical physics activities, beam line commissioning, and collecting data for treatment planning systems (TPS), quality assurance (QA) and for research and development. ICRU 78 provided detailed analysis of the appropriate sensitivity, energy independence, response linearity and spatial resolution for different detectors and summarized that depending upon the clinical task, ionization chambers, silicon diodes, radiographic films, diamond detectors, gels, scintillators, thermoluminescence dosimeters (TLDs), and radiochromic films can be employed for relative measurements. Nevertheless, all measurements with different detectors should be verified through the comparison with an ionization chamber.

The measurements used for controlling the dose and the shape of the dose distribution delivered with scanned beams differ from those with passive-beam scattering only from the point of view of the longer time needed for the measurements. The simultaneous use of several dosimeters distributed either at discreet positions in a volume or aligned along arrays (for measuring dose profiles) was recommended. Alternatively, 2-D dosimeters, such as radiochromic films, scintillating screens or gel dosimeters can be employed.

2.3. Quality Assuarnce

A comprehensive QA program for a proton-beam therapy facility includes the procedures that ensure a consistent and safe fulfilment of the dose prescription as well as minimal radiation exposure to the personnel and the public. Practical implementation of a QA program depends on the details of the proton accelerator and the selected beam-delivery technique. The QA measurements described in ICRU 78 follow the steps of the proton-therapy and focus on dose delivery and treatment planning. Commissioning and validation of proton-beam delivery and treatment-planning systems include machine-specific beam-data acquisition, data entry into the treatment planning system, validation of the calculations, development of operational procedures and constancy checks, as well as training of all staff concerned with the operation of the system. New types of proton-beam delivery systems might also require biological assessment as a part of commissioning[10] whereas preclinical testing of commercially available facilities is usually limited to physics and dosimetry acceptance checks[11]. The data obtained during the commissioning and validation process are used later as benchmarks and thresholds for periodic QA checks.

Periodic QA checks for wobbling and scanning delivery techniques are similar to those for the passive-beam scattering technique. However, because these delivery systems are dynamic and also because the accurate delivery of the planned dose depends on the accurate deposition of individually weighted pencil beams, additional QA methods are required for scanned-beam systems. An important part of QA procedures is related to beam

monitoring with multiple-wire and multiple-segment ionization chambers that control deviations in beam position, check the beam size and its uniformity, and control the dose delivered to the patient during the treatment. The stability of the monitors with gantry angle and reproducibility of the beam from the accelerator should be verified as a part of periodic QA checks[12].

Accurate positioning of the patient in the proton beam requires location of the patient on the support system and precise operation and correct interaction of two systems: one that performs and controls the movements required to place the patient in the prescribed position, and another that verifies the position of the patient relative to the beam axis. The periodic QA checks of positioning systems and digital x-ray imaging systems should be deal with the calibration of CCD cameras and verification of the alignment of the axial x-ray imaging system[12]. Patient positioners can also include high-precision robotic systems[13),14)] that are capable, in combination with gantry angulations, of locating the treatment isocenter at any point within the patient and direct the beam from any angle through that point. The accuracy of robotic patient positioning depends mainly on the capability of the robot control and safety software rather than on the mechanical accuracy of the couch, therefore periodic quality control involves a substantial amount of software and safety checks[14].

The TPSs used at proton centers with a passive scattering beam delivery system are mostly based on scatter-convolution algorithms[12]. This method employs as input data the measured depth-dose tables, off-axis profiles and output factors for each energy and modulator combination. During commissioning, the dosimetric characteristics of the proton beams, such as depth doses, off-axis profiles, field-size factors, modulation factors for different field sizes, penumbra sizes, and beam ranges, should be measured and recorded for validation of the TPS and also stored in a database to be referenced in future periodic QA checks[12),15)]. Again, for scanning systems, the beam data-acquisition procedure is somewhat different, and requires the measurement of depth-dose curves and lateral profiles of pencil beams, requiring small-field dosimetry equipment with a good spatial resolution[11]. Given the importance of the accuracy of the CT HU values, ICRU 78 strongly recommends that regular checks of the consistency of the CT HU values be performed.

Patient-specific periodic QA checks for passive-scattering techniques include portal calibrations and verification of beam-shaping devices (apertures and compensators/boluses)[12),15)]. Precision in manufacturing the bolus directly affects the distal part of the depth-dose distribution, while the errors in the patient aperture impinge on the lateral-dose distribution. Although milling machines provide high manufacturing precision, the manufactured beam- shaping devices for each patient should be checked against TPS data files by comparing aperture shapes and bolus thicknesses at pre-selected points[12]. Improvement in quality control of dose delivery can be achieved through the use of proton radiography that provides verification of the relative range of protons in vivo in the patient[16]. The use of PET monitoring to check proton range, dose localization, and stability of the treatment during different fractions could be considered a potentially useful tool for QA in proton therapy[17),18)].

Patient-specific QA checks for TPS used for scanned-beam system[19] include manual calculations of the MU, range checks and, most importantly, independent dose calculations based on the control file itself, which is directly compared to that calculated by the treatment planning system. If respiratory-synchronized irradiation is employed, CT images used for treatment planning must also be taken in respiratory-gating mode. The same specifications for irradiation gating, synchronizing timing and thresholds, should be applied for acquisition of treatment-planning CT images[15].

## 3. Conclusion

The implementation of recommendations of ICRU 78 will help to harmonize the clinical descriptions of pro-

ton treatments and provide standardization for the design of new facilities, for the evaluation of clinical data, and for assessing the efficacy of proton beam radiation therapy relative to photons or other modalities.

**4. Acknowledgement**

The input of members of the ICRU/IAEA Report Committee on Prescribing, Recording, and Reporting Proton Beam Therapy is gratefully acknowledged.

**5. References**

1. International Commission on Radiation Units and Measurements, (ICRU) /International Atomic Energy Agency (IAEA) Prescribing, Recording, and Reporting Proton Beam Therapy Report 78 (ICRU) in print (2008).
2. International Commission on Radiation Units and Measurements, (ICRU) Clinical Proton Dosimetry Part I: Beam Production, Beam Delivery and Measurement of Absorbed Dose. Report 59 ICRU, Bethesda, MD, (1998).
3. Vatnitsky, S., Moyers, M., Miller, D., et al. Proton dosimetry intercomparison based on the ICRU Report 59 protocol." Radiother. Oncol. 51 273-279 (1999).
4. International Atomic Energy Agency (IAEA), Absorbed dose determination in external beam radiotherapy: an International Code of Practice IAEA (Technical Report Series 398) (Vienna: IAEA) (2000).
5. Medin, J., Andreo, P., and Vynckier, S. Comparison of dosimetry recommendations for clinical proton beams. Phys. Med. Biol. 45 3195-3211 (2000).
6. Jones D.T.L. The w-value in air for proton therapy beams. Rad. Phys. Chem. 75-541-550 (2006).
7. International Commission on Radiation Units and Measurements (ICRU), Stopping Powers and Ranges for Protons and Alpha Particles, Report 49 ICRU, Bethesda, MD (1993).
8. Medin, J. and Andreo, P. Monte Carlo calculated stopping-power ratios water/air for clinical proton dosimetry (50-250 MeV)," Phys. Med. Biol. 42, 89-105 (1997).
9. Coray, A., Pedroni, E., Boehringer, et al. Dosimetry with the scanned proton beam on the Paul Scherrer Institute gantry," in Proc. Int. Symp. on Standards and Codes of Practice in Medical Radiation Dosimetry. IAEA-CN-96 (International Atomic Energy Agency, Vienna). pp. 295-302 (2002).
10. Pedroni, E., Bacher, R., Blattmann, H., Boehringer, et al. The 200 MeV proton therapy project at the Paul Scherrer Institute: Conceptual design and practical realisation. Med. Phys. 22, 37-53 (1995).
11. Kooy, H.M., Clinical commissioning of Gantry 1 at the Northeast Proton Therapy Center. Particles 31 Abstracts of the XXXVI PTCOG Meeting Catania, Italy May 29 - 31(2002).
12. Moyers, M., Proton therapy Ch.20, (Van Dyk J. Ed), The Modern Technology of Radiation Oncology: A Compendium for Medical Physicists and Radiation Oncologists, Medical Physics Publishing, Madison, WI (1999).
13. Schroeder, N., "The MPRI robotic patient positioner Particles 34 Abstracts of the XLth PTCOG meeting Paris ? Institute Curie ? CPO June 16 - 18 (2004).
14. De Kock, E.A., "The robot-based patient positioning system for high precision radiotherapy at iThemba LABS. Particles 32 Abstracts of the XXXVII PTCOG Meeting, Cape Town, South Africa October 28 - 30 (2002).
15. Guidelines of physical and technological quality assurance for particle beam therapy Recommendation of Japanese Association of Therapeutical Radiation Oncology-JASTRO (2004)

16. Schneider, U., and Pedroni, E. Proton radiography as a tool for quality control in proton therapy. Med. Phys. 22, 353-363 (1995)
17. Hishikawa, Y., Kagawa, K., Murakami, M., et al. Usefulness of positron-emission tomographic images after proton therapy. Int. J Radiat. Oncol. Biol. Phys. 53, 1388-91 (2002).
18. Parodi, K., and Englhardt, W. Potential application of PET in quality assurance of proton therapy. Phys. Med. Biol. 45, N151-N156 (2000).
19. Lomax, A., Böhringer, T., Bolsi, A., et al. Treatment planning and verification of proton therapy using spot scanning: Initial experiences. Med. Phys. 31, 3150-3157 (2004).

# 炭素線治療における二次中性子の評価

独）放射線医学総合研究所　重粒子医科学センター　米内俊祐

Corresponding: yonai@nirs.go.jp

## 1．はじめに

HIMACで行われている炭素線治療は、多くの疾患に対してその有用性を示す臨床結果を得ており、その普及が期待されている。炭素線治療の普及のためには、建設コストの削減等の研究開発のみならず、患者の治療患部以外の組織、臓器の後発性障害に対する評価、つまり、二次がんリスク評価を行うことが必要である。粒子線治療では、粒子線が照射機器や人体と相互作用し、生物学的効果の高い二次中性子が生成するために、一次、二次荷電粒子による治療患部周辺の組織、臓器に対する比較的高い線量の被曝と同時に、患部から離れた組織、臓器に対する低線量被曝を評価することも重要である。

この二次中性子による被曝線量を算出するためには、生体内もしくは、ファントム内の線量分布を評価する必要がある。しかし、それらの二次中性子をファントム内で測定するためには、広いエネルギー領域に感度があり、かつ、分布を評価するのに十分な位置分解能の高い検出器が必要となる。現在これを満足する検出器は存在しないことから、測定で直接それを評価するには検出器の開発を行う必要があり容易ではない。よって、二次中性子を評価する場合には、シミュレーション計算により算出することが現実的である。シミュレーション計算の本質は、中性子源から放出される中性子エネルギースペクトルを正確に模擬することであり、それを測定により正確に得ることが正確な二次がんリスク評価につながる。

陽子線治療においては、照射機器と人体を模擬した水ファントムから生成する中性子のエネルギースペクトル及び周辺線量当量の測定、シミュレーション計算の研究結果がこれまでに発表されている[1)-4)]。一方で、炭素線治療における二次中性子の測定に関する研究は、これまで成されておらず、また、組織等価物質から生成する二次中性子の実験データが極めて少ない。そこで、我々は、HIMACにおいて、シミュレーション計算の妥当性を評価するために、炭素線入射により照射機器及び水ファントムから生成する二次中性子のエネルギースペクトルの測定を行った。ここでは、その測定方法の確立と、治療室における中性子エネルギースペクトルの測定結果を報告する。

また、E. Hallは、陽子線治療においてこれまで行われた二次中性子の（周辺）線量当量の測定を基に、陽子線治療における二次がんリスクの評価を行った[5)]。この結果は、HIMAC及び他の多くの治療施設が用いてPassive法による照射は、Scanning法を用いた照射よりも100倍以上の二次中性子による被曝があり、Passive法を用いた陽子線治療に潜在する高い二次がんリスクについて警告するものであった。そこで、上述した炭素線治療場の中性子エネルギースペクトルの測定から、周辺線量当量を算出し、陽子線治療施設の結果と比較することで、炭素線治療場の二次がんリスクを定性的に評価した。

さらに、筑波大学陽子線医学利用研究センターに（PMRC）おいて、HIMACで用いた測定方法および測定条件で、中性子エネルギースペクトルを測定し、E. Hallが評価の用いた測定結果の妥当性を評価した。

## 2．測定方法

図１に測定体系を示す。測定は、HIMAC治療室BHCコースで行った。水ファントム（21×20×39

cm³）を、治療台の上に設置し、図１に示す角度θ、距離d、およびマルチリーフコリメータ（MLC）の開口幅lを変えた場合の依存性を測定した。角度及び距離の基準点はそれぞれ、ファントム中心と検出器中心である。表１に、本測定における各依存性取得のための検出器およびMLCの幾何学的条件を示す。また、本測定では、炭素ビームは、エネルギー290 MeV/u、一様照射野10 cmϕ、SOBP幅60 mmに固定している。

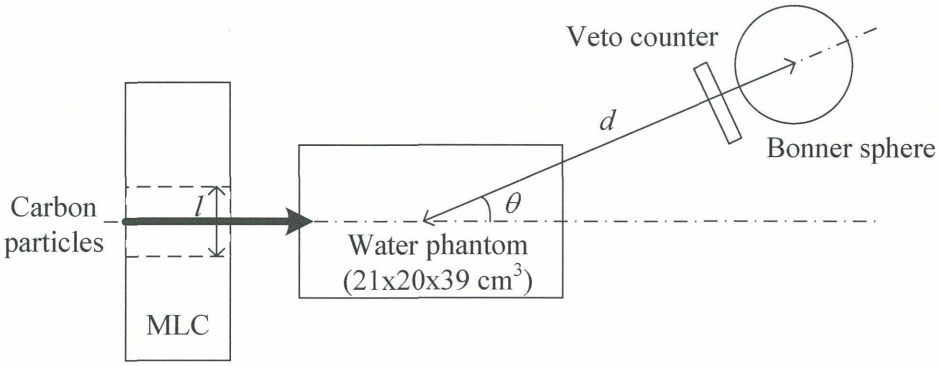


図１：実験体系

| Dependence | MLC ($l$×$l$ [cm$^2$]) | $\theta$ [degree] | $d$ [cm] |
|---|---|---|---|
| Angular | 10x10 | 0, 15, 30, 45, 60, 90 | 173 |
| Distance | 10x10 | 0,15 | 100, 173, 250 |
| MLC | 5x5, 10x10, open | 0, 15, 30, 90 | 173 |

表１：本測定における各依存性取得のための検出器およびMLCの幾何学的条件

中性子エネルギースペクトル測定には、従来から広いエネルギー領域の中性子測定に用いられているボナーボールを用いた。ボナーボールは、ポリエチレン減速材により入射中性子のエネルギーを熱領域まで減速させ、減速材中央に位置する熱中性子検出器で測定するものである。本測定では、$^6$LiIシンチレータを熱中性子検出器として用いていた。図２に本測定に用いたボナーボールの応答関

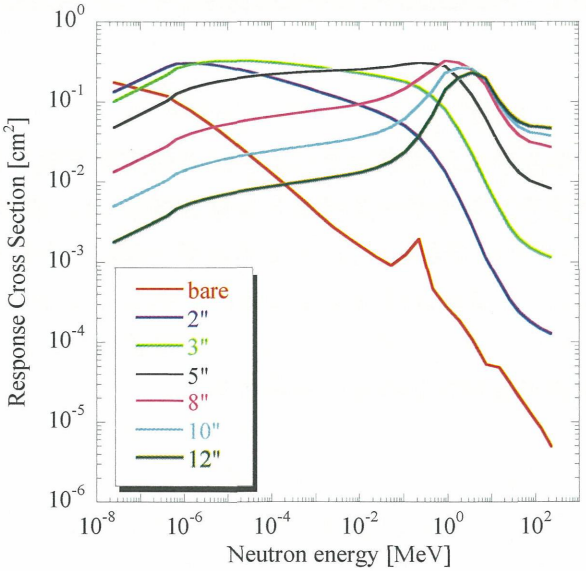


図２：$^6$LiIシンチレータ（４mm×４mm）を用いたボナーボールの応答関数[6]

数[6]を示す。厚さの違う減速材は異なる応答関数を与えるために、複数の測定値をアンフォールディングすることにより、中性子エネルギースペクトルが得られる。ここでは、一般的に用いられているSAND-IIコード[7]を用いて、アンフォールディングを行った。また、アンフォールディングに必要な初期スペクトルにはモンテカルロコードPHITS[8]による計算値を用いた。

炭素線治療場では、二次中性子と同時に、二次荷電粒子も多数生成される。$^{6}$LiIシンチレータは荷電粒子にも感度があることから、荷電粒子混在場において中性子エネルギースペクトルを得るためには、中性子イベントと荷電粒子イベントを弁別する必要がある。この弁別のために、本測定では、図１に示すように、ボナーボールの前方に薄いプラスチックシンチレータをveto検出器として設置した。図３に、veto検出器を用いた荷電粒子イベントの弁別を示す。この図からわかるように、veto検出器を用いることにより、中性子イベントを二次荷電粒子イベントから弁別可能なことが分かった。また、この二次荷電粒子イベントは、ほぼすべてが、水ファントムから生成するものであり、veto検出器をファントム方向のみに設置すればよいことが分かった。

上述した方法で得た中性子エネルギースペクトルに周辺線量当量換算係数を乗じることにより、周辺線量（H*（10））分布の角度、距離、MLC開口幅依存性も取得した。周辺線量当量換算係数は、201MeV以下はICRP74[9]の値を用い、それ以上のエネルギーでは、PHITSによる計算値[10]を用いた。また、周辺線量当量の結果は、水ファントム中のSOBP中心における吸収線量によって規格化した。

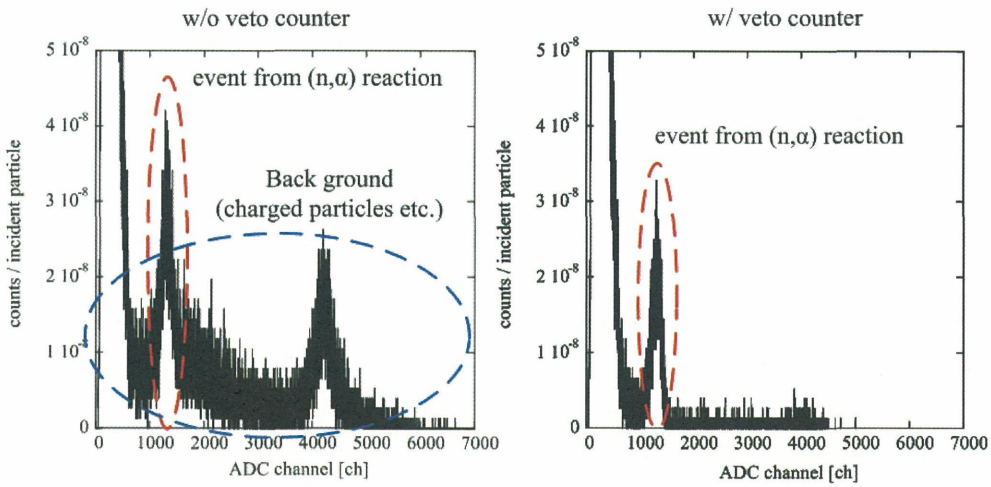


図３：veto検出器を用いた荷電粒子イベントの弁別

## ３．測定結果

ａ）角度依存性

図４に測定により得た中性子エネルギースペクトルの角度依存性を示す。この図からわかるように、炭素線治療場の中性子エネルギースペクトルを３成分：1）10keV以下、2）10keV-10MeV、3）10MeV以上、に分けることができる。1）のエネルギー領域の中性子は、天井や床などによる散乱中性子成分と考えられ、角度依存性は全くない。2）のエネルギー領域では、角度が大きくなるほど増加する傾向がみられるが、０度以外では、大きな差はない。3）のエネルギー領域では、角度が小さくなるほど増加する傾向が顕著にみられる。

重荷電粒子入射による厚いターゲットからの中性子生成量の測定11）から、2）のエネルギー領域の中性子は、おもに蒸発過程から放出されるもので、重核ターゲットほど生成量が大きく、3）のエネルギー領域の中性子は、おもに直接過程及び入射粒子自身のブレイクアップにより放出されるもので、軽核ターゲットほど生成量が大きいことが分かっている。つまり、2）の成分はMLC（鉄）に寄与するものであり、3）の成分は水に寄与するものであることがわかる。また、2）の成

分は、蒸発過程により、ターゲットから等方に放出されるので、角度が小さいほど中性子量が減少するのは、MLCと測定位置の距離によるものであると考えられる[1]。

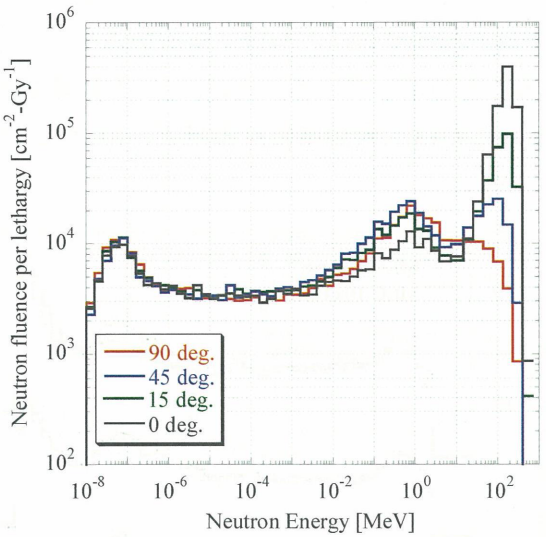


**図４：炭素線治療場における中性子エネルギースペクトルの角度依存性**

b）距離依存性

図５に測定により得た中性子エネルギースペクトルの距離依存性を示す。ファントムと測定位置の距離が長くなるほど、中性子量が減少していることがわかる。しかし、０度では、上述した治療室内の散乱成分である10keV以下の中性子ではほとんど影響していない。散乱中性子は、治療室の空間に影響されるために、部屋内の散乱物質に強く影響される。90度、50, 100cmの位置では、散乱成分が他の測定位置より多くなったが、これは、散乱物であるMLCなどの照射機器に近いためではないかと推測できる。a）で述べた2), 3）のエネルギー領域はターゲットにより生成するものが主であり、治療室の空間には強く影響されず、反応点から距離を離せば単位面積当たりの中性子量が減少するのは当然である。

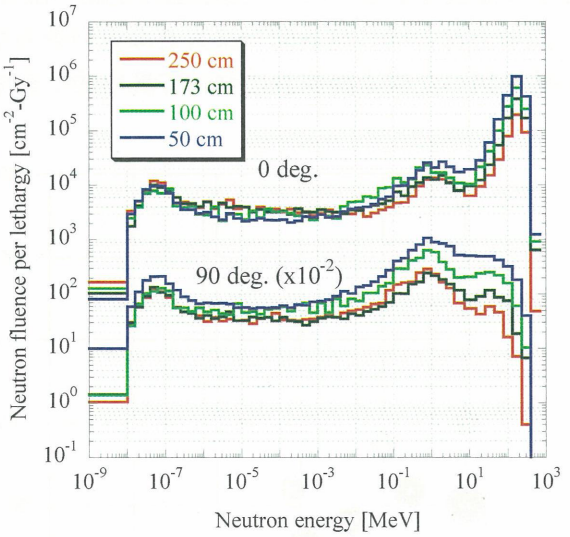


**図５：炭素線治療場における中性子エネルギースペクトルの距離依存性**

[1] 測定位置は、水ファントムを基準にしているため、MLCと各測定位置の距離は角度毎に異なり、０度が最もMLCから離れている。

c）MLC開口幅依存性

図６に測定により得た中性子エネルギースペクトルのMLC開口幅依存性を示す。散乱成分には、MLC開口幅の依存性は全くみられないが、MLCを閉めると、a）で述べた2）のエネルギー領域が増加し、3）のエネルギー領域が減少する。これは、角度依存性と矛盾がなく、2）の成分がMLC、3）の成分が水の寄与であることを示している。また、3）の領域では、大角度になるほどMLCの開口幅の依存性はなくなる。これは、大角度になるほど、3）のエネルギー領域もMLCの寄与が非常に大きいことを示している。

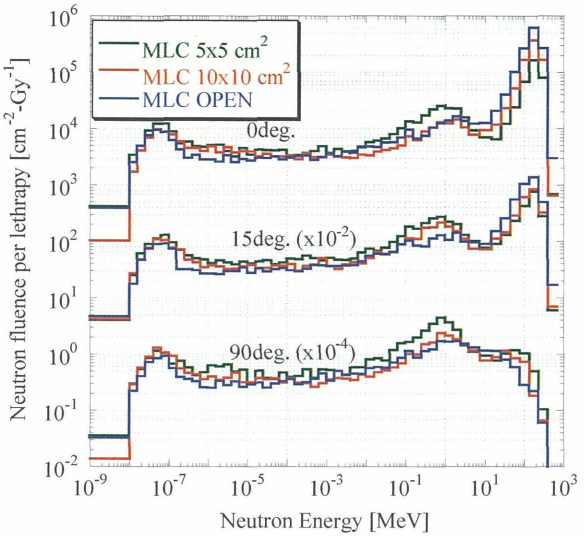


**図６：炭素線治療場における中性子エネルギースペクトルのMLC開口幅依存性**

d）周辺線量当量分布

図７にMLC開口幅10×10 ㎠における周辺線量当量分布を示す。また、図８に、中性子エネルギースペクトルに周辺線量当量換算係数を乗じた周辺線量当量エネルギースペクトル（$d$=173 ㎝、$l$=10 ㎝）を示す。図８からわかるように、周辺線量当量は10keV以上の中性子に大きく依存する。つまり、散乱線による中性子には依存しないため、治療室の空間の広さには依存しない。これは、測定値が治療室もしくは、照射方法の同じ施設間では大きな違いをもたらさないことを示唆しており、我々の測定がpassive法を用いた炭素線施設において汎用的に適応できると考えられる。

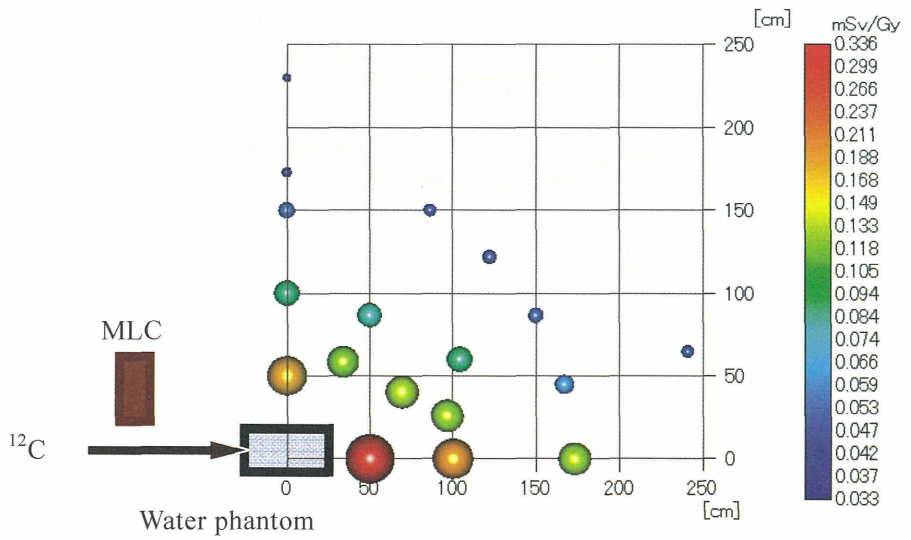


**図７：炭素線治療場における二次中性子による周辺線量当量分布**

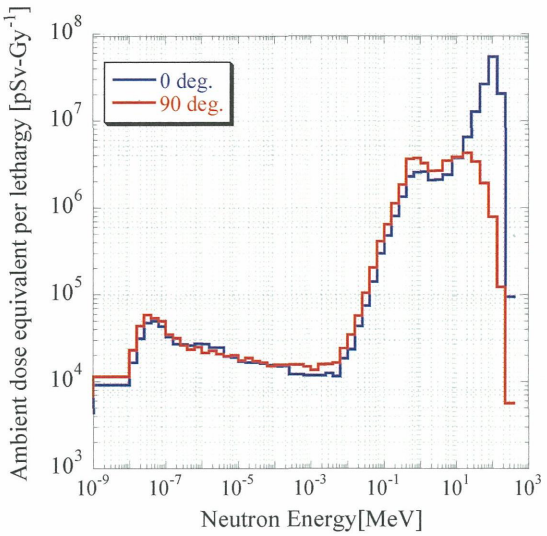


**図８：周辺線量当量エネルギースペクトル（d=173cm、l=10cm）**

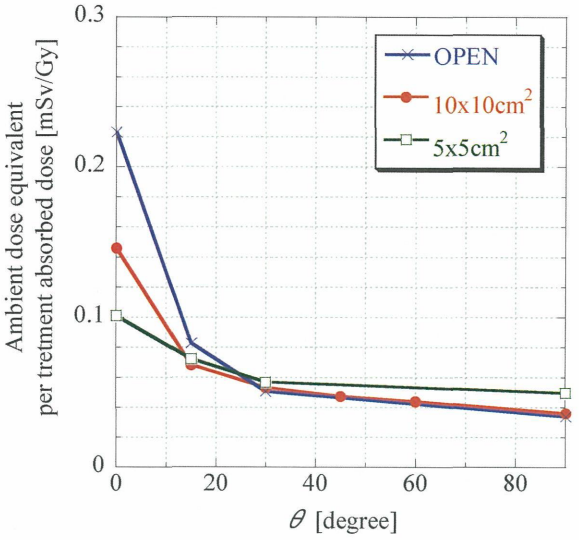


**図９：周辺線量当量のMLC開口幅依存性**

図７から、周辺線量当量は測定を行った領域で、治療吸収線量1Gy当たり、0.336-0.033 mSvの範囲であり、中性子エネルギースペクトルの測定結果から推測できるように非常に前方性の強いものであることがわかる。

図９に周辺線量当量のMLC開口幅依存性を示す。前方では大きなMLC開口幅依存性があるが、90度ではその依存性は小さい。患者の被曝を考える場合に重要となるのは90度方向の線量であることから、MLCの開口幅による被曝線量の依存性は中性子エネルギースペクトル（図６）と同様に小さいと考えられる。

## ４．陽子線治療との比較

E. Hallは、参考文献１，３の測定データから90度方向の周辺線量当量[2]を用いて、陽子線治療のpassive法[1]とscanning法[3]を比較している[5]。ここでは、それらの結果に我々の実験値を追加し、passive法を用いた炭素線治療と陽子線治療の中性子被曝量を比較した。しかし、E. Hallの比較には、いくつかの問題があり、ここでは以下のように修正し比較した。

a）SOBP幅

参考文献５では、SOBP幅を統一せずに比較している。参考文献1では、SOBP幅8.2 cmであり、参考文献３では、10 cmである。ここでは、SOBP幅を我々の実験条件である6 cmに統一した。周辺線量当量は、SOBP幅に比例すると仮定し、参考文献１，３の実験結果を補正した。

b）照射野

参考文献５では、照射野は10×10cm$^2$に統一している。そのため、passive法の測定結果である参考文献１の実験結果を、周辺線量当量が照射野面積に比例するとして、補正している。この補正は、scanning法の場合はMLCが存在しないために正しい補正であろう。しかし、passive法の場合、同一のビーム条件で照射野を拡大するということは、水ファントムに入射する粒子が増加し、MLCに入射する粒子が減少することであるから[3]、照射野面積には比例せず、図９を参考にすれば、むしろ周辺線量当量は減少するかもしれない。ここでは、照射野5×5 cm$^2$で測定を行っている参考文

[2] 参考文献１では、NCRP38[12]の換算係数を用いているため、定義上、結果は線量当量で与えられている。

[3] 参考文献１の照射条件では、19×19 cm$^2$まで一様照射野が形成されている[13]。

献１に条件を合わせ、参考文献３にのみ照射野面積の比率で補正した。

c）線質係数（放射線荷重係数）

参考文献５では、測定で得た実効線質係数を10になるように補正している。しかし、周辺線量当量の比較において、そのような補正をする必要がないために、ここでは、そのような補正はしないこととした。

d）入射陽子数

参考文献3では、10×10×10 $cm^3$のターゲットに対して、吸収線量1Gyを投与するのに必要な入射陽子数を$1\times10^{11}$と仮定している。しかし、この値は誤っており、実際は、$1.75\times10^{11}$が正しいと指摘されている[13]。そのため、ここでは、正しい入射陽子数を用いて、参考文献３の値を修正した。

我々の実験データは炭素エネルギーが290 MeV/uのみであるが、HIMACで治療に用いている最大エネルギーである400 MeV/uでの周辺線量当量を見積もるために、重荷電粒子入射による厚いターゲットから90度方向に生成される5 MeV以上の中性子量[14] のエネルギー依存性を算出した。参考文献14では、炭素入射に対し、炭素、アルミニウム、銅、鉛ターゲットの測定を行っており、90度方向に生成される5 MeV以上の中性子量は、入射炭素エネルギーにほぼ線形に増加する。290 MeV/uと400 MeV/u入射の炭素による中性子生成量の比率は、ターゲットに依存せず、1.57倍であったために、400 MeV/uを用いた場合の周辺線量当量は、290 MeV/uの実験値を1.57倍することで概算した。

また、passive法を用いた陽子線治療施設、PMRCにおいて、陽子160 MeVを用いて、上述の照射条件、測定方法で測定を行った。

図10に炭素線治療場と陽子線治療場の二次中性子による周辺線量当量の比較を示す。炭素線治療では、治療に用いる線量は吸収線量ではなく、RBEを考慮した治療線量を用いるために、図10には参考として治療線量で規格化した値も示している。また、現在のところ、我々のデータは各条件で一点のみしか測定していないため、照射野10×10 $cm^2$の結果を分布の参考として示している。

図10からわかるように、passive法を用いた炭素線治療における中性子による周辺線量当量はpassive法を用いた陽子線治療によるものより小さく、また、scanningによるものより大きいことがわかる。しかし、我々のPMRCで行った測定と参考文献１の結果には数倍の差がある。これは、用いている周辺線量当量換算係数が異なることや、施設間の差等が考えられる。図11に各研究に用いられた周辺線量換算係数を示す。参考文献１では、測定は我々と同じようにボナーボールを用いており、NCRP38の換算係数を使って線量当量を算出している。また、参考文献３では、レムカウンター

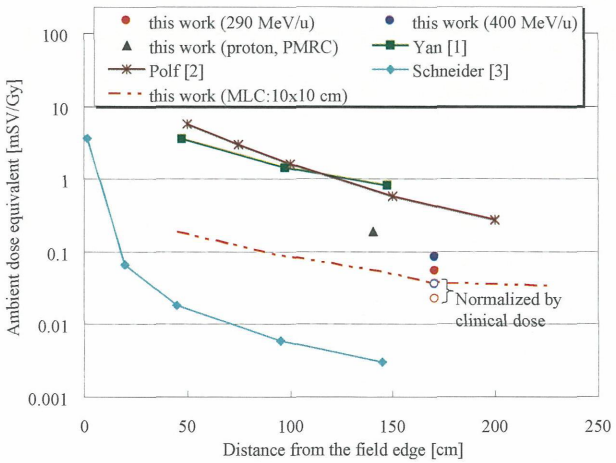


**図10：炭素線治療場と陽子線治療場の二次中性子による周辺線量当量の比較**

陽子線治療場の測定で用いられた入射陽子エネルギーは、PMRC及び参考文献１，２が160MeV、参考文献３が177MeVである。

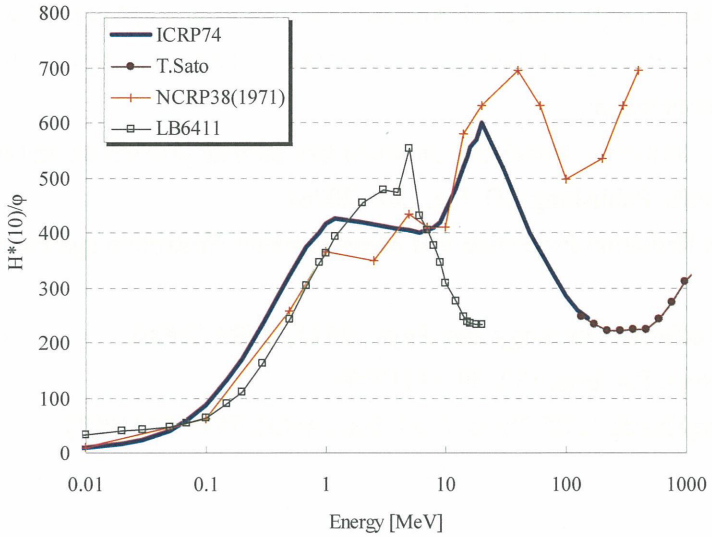


**図11：各研究に用いられた周辺線量換算係数及び検出器のレスポンスの比較**

ICRP74及びT. Satoが我々が用いた係数、NCRP38が参考文献１、LB6411が参考文献３に対応する。

（LB6411[15]）を用いた測定であるために、レムカウンターのレスポンスが線量換算係数に対応する。この図からわかるように、参考文献１で用いている線量換算係数は、10MeV以上で、我々が用いた係数（ICRP74）と、で２倍以上異なることがわかる。さらに、参考文献３では、10MeV以上では、エネルギーの増加とともにレスポンスが減少し、このエネルギー領域の中性子による線量を過小評価していることがわかる。施設間など、これらの差を検証するために、今後、HIMACでの測定と同時に、複数の陽子線治療施設での測定を今後行う必要があると考えている。

## ５．終わりに

HIMACで行われている炭素線治療に潜在する二次がんリスクを評価するために、基礎データとなる二次中性子エネルギースペクトルの取得を行った。現在までに、その測定方法を確立し、また、治療室内の各位置における中性子エネルギースペクトルを取得した。HIMAC及びPMRCでの測定結果から、passive法を用いた場合、炭素線治療場での二次中性子による周辺線量当量は陽子線治療によるものより小さいことを明らかにした。しかし、粒子線治療場における二次中性子線量を、定量的かつ一般的に議論するためには、複数の治療施設において同一の実験条件、実験方法を用いて測定を行う必要がある。今後、日本の他の陽子線治療施設において、同一の測定を行う予定である。また、これらの測定データから、モンテカルロ計算の精度を検証し、等価線量、実効線量を算出する予定である。

参考文献

1) X. Yan et al.: Nucl. Instr. and Meth. A 476, 429-434 (2002).
2) J.C. Polf and W.D. Newhauser: Phys. Med. Biol. 50, 3859-3873 (2005) .
3) U. Schneider et al.: Int. R. Radiation Oncology Biol. Phys., 53(1), 244-251 (2002) .
4) H. Jiang et al.: Phys. Med. Biol. 50, 4337-4353 (2005) .
5.) E. Hall: Int. J. Radiation Oncology Biol. Phys., 65(1), 1-7 (2006) .
6.) M.Awschalom and R.S.Sanna: Radiat.Prot.Dosim., 10, 89-101 (1985) .
7) W.N. EcElroy et al.; AFWL-TR-67-41, Air Force Weapons Lab. (1967).
8) H. Iwase et al., J. Nucl. Sci. Technol. 39(11), 1142-1151 (2002).

9) International Commission on Radiological Protection: Conversion coefficients for use in radiological protection against external radiation. ICRP Publication 74, (Oxford: Pergamon Press) (1996).
10) S. Sato, private communication
11) T. Nakamura and L. Heilbronn: Handbook on secondary particle production and transport by high-energy heavy ions, World Scientific Publishing CO. Pte. Ltd. (2006)
12) National Council on Radiation Protection and Measurements: Protection against neutron radiation NCRP Report 38, (1971).
13) B. Gottschalk: I.J. Radiation Oncology Bio. Phys., 66 (5), 1594 (2006).
14) T.Kurosawa et al.: Nucl. Sci. Eng, 132, 30-57 (1999).
15) A. Klett1 and B. Burgkhardt, IEEE Trans. Nucl. Sci. , 44(3), 757-759 (1997).

# 照射機器内に生じた残留放射能からの放射線強度測定

兵庫県立粒子線医療センター　赤城　卓

Corresponding: t.akagi@hibmc.shingu.hyogo.jp

## 1　はじめに

### 1.1　背景

重粒子線等（陽子線及び重粒子線）は放射線治療において光子線（X線・γ線）と比べ有利な物理学的・生物学的性質を有している。またその臨床研究においても非常に良好な治療成績を示している。そのため有望な放射線治療の一つと考えられている。今後重粒子線等を用いた放射線治療（粒子線治療）は徐々に普及していくことが予想される。

### 1.2　目的

重粒子線等には物質を放射化する能力があり、粒子線治療によって照射機器内および患者体内に放射性物質が生成され照射後も残留する。そのため粒子線治療に従事する医師・診療放射線技師・看護師、及び患者に付き添う家族等へ残留放射能からの放射線による被曝が懸念される。現在は、粒子線治療も現行の放射線障害防止法及び医療法に従うことによってその安全性が十分担保されていると考えている。但し、根拠となるべきデータがなかったため、現存する６つの粒子線治療施設が協力し、陽子線及び炭素線によって生じた残留放射能からの放射線量を測定することとなった。

## 2　方法

### 2.1　測定対象

日本で行われている陽子線及び炭素線を用いた粒子線治療ではブロードビーム法が一般的である。Fig. 1にブロードビーム法の粒子線治療に用いられる照射機器を示す。残留放射能によ

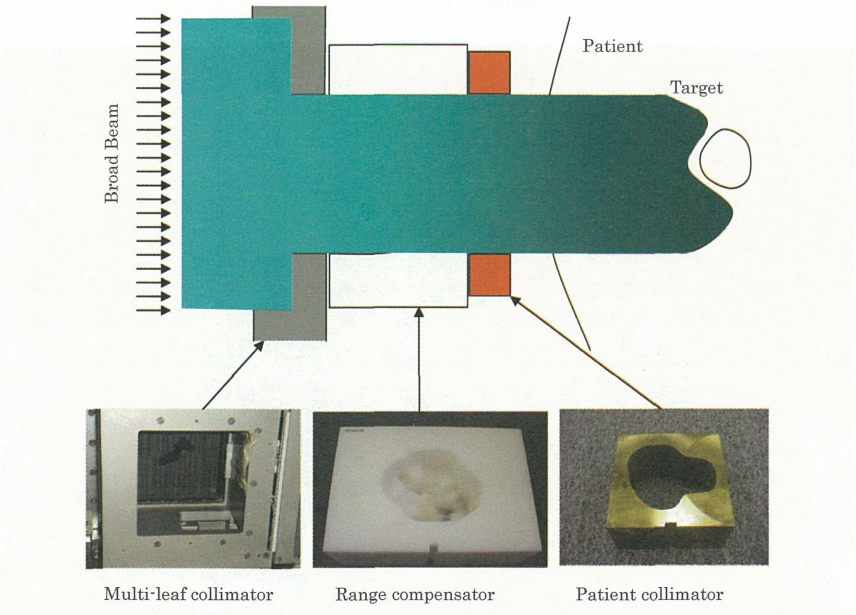


Fig.1: Beam modifying devices for the broad beam delivery system, the collimators and the range compensator. Either the multi-leaf collimator or the patient collimator is used for the treatment. The radiation from the radioactivity remaining in the devices was measured.

る放射線強度を測定すべき機器は治療従事者の近くにあるもので、マルチリーフコリメータ、患者ボーラス、患者コリメータ、である。患者家族への影響を評価するために、患者はタフウォーターファントムに置き換えて放射線量を測定する。Table 1及びTable 2に測定対象物の照射・測定条件をまとめた。

| Objects | Materials | Size | Distance |
|---|---|---|---|
| Patient collimator | Brass | Aperture 3×3 $cm^2$ | Surface |
| | | | 30 cm away |
| Range compensator | Polyethylene/ | 10cm water equivalent | Surface |
| | Chemical wood | thickness | 30 cm away |
| Multi-leaf collimator | Iron | Aperture 5×5 $cm^2$ | Surface |
| | | | 50 cm away |
| *Patient* | Tuff water | 30×30×30 $cm^3$ | Surface |
| | | | 30 cm away |

Table 1: Specifications of the measuring objects and the measuring distance from the object.

| | Protons | Carbon-ions |
|---|---|---|
| Beam energy in residual range (cm) | ～25 | ～15(25) |
| Field size in diameter (cm) | 15 | 15 |
| SOBP width (cm) | 6 | 6 |
| Physical dose at the mid-peak (Gy) | 5 | 5 |
| Dose rate (Gy/min) | Equivalent to treatments | Equivalent to treatments |
| *Measuring interval* | Every 30 sec | Every 30 sec |

Table 2: Protocol of the radiation measurements for the proton and carbon-ion beams. The higher beam energy of the carbon-ion beam was optional.

## 2. 2　測定器

電離箱式サーベイメータ（Fig. 2）を用いて機器からの放射線強度を30秒ごとに測定した。電離箱のキャップをはずすことにより$\beta$線による皮膚線量の測定も行った。各施設の測定器は国家標準とトレーサビリティーのある標準場において１年以内に校正済みであった。

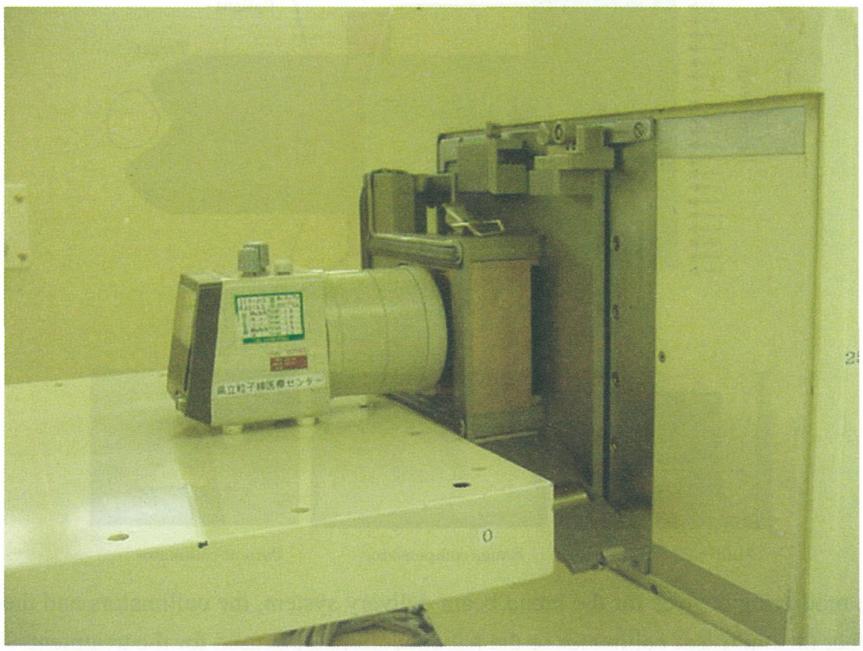

Fig.2: Photo of the Ionization survey meter used for the radiation measurements.

## 3　結果

### 3.1　データ解析

6施設中4施設から測定データが提出された。ある施設で測定された30秒ごとの線量率をグラフにした結果を測定対象物ごとにFig. 3に示す。得られたデータを２つの減衰曲線の和、

$$\dot{H} = p_1 \exp(-t / p_2) + p_3 \exp(-t / p_4) \tag{1}$$

で表現した。ここで、$H$は線量率（μSv）、$t$は時間（h）である。$p_1$、$p_3$は生成された放射能の量、$p_2$、$p_4$は放射能の寿命に相当する量である。$p_1$～$p_4$はフィッテングパラメータである。

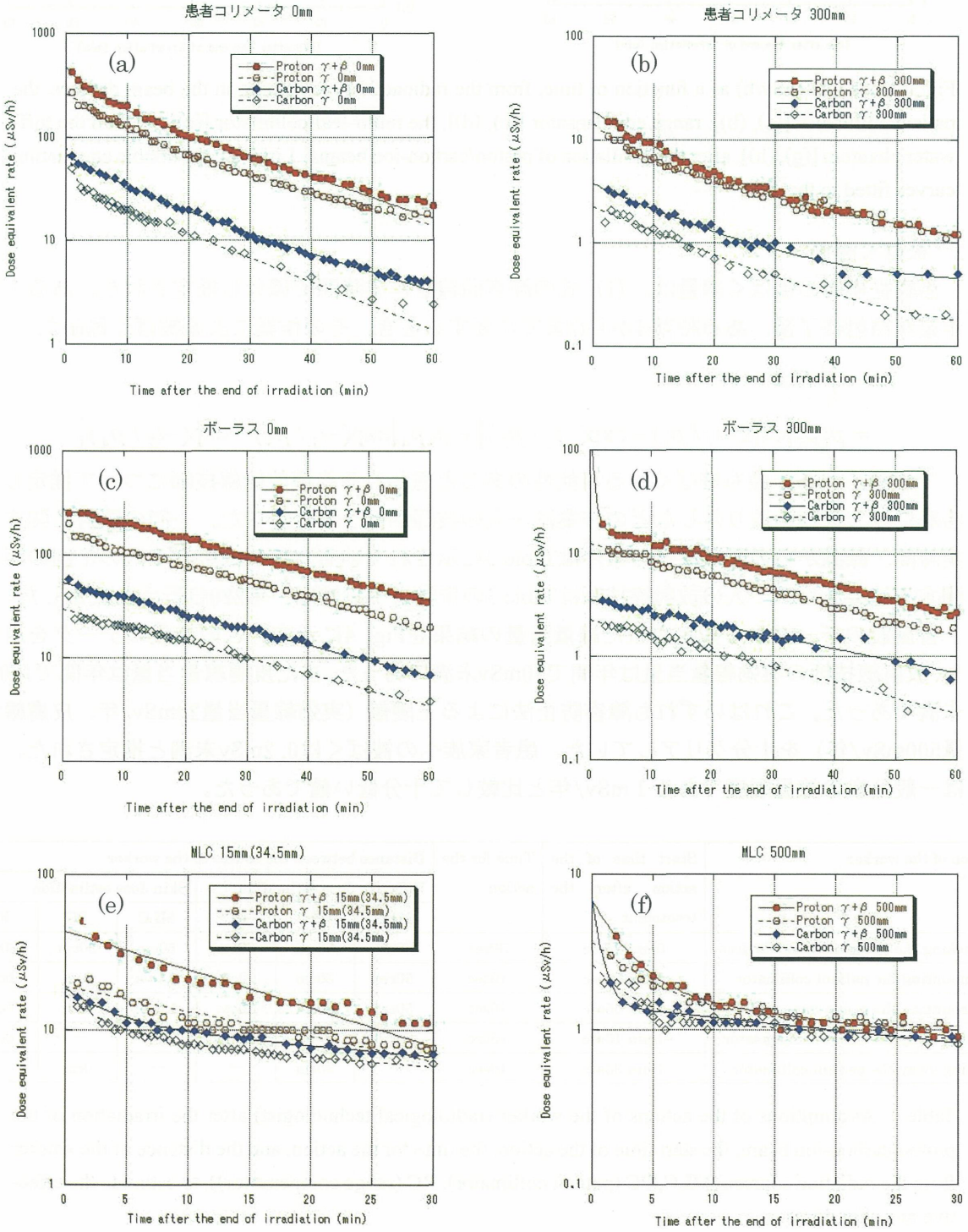

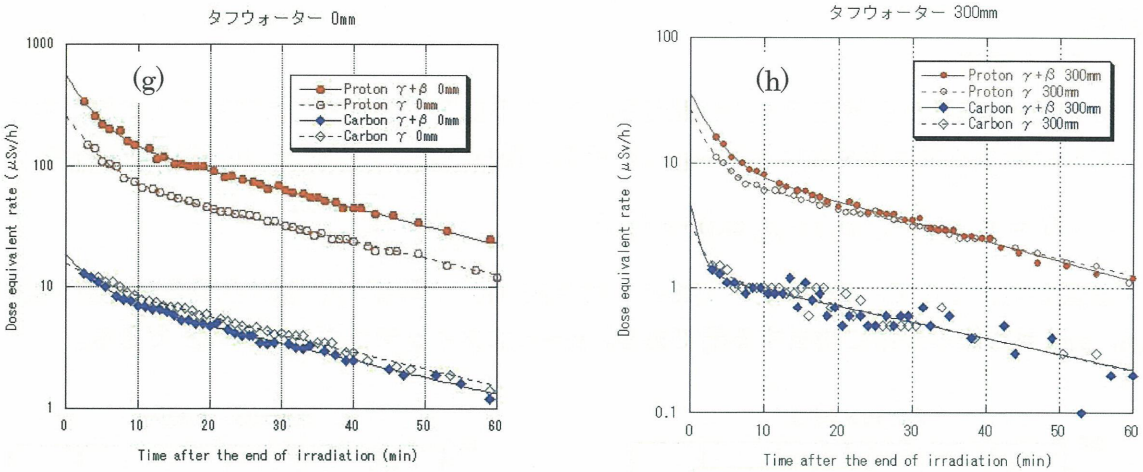


Fig.3: Dose rate (μSv/h) as a function of time, from the radioactivity remaining in the beam devices, the patient collimator [(a), (b)], range compensator [(c), (d)], the multi-leaf collimator [(e), (f)], and the tuff-water phantom [(g), (h)], after the irradiation of proton/carbon-ion beams. Lines are the double attenuation curves fitted to the data.

## 3. 2　被ばく評価

治療従事者の被ばく線量は、(1) 式の減衰曲線を作業時間で積分し推定された。ある１つの作業が照射終了後、ある時刻t1からt2までに要するとき、その作業による被ばく量$H$は、

$$H = \int_{t_1}^{t_2} \dot{H} dt$$
$$= p_1 p_2 \left[\exp(-t_1 / p_1) - \exp(-t_2 / p_2)\right] + p_3 p_4 \left[\exp(-t_1 / p_3) - \exp(-t_2 / p_4)\right] \quad (2)$$

で求められる。最も被ばくする可能性のあると思われる診療放射線技師について推定した。治療に伴う機器の取り外しなどの作業は一人の技師が行うと仮定した。一回の照射に関する作業時間、線源からの距離などの条件はTable 3に示されている。これは患者１人の１回の照射に関する値であり、一人の放射線技師はTable 3の作業を１日20回、年260日行うと仮定した。

各施設のデータから推定された線量当量の結果をFig. 4に示す。どの施設のデータを用いても、放射線技師の実効線量当量は年間で10mSv未満であった。また皮膚線量当量は年間で100mSv未満であった。これはいずれも障害防止法による上限値（実効線量当量20mSv/年、皮膚線量当量500mSv/年）を十分クリアしていた。患者家族への被ばくは0. 2mSv未満と推定された。これは一般公衆の線量限度である１mSv/年と比較して十分低い値であった。

| Action of the worker | Start time of the action after the treatment | Time for the action | Distance between the source to the worker | | | | | |
|---|---|---|---|---|---|---|---|---|
| | | | Effective dose estimation | | | Skin dose estimation | | |
| | | | MLC | PC | RC | MLC | PC | RC |
| Detaching the immobilization devices | 0min 25sec | 30sec | 50cm | 30cm | 30cm | 50cm | 30cm | 30cm |
| Dismounting the patient collimator | 0min 55sec | 10sec | 50cm | 30cm | 30cm | 1.5cm | 0cm | 0cm |
| Dismounting the range compensator | 1min 05sec | 10sec | 50cm | 30cm | 30cm | 1.5cm | 30cm | 0cm |
| Putting away the range compensator | 1min 15sec | 15sec | — | — | 30cm | — | — | 0cm |
| Putting away the patient collimator | 1min 30sec | 10sec | — | 30cm | — | — | 0cm | — |

Table 3: Assumptions of the actions of the worker (radiological technologist) after the irradiation of the proton/carbon-ion beam, the start time of the action, the time for the action, and the distance of the worker from the radiation sources (MLC, PC (patient collimator), RC (range compensator)), to estimate the effective and skin doses.

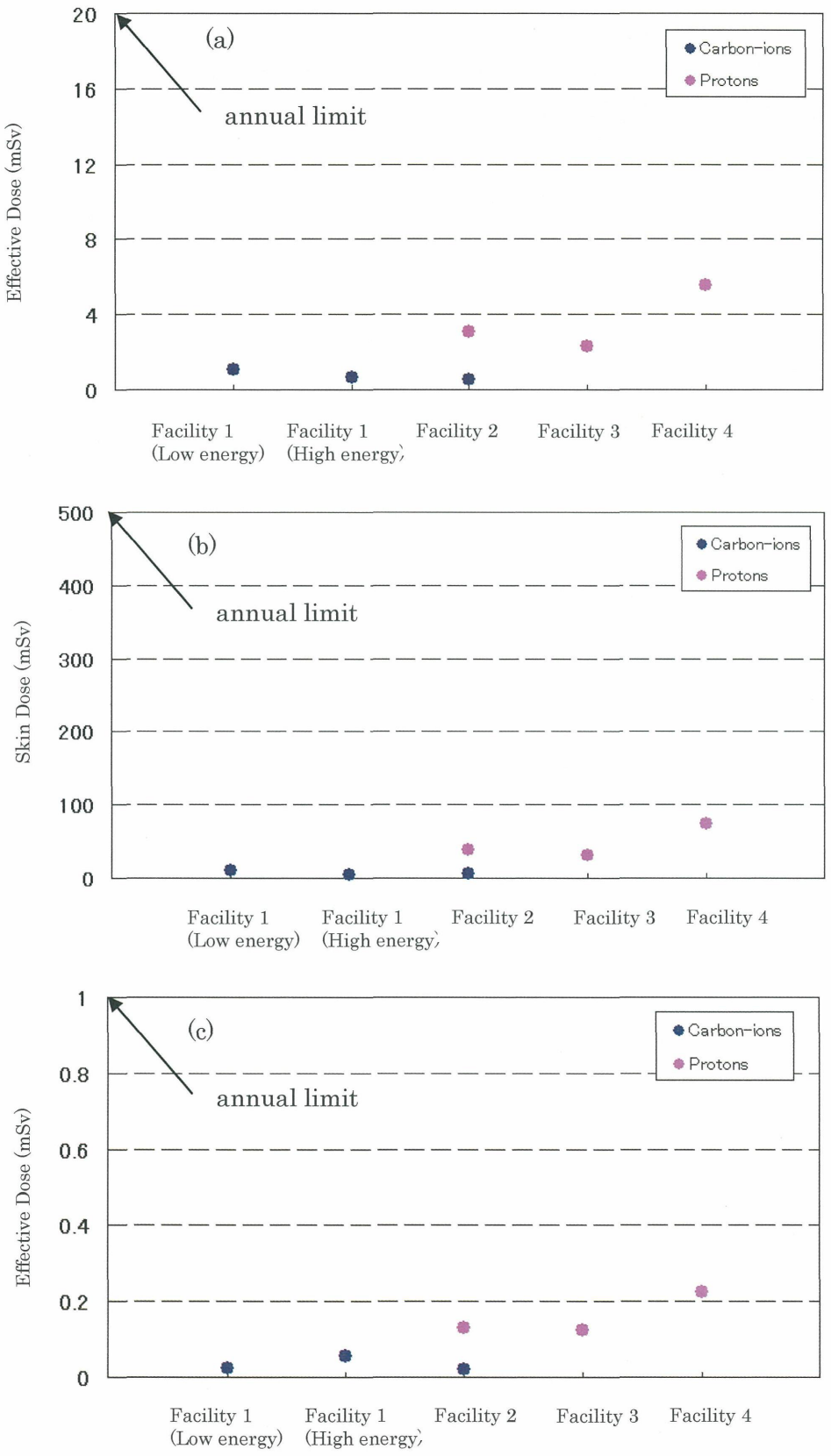


Fig.4: Effective doses estimated from the attenuation curves with four facilities' data. All of the doses are much lower than the annual limits by the Japanese regulations.

## 4　おわりに

粒子線治療による照射機器及び患者の放射化について実験を行った結果、放射化物からの放射線による治療従事者及び患者家族への影響は現行の規制基準を十分満足していた。この研究は厚生労働省科学研究費補助金を受けて行われている「重粒子線治療等新技術の医療応用に係る放射線防護のあり方に関する研究」の一部である。

# 粒子線治療施設における放射線防護と管理

独立行政法人理化学研究所・仁科加速器研究センター　上蓑　義朋

Corresponding: uwamino@riken.jp

## 1．はじめに

高エネルギーに加速された重イオンや陽子を用いた粒子線治療は、従来のX（γ）線や電子線を用いた治療と異なり、機器のみならず患者自体も有意に放射化し、中性子の発生も顕著である。加速器の使用については放射線障害防止法が施設の遮へい能力等に関して安全上の規制をしているが、機器や患者の放射化、患者の中性子被ばく等については国内の法令では考慮されていない。粒子線治療の安全に関して、特別な規制が必要であるかを検討してきた。

患者の中性子被ばく、機器の放射化による医療従事者の被ばくについて、国内の粒子線治療施設において実験的に評価した結果は前の２つの報告で明らかにされている。ここでは諸外国の実態調査と、患者の放射化による家族の被ばくおよび環境への影響を評価した結果について報告する。

なおこの報告の内容は、厚生労働科学研究費補助金（研究課題名：重粒子線治療等新技術の医療応用に係る放射線防護のあり方に関する研究、主任研究者：辻井博彦）を受けて平成17年度から３年間の計画で行われてきた研究の成果の紹介である。従って調査研究はすべて主任研究者、研究分担者、研究協力者によって実施されたものである[1)]。

## 2．諸外国の実態調査

諸外国の規制の状況を、既に患者への照射を実施しているドイツ、アメリカ、スウェーデン、南アフリカ、スイスおよび治療はしていないが加速器について発展途上国であるインドについて調査した。表１に調査を行った国と施設、治療に用いている粒子の種類と最大エネルギーを示す。

| country | code | organization | particle used for therapy | energy (MeV/u) |
|---|---|---|---|---|
| Germany | DE | GSI, Darmstadt | $^{12}$C | 430 |
| | | HIT/DKFZ, Heidelberg | $^{12}$C | 430 |
| USA | US | Loma Linda U., CA | p | 250 |
| | | MD Anderson, TX | p | 250 |
| | | Florida U., FL | p | 235 |
| Sweden | SE | Upsala TSL | p | 180 |
| S. Africa | ZA | iThemba LABS, Cape Town | p | 200 |
| Switzerland | CH | PSI, Aargau | p | 214 |
| India | IN | VECC, Kolkata | Therapy is not conducted. | |

**表１　実態調査を行った国と施設。**

粒子線治療施設の安全を担当する規制当局に関しては、スウェーデンは日本と同様施設の放射線安全と治療については異なった機関が担当しているが、両者をまとめて一つの機関が規制している国が多いようである。米国では州によって体制が異なる。

管理区域などの場所にかかる外部線量率限度については、ドイツは日本よりも厳格にICRP勧告を取り入れているなど、実態は国によってかなり異なっている。南アフリカとインドでは大雑把に規制しているが、インドの規制値は必要以上に厳しいように思える。

ボーラスやコリメータなど、微弱に放射化するが短時間で減衰する物品の廃棄に対する規制では、ドイツは法で明確にクリアランスレベルが決められているため、管理者はそれに従って判断すればよい。日本を含め大方の国では、明確な基準は定められておらず、管理者の判断に任されているのが現状である。

粒子線治療に関して、医療従事者の防護や患者の放射化に対する特別な法規制について聞き取りをした。照射終了後は立入までに２，３分要することから、極めて短半減期の放射能は減衰してしまうため、被ばくはほとんど観測されておらず、いずれの施設も医療従事者に対する特別な規制は不要と考えていた。また患者の放射化についてもレベルは低いため、すべての施設において特別な配慮は取られていなかった。ペースメーカや心電図を装着した患者の照射についてはGSIだけで経験があり、基本的には機器を直接照射しなければ治療可能と考えられていた。

## ３．患者放射化の評価

### 3.1　タフウォータの照射実験

粒子線照射によって患者の照射部位は微弱に放射化する。これによって患者に付き添う家族は被ばくする可能性があり、また患者の排泄物に放射性物質が含まれる。これらの影響を評価するために、患者を模擬するファントムとしてタフウォータを4施設（筑波大学陽子線医学利用研究センター、静岡県立がんセンター、兵庫県立粒子線治療センター、放射線医学総合研究所重粒子医科学センター）において、表2に示す6種類の陽子または炭素線ビームを用いて照射した。

照射条件は、図１（A）に示すとおり厚さ30cmのタフウォータに50cmの距離で10cm×10cmに絞ったビーム（SOBPは６cm、およその水中飛程は陽子で25cm、炭素で15cmまたは25cm）を、SOBP中点における線量で5Gy照射した。

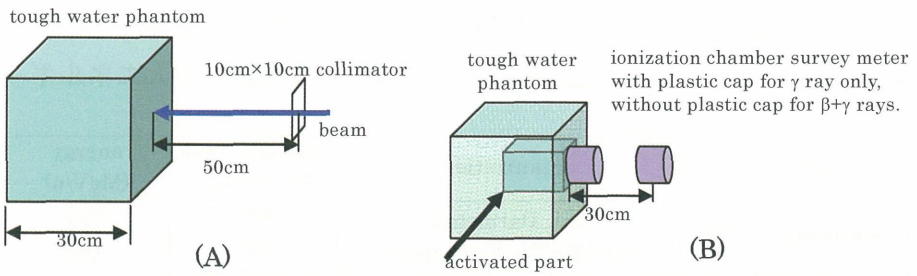


**図１　（A）はタフウォータ照射の条件。（B）は照射後の測定条件**

照射後タフウォータをバックグランドの低い照射室外に持ち出し、図１（B）に示すように、電離箱式サーベイメータで表面および表面から30cm（電離箱の実効中心までの距離）における$\gamma$線量率（キャップ付で測定）および$\beta+\gamma$線量率（キャップなしで測定）をおよそ30秒間隔で測定した。

タフウォータの組成を表３に示す。比較のために示した人体軟組織の組成（ICRU soft tissue）に比べ、酸素が少なく炭素が多い。

測定結果の例として、照射終了５分後の線量率を表２に示す。陽子線照射では炭素線に比較して数倍から十数倍線量率が高いことが分かる。放医研の測定ではエネルギーが高いと線量率はエネルギーの比以上に上昇しているが、兵庫との同じ炭素線の比較では逆にエネルギーが若干高い兵庫のほうが線量率は小さい。原因は不明である。

時系列の測定値を、次の２成分の指数関数で近似した結果を図２に示す。

| facility | beam | dose rate (μSv/h) | | | | $\beta^+$ emitter concentration* (Bq/g) |
|---|---|---|---|---|---|---|
| | | at surface | | at 30cm | | |
| | | β+γ | γ | β+γ | γ | |
| 筑波 | 200MeV p | 298 | 136 | 19 | 11 | 387 |
| 静岡 | 220MeV p | 286 | 134 | 18 | 9.8 | 353 |
| 兵庫 | 210MeV p | 230 | 116 | 13 | 8.9 | 323 |
| | 320MeV/u $^{12}$C | 10 | 11 | 1.1 | 1.3 | 45 |
| 放医研 | 290MeV/u $^{12}$C | 21 | 15 | 3.1 | 2.1 | 76 |
| | 400MeV/u $^{12}$C | 35 | 22 | 4.9 | 3.9 | 142 |

* Weight of patient is assumed to be 50kg.

**表２　Tough Waterの照射を行った施設、用いたビームと5分後の線量率および30cmの位置で測定したγ線量率から計算で求めた、陽電子放出核種の患者体内の比放射能**

| 元素 | H | C | N | O | Cl | Ca |
|---|---|---|---|---|---|---|
| Tough Water | 8.2 | 66.2 | 2.2 | 20.7 | 0.4 | 2.3 |
| ICRU soft tissue | 10.1 | 11.1 | 2.6 | 76.2 | 0 | 0 |

**表３　Tough Water（密度1.018g/cm$^3$）とICRU軟組織の成分。数値は質量分率（wt%）。**

$$H = H_{01}e^{-\lambda_1 t} + H_{02}e^{-\lambda_2 t} \tag{1}$$

放医研における290MeVの測定値はばらつきが大きく、1成分でしか近似できなかった。タフウォータの成分から、放射性核種は$^{15}$O（半減期2.037分）と$^{11}$C（半減期20.39分）であることが推測される。主な生成反応は、$^{16}$O（p, pn）$^{15}$O、$^{12}$C（p, pn）$^{11}$C〔pは陽子または炭素イオン〕である。タフウォータは軟組織に比較して炭素が多く酸素が少ないため、実際の患者では図２よりも早い減衰成分が大きく、遅い減衰成分が小さくなることが予測される。

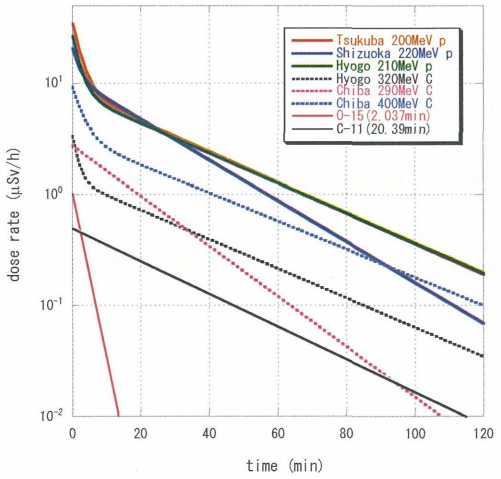


**図２　タフウォータの表面から30cmの位置におけるγ線量率の減衰曲線。参考のために赤い実線と黒い実線で$^{15}$O（半減期2.037分）と$^{11}$C（半減期20.39分）の減衰（絶対値は任意）も示した。**

### 3.2　患者家族の被ばく評価

患者が照射終了２分後に照射室から出た後、家族が2時間付き添った場合の積算線量を求めた。これはタフウォータの表面から30cmの位置におけるγ線の線量率をフィットした式を、２分から120分まで積分した値である。粒子線治療では、患者に対し20～30回程度の分割照射が行われる。可能性

のある被ばくの最大値を求めるため、この積分値を30倍した値を、家族一人の被ばく量と仮定した。結果は陽子線照射では123から138μSv、炭素線照射では21から56μSvであった。

この値はタフウォータ照射の場合の値であり、実際の患者での被ばくを推定するため、成分の違いを考慮して補正した。(1) 式の第1項を短半期成分、第2項を長半減期成分とする ($\lambda_1 > \lambda_2$)。短半減期成分を酸素の放射化、長半減期成分を炭素の放射化と仮定し、それぞれ成分の違いから次式の補正をし、患者からの線量率とした。

$$H' = H_{01} \times \frac{76.2}{20.7} \times e^{-\lambda_1 t} + H_{02} \times \frac{11.1}{66.2} \times e^{-\lambda_2 t} \qquad (2)$$

(2) 式を同様に2分から120分まで積分し、30倍した値は、陽子線では33から73μSv、炭素線では5から25μSvであった。これらの値はいずれも一般人の年間被ばく限度である1mSvに比較して10分の1以下である。このように極めて過大と思われる評価を行っても、患者家族の被ばくは十分低い値である。

### 3.3 患者からの排泄物の放射能濃度評価

照射5分後に患者が照射室から退室した直後のトイレでの排泄を想定した場合の排水中の放射能濃度を評価した。

光子と電子の挙動をモンテカルロ法で計算するEGS4プログラム[2] を用いて、照射領域（10cm×10cm×25cmの水と仮定）中の任意の位置で消滅放射線が1個発生した際に、表面から30cm離れた場所での線量を計算すると、平均$7.7\times10^{-17}$Svであった。保守的に評価をするため、血流によって生成した放射能が患者の身体全体に分散すると仮定した場合の照射5分後の患者（体重50kgと仮定）の比放射能を計算した結果を表2の最右欄に示す。

比放射能は45から390Bq/gである。半減期が比較的長く危険性が高い$^{11}$Cの排水中濃度限度は40 Bq/cm$^3$である。安全側に放射能はすべて$^{11}$Cであると仮定しても、炭素線では患者の比放射能は排水中濃度限度の1から4倍、陽子線でも8から10倍であり、水洗による希釈を考慮すると、トイレの排水だけに注目した場合でも濃度限度を下回る。さらに病院の他の排水による希釈を考えると、まったく問題とすべき値ではないことが分かる。

## 4．おわりに

諸外国における調査では、いずれの施設においても粒子線治療特有の安全規制は行われておらず、必要性も認識されていなかった。また患者の放射化を評価したところ、放射化の程度はきわめて低く、特別な配慮の必要性は認められなかった。従って粒子線治療の安全に関し、科学的見地からは新たに規制を設ける必要はないと判断できる。

引用文献

1）辻井博彦：「重粒子線治療等新技術の医療応用に係る放射線防護のあり方に関する研究」、厚生労働科学研究費補助金、総括・分担研究報告書（2007年4月）.

2）W. R. Nelson, et al.: The EGS4 code system, SLAC-245 (1985).

National Institute of Radiological Sciences

4-9-1 Anagawa,Inageku,Chiba 263-8555,Japan
International and Research Cooperation Section
E-mail: kokukou@nirs.go.jp
Tel: +81-43-206-3024
Fax: +81-43-206-4061